amU
Aix Marseille Université

NNT : 02VEHV043E6

THÈSE DE DOCTORAT

Soutenue à AMU — Aix-Marseille Université
dans le cadre d'un co-encadrement avec FEMTO-ST
le 18 décembre 2024 par

Walid TOUIL

Predictive Modeling Approach for Aging Analysis and Durability Enhancement of PEM Fuel Cells

Modélisation prédictive pour l'analyse du vieillissement et l'amélioration de la durabilité des piles à combustible PEM

Discipline
Automatique

École doctorale
ED 184 Mathématiques et Informatique

Laboratoire/Partenaires de recherche
Laboratoire d'Informatique et des Systèmes (LIS), Marseille FRANCE

Institut de Franche-Comté Electronique Mécanique Thermique et Optique – Sciences et Technologies (FEMTO-ST), Besançon FRANCE

Composition du jury

M.Belkacem OULDBOUAMAMA PU (CRIStAL/UL)	Rapporteur
M.Jean-Christophe OLIVIER MCF (IREENA/UN)	Rapporteur
Mme.Mitra FOULADIRAD PU (M2P2/CM)	Présidente
M.Cédric DAMOUR MCF (Energy-Lab /UR)	Examinateur
M.Christophe TURPIN DR (Laplace/CNRS)	Examinateur
M.Rachid OUTBIB PU (LIS/AMU)	Directeur de thèse
M.Zhongliang LI Chaire de professeur junior (FEMTO-ST/UFC)	Co-directeur de thèse

femto-st SCIENCES & TECHNOLOGIES

LIS LABORATOIRE D'INFORMATIQUE & SYSTÈMES

Affidavit

I, undersigned, Walid TOUIL, hereby declare that the work presented in this manuscript is my own work, carried out under the scientific supervision of M.Rachid OUTBIB and M.Zhongliang LI, in accordance with the principles of honesty, integrity and responsibility inherent to the research mission. The research work and the writing of this manuscript have been carried out in compliance with both the french national charter for Research Integrity and AMU charter on the fight against plagiarism.

This work has not been submitted previously either in this country or in another country in the same or in a similar version to any other examination body.

Marseille, October 23, 2024



This work is licensed under Creative Commons Attribution-NonCommercial-NoDerivatives 4.0 International Public License

List of publications and conference participation

List of publications produced within the framework of the thesis project :

1. W. Touil, Z. Li, R. Outbib, D. Hissel, and S. Jemei, "A System-Level Modeling Framework for Predicting Pt Catalyst Degradation in Proton Exchange Membrane Fuel Cells," *Journal of Power Sources*, 2024. DOI : 10.1016/j.jpowsour.2024.235628.

Participation in conferences during the thesis period :

1. W. Touil, Z. Li, R. Outbib, D. Hissel, and S. Jemei, « Model predictive control energy management strategy of fuel cell hybrid electric vehicle » in the 48th Annual Conference of the IEEE Industrial Electronics Society (IECON), oral presentation, October 2022, Brussels, Belgium. DOI : 10.1109/IECON49645.2022.9968429.
2. W. Touil, Z. Li, R. Outbib, D. Hissel, and S. Jemei, « A dual-scale modelling framework for predicting catalyst degradation in Polymer Electrolyte Fuel Cells » in the 9th International Conference on Fundamentals & Development of Fuel Cell (FDFC), oral presentation, September 2023, Ulm, Germany.
3. W. Touil, Z. Li, R. Outbib, S. Jemei, and D. Hissel, « A dual-scale modelling framework for predicting catalyst degradation in Polymer Electrolyte Fuel Cells » in the 3rd French Hydrogen Research Federation annual conference (3ième plénières FRH2), oral presentation, May 2023, La Réunion, France.
4. W. Touil, Z. Li, R. Outbib, D. Hissel, and S. Jemei, « Control oriented modeling of integrated catalyst and membrane degradation in PEM fuel cells » in 2024 IEEE Transportation Electrification Conference and Expo (ITEC), oral presentation, June 2024, Chicago, USA. DOI : 10.1109/ITEC60657.2024.10598861.

Résumé et mots clés

Les piles à combustible, notamment les PEMFC, souffrent d'une durabilité limitée freinant leur adoption. Les recherches actuelles visent à mieux comprendre leurs mécanismes et optimiser la conception des composants pour prolonger leur durée de vie et réduire les coûts. Les progrès récents montrent que l'intégration de matériaux avancés et de stratégies de contrôle intelligentes peut significativement améliorer la durabilité, soulignant le rôle crucial des systèmes de contrôle dans l'adaptation aux tendances de dégradation des PEMFC.

Cette thèse développe un cadre de modélisation à double échelle pour prédire la dégradation des piles à combustible dans diverses conditions, facilitant la mise en œuvre de stratégies de contrôle optimales. Elle combine des modèles microscopiques des mécanismes de dégradation affectant le catalyseur et la membrane, avec un modèle macroscopique de l'état interne de la cellule et des performances globales. Cette approche permet des mises à jour en temps réel des performances et des prédictions de la dégradation, améliorant la gestion proactive et prolongeant la longévité du système.

Dans la modélisation microscopique, l'impact du vieillissement sur l'assemblage membrane-électrode, en particulier la membrane échangeuse de protons et le catalyseur en platine, est étudié en détail. Ce modèle éclaire les mécanismes de dégradation, tels que la dissolution et l'oxydation du platine, la corrosion du support en carbone et la dégradation de la membrane, servant d'indicateur pour évaluer l'état de vieillissement de la pile. Il permet également de comprendre l'influence des conditions de fonctionnement sur le taux de dégradation.

L'approche de modélisation globale couple le modèle microscopique des mécanismes de dégradation électrochimique avec la performance globale de la pile, reliant les échelles pour développer un contrôle optimisé du PEMFC. Cette stratégie permet d'équilibrer les conditions de fonctionnement, assurant des performances optimales tout en respectant les contraintes de la membrane et du catalyseur en platine.

Cette recherche implique la formulation du problème de contrôle pour la gestion de la santé des piles à combustible et l'amélioration de leur durabilité, en définissant les objectifs spécifiques de contrôle. Elle traite également de la nécessité d'un contrôle optimal, avec la mise en place d'un cadre de contrôle prédictif basé sur modèle, conçu pour optimiser les conditions de fonctionnement, en particulier la température, et prolonger la durée de vie des piles à combustible.

Mots clés : PEMFC, Modélisation de la dégradation, Dégradation du catalyseur à base de platine, Dégradation de la membrane, Contrôle-commande.

Abstract and keywords

Fuel cells, particularly PEMFCs, suffer from limited durability, hindering their widespread adoption. Current research aims to better understand their mechanisms and optimize component design to extend their lifespan and reduce costs. Recent advancements show that integrating advanced materials and intelligent control strategies can significantly improve durability, highlighting the crucial role of control systems in adapting to the degradation trends of PEMFCs.

This thesis develops a dual-scale modeling framework to predict fuel cell degradation under various conditions, facilitating the implementation of optimal control strategies. It combines microscopic models of the degradation mechanisms affecting the catalyst and membrane with a macroscopic model to estimate the internal state of the cell and overall performance. This approach enables real-time updates of performance and degradation predictions, enhancing proactive management and extending the system's longevity.

In microscopic modeling, the impact of aging on the membrane-electrode assembly, particularly the proton exchange membrane and platinum catalyst, is studied in detail. This model sheds light on degradation mechanisms, such as platinum dissolution and oxidation, carbon support corrosion, and membrane degradation, serving as an indicator to assess the aging state of the fuel cell. It also helps understand the influence of operating conditions on the degradation rate.

The global modeling approach couples the microscopic model of electrochemical degradation mechanisms with the overall performance of the fuel cell, linking the scales to develop optimized control of the PEMFC. This strategy allows for balancing operating conditions, ensuring optimal performance while respecting the constraints of the membrane and platinum catalyst.

This research involves formulating the control problem for fuel cell health management and improving their durability by defining specific control objectives. It also addresses the need for optimal control, implementing a model-based predictive control framework designed to optimize operating conditions, particularly temperature, and extend the lifespan of fuel cells.

Keywords: Proton exchange membrane fuel cell (PEMFC), Degradation modeling, Catalyst degradation, Membrane degradation, Durability enhancement control.

Acknowledgments

I would like to express my deepest gratitude to my thesis supervisors, M. Zhongliang Li and M. Rachid Outbib, for their unwavering support, patience, and invaluable suggestions throughout my research. Their insightful guidance and encouragement have been instrumental at every stage of this thesis.

I also extend my sincere appreciation to my research project DEAL team members, M. Daniel Hissel and M. Samir Jemei, for their invaluable support. Additionally, I am grateful to my thesis committee members, M. Belkacem OULD BOUAMAMA, M. Cédric DAMOUR, Mme. Mitra FOULADIRAD, M. Jean-Christophe OLIVIER, and M. Christophe TURPIN, for their constructive comments and the dedicated time they devoted to reviewing my work.

I am especially thankful to my family, particularly my parents, for their boundless love, understanding, and unwavering support throughout my studies. I also wish to thank my friends and colleagues for their encouraging conversations and support over the years; your assistance has been crucial to this enlightening experience.

Finally, this work was supported by the French National Research Agency (ANR) through the DEAL project and was conducted at the LIS laboratory of Aix-Marseille University in collaboration with the FEMTO-ST laboratory at Franche-Comté University. I am grateful to these institutions for providing me with the opportunity to pursue my research.

Contents

Nomenclature 9

List of Figures 12

List of Tables 14

General Introduction 15

1 Introduction 17
- 1.1 Motivation . . . 17
- 1.2 Principles and Structure of PEM Fuel Cells . . . 19
- 1.3 Literature Review on Degradation Mechanisms in PEM Fuel Cells . . . 22
  - 1.3.1 Pt Catalyst Degradation Mechanism . . . 22
  - 1.3.2 Proton Exchange Membrane Degradation Mechanism . . . 24
  - 1.3.3 Reversible Degradation of PEMFC . . . 26
- 1.4 Literature Review on Operating Condition Effects . . . 27
- 1.5 Literature Review on PEMFC Degradation Modeling . . . 30
  - 1.5.1 Pt Catalyst Degradation Modeling . . . 30
  - 1.5.2 Membrane Degradation Modeling . . . 31
  - 1.5.3 System Level Degradation Model . . . 34
- 1.6 Literature Review on PEM Fuel Cell Modeling Approaches . . . 35
- 1.7 Literature Review on Control Strategies for PEMFC . . . 37
- 1.8 Summary and Conclusion . . . 40

2 Micro-Scale Model : PEM Fuel Cell Degradation Model 41
- 2.1 Inroduction . . . 41
- 2.2 Development of a Pt Catalyst Degradation Model . . . 42
  - 2.2.1 Pt degradation processes and kinetics . . . 44
  - 2.2.2 Physical Pt catalyst degradation model . . . 48
- 2.3 Results and Discussion . . . 51
- 2.4 PEM Model Development . . . 61
  - 2.4.1 Hydrogen peroxide formation . . . 62
  - 2.4.2 Fluoride release rate . . . 63
  - 2.4.3 Membrane thinning . . . 64
  - 2.4.4 Results and Discussion . . . 66
- 2.5 Summary and Conclusion . . . 69

3 Macro-Scale Model: PEM Fuel Cell Dynamic Model **70**
3.1 Introduction . . . 70
3.2 PEMFC Dynamic Model . . . 72
3.2.1 Model Assumption . . . 73
3.2.2 Mass Transport across the MEA . . . 74
3.2.3 Heat Transport Model . . . 80
3.2.4 Terminal voltage Model . . . 81
3.3 Modeling Framework for Predicting PEMFC Degradation . . . 83
3.3.1 Analysis of Internal States and Parameters . . . 84
3.3.2 Performance . . . 86
3.3.3 Results and discussion . . . 88
3.4 Summary and Conclusion . . . 92

4 Control Strategies for Enhancing PEMFC Longevity **93**
4.1 Inroduction . . . 93
4.2 PEMFC system control overview and durability enhancement control . 95
4.2.1 Overview of two-layer control . . . 95
4.2.2 Durability enhancement control design . . . 96
4.3 Control Objective . . . 96
4.4 Modeling . . . 97
4.4.1 Assumptions . . . 98
4.4.2 MEA Degradation Modeling . . . 98
4.4.3 State-Space Model for Control . . . 101
4.4.4 Simulation Results . . . 103
4.5 Control Problem Formulation . . . 105
4.6 Control Method: Economic Model Predictive Control . . . 106
4.6.1 MPC principle and EMPC . . . 107
4.6.2 Application to the Fuel Cell Case . . . 109
4.6.3 EMPC Implementation Overview . . . 110
4.6.4 Simulation Results . . . 111
4.7 Experimental Results . . . 113
4.7.1 Test Bench Presentation . . . 113
4.7.2 Test Protocol . . . 113
4.7.3 Future Validation Results . . . 115
4.8 Summary and Conclusion . . . 116

Conclusion and Perspectives **117**

Bibliography **120**

ANNEXES **137**

5 Appendix **138**
5.1 Pt Catalyst Model Simplification . . . 138

Nomenclature

Physical quantities

α	Transfer Coefficient
α_i	Transfer Coefficients for Reactions $i = 1,2,4,5$ [-]
$\Delta\mu$	Chemical Potential [J/mol]
δ_{band}	Platinum Diffusion Length [cm]
δ_{CL}	Catalyst Layer Thickness [cm]
δ_{mb}	Membrane Thickness [cm]
Γ_{max}	Maximum Oxide Coverage on Pt Surface [mol/cm²]
ω	Pt-O Interaction Energy [J/mol]
ψ	Membrane Gas Permeability [mol/(cm·bar·s)]
ρ	Density [g/cm³]
σ	Surface Tension [J/cm²]
θ	PtO Oxide Coverage [-]
A_{fc}	Cell Active Area [cm²]
c	Concentration [mol/cm³]
c^{ref}	Reference Concentration [mol/cm³]
D_{Pt}	Platinum Ion Diffusion Coefficient [cm²/s]
EW	Ionomer Equivalent Weight [g/mol]
F	Faraday Constant [C/mol]
f_N	Particle Density for Each Group of Radius dr [-]
G_i	Activation Energy of Reaction $i = 1,2,4$ [eV]
k_i^{ref}	Reference Reaction Rate for Reaction i [mol/(cm³·s)]
k_5^{ref}	Coagulation Rate Constant [1/s]
k_b	Boltzmann Constant [eV/K]
$k_{a,d}$	Interfacial Water Transfer Coefficient [cm/s]

M Molar Mass [g/mol]

N_{mb} Water Flux in the Ionomer Phase [mol/(cm²·s)]

$P_{\mathrm{H_2}}$ Hydrogen Partial Pressure [bar]

$P_{\mathrm{O_2}}$ Oxygen Partial Pressure [bar]

$q_{\mathrm{Pt,loss}}$ Platinum Loss in Membrane [mol/(cm³·s)]

R Universal Gas Constant [J/(mol·K)]

r Radius of Nanoplatinum Particles [cm]

R_4 Detachment Rate of Platinum [1/s]

R_i Reaction Rate for $i = 1,2,3$ [mol/(cm³·s)]

RH Relative Humidity [-]

S_{Pt} Source Term for Platinum Species [mol/(cm³·s)]

T Temperature [K]

U Cell Voltage [V]

U^{eq} Equilibrium Potential [V]

U_i^0 Standard Equilibrium Potential for Reaction i [V]

$V_{\mathrm{H_2}O}$ Molar Volume of Liquid Water [cm³/mol]

Subscripts and superscripts

an Anode

ca Cathode

cc Carbon

H^+ Proton

H_2 Hydrogen

H_2O_2 Hydrogen Peroxide

$i = 1,2,3,4$ Reactions: Dissolution/redeposition, oxidation, chemical dissolution, carbon corrosion

n Nafion

O_2 Oxygen

Pt Platinum

Pt^{2+} Platinum Ion

PtO Platinum Oxide

sat Saturation

v Vapor

w Water

Abbreviation

H_2O_2 Hydrogen peroxide

ACL Anode Catalyst Layer

AST Accelerated Stress Test

CCM Catalyst Coated Membrane

CL Catalyst Layer

$ECSA$ Electrochemical Surface Area

EOD Electro-Osmotic Drag

FC Proton Exchange Membrane Fuel Cell

$FCEV$ Fuel Cell Electric Vehicle

FRR Fluoride Release Rate

GC Gas Channel

GDL Gas Diffusion Layer

HOR Hydrogen Oxidation Reaction

LPL Lower Potential Limit

MEA Membrane Electrode Assembly

MPC Model Predictive Control

MPL Micro-Porous Layer

OCV Open Circuit Voltage

OH Hydroxyl

ORR Oxygen Reduction Reaction

PEM Proton Exchange Membrane

$PEMFC$ Proton Exchange Membrane Fuel Cell

$PFSA$ Perfluorosulfonic Acid

PRD Particle Radius Distribution

Pt Platinum

SW Square Wave

TW Triangular Wave

UPL Upper Potential Limit

List of Figures

1.1 Comprehensive Overview of Degradation Mitigation Techniques in PEM-FCs . . . 19
1.2 PEM fuel cell operational principle . . . 20
1.3 PEM fuel cell structure . . . 21
1.4 Pt catalyst degradation mechanism . . . 23
1.5 Influence of different operating conditions on degradation . . . 28

2.1 Micro scale modeling structure . . . 43
2.2 Schematic Presentation of Catalyst Degradation . . . 44
2.3 Adjusted thermodynamic potentials . . . 46
2.4 Load cycling voltage profile . . . 52
2.5 Initial particle radius distribution . . . 53
2.6 Comparison of PtO evolution and coverage under varying conditions . . . 55
2.7 Dissolution/redeposition rates for two radius . . . 56
2.8 Concentration of Pt^{2+} ions in the ionomer . . . 56
2.9 Comparison of particle radius and ECSA evolution . . . 58
2.10 ECSA evolution over 30k cycles . . . 59
2.11 Evolution of ECSA for datasets (2) & (3) & (4) . . . 60
2.12 Evolution of ECSA for datasets (4) & (5) & (6) . . . 60
2.13 Evolution of ECSA for datasets (4) & (7) & (8) . . . 61
2.14 Schematic Representation of Membrane Degradation . . . 62
2.15 Fluoride release accumulation . . . 66
2.16 MT evolution under different potentials . . . 67
2.17 MT degradation over 250 hours . . . 67

3.1 Modeling domain and discretization . . . 73
3.2 The relationship between ECSA and transport resistance within CL [170] . . . 75
3.3 Interactions across various levels within the fuel cell system . . . 84
3.4 Overview of PEM fuel cell parameters . . . 85
3.5 Framework for coupling component level degradation to PEMFC performance model . . . 86
3.6 Flowchart for simulating the dual-scale model of PEM fuel cell degradation 87
3.7 Comparative analysis of OCV and hydrogen crossover behavior over time. 88
3.8 ECSA and MT evolution over time . . . 89
3.9 Power and Voltage Load for FC-DLC . . . 90
3.10 ECSA evolution under NEDC . . . 90
3.11 Polarisation curve decay over time under NEDC . . . 91

4.1 Lifetime Management concept for PEM fuel cell systems 94
4.2 Overview of the PEMFC system control 95
4.3 Durability enhancement control in MPC paradigm 96
4.4 Presentation of the input/output system 97
4.5 Comparison of ECSA Evolution: Detailed vs. Simplified Model 103
4.6 Effect of Temperature on Polarization and Power Density 104
4.7 ECSA and MT degradation under T = 80°C and T = 90°C 105
4.8 Principle and Structure of MPC [198] 108
4.9 Temperature trajectory 112
4.10 Power density for case (1) & (2) &(3) 112
4.11 Degradation in different cases 113

List of Tables

2.1 Pt catalyst specification 53
2.2 Summary of experimental conditions used for validation purposes. . . 54
2.3 Model Parameters for MEA Degradation 65

3.1 Diffusion coefficients of various species 75
3.2 Parameters Used in the Model Adapted from [118] 76
3.3 Physical parameters for water transport 78
3.4 Membrane gas permeability 78
3.5 Heat source terms for equation 3.28 81

4.1 Constants Used in the PEMFC Degradation Model 103
4.2 Parameters and Ranges Used in the PEMFC Degradation Model 110

General Introduction

As the automotive industry moves to address environmental concerns and improve fuel efficiency, hydrogen-powered fuel cell electric vehicles (FCEVs) have attracted attention as a promising alternative. FCEVs, based on proton exchange membrane (PEM) fuel cells, offer several advantages, including high energy efficiency, zero emissions at the point of use and the possibility of using hydrogen as a clean fuel. Despite these advantages, the large-scale commercialization of FCEVs is hampered by problems associated with the high cost and limited durability of PEM fuel cells, mainly due to the degradation of critical components such as platinum catalysts and polymer membranes [1–4].

While extensive research has focused on material development, recent findings indicate that intelligent control strategies can significantly enhance the durability of fuel cell stacks using existing materials [5–7]. Therefore, a combined approach integrating advanced materials with sophisticated control strategies offers the most effective solution to these challenges. Optimizing system control is crucial among various methods for improving fuel cell durability [8]. Although many optimal control strategies have been proposed, they often overlook the aging effects on system behavior. Notably, a control design that adapts to the degradation status and trends of fuel cells is still lacking. As improving fuel cell durability through control design is an emerging field, significant efforts are needed to develop a predictive model that encompasses component degradation and fuel cell performance.

This dissertation focuses on developing a component-level framework to predict the performance and durability of PEM fuel cell systems. To achieve this, a novel dual-scale framework will be established, incorporating microscale models that capture the primary degradation mechanisms affecting the microstructures of fuel cell components under varying operating conditions. A comprehensive physical degradation model for the platinum catalyst and membrane have been synthesized, addressing the main degradation mechanisms.

The microscale models will be integrated with a macroscale model to provide detailed insights into the cell's internal states. This integration enables real-time updates on the fuel cell system's performance in response to degradation, establishing a correlation between microscopic degradation processes, macroscopic performance, and operational variables. Consequently, this predictive framework allows for forecasting combined catalyst and membrane degradation under diverse operating conditions. The influence of load, temperature, and relative humidity on the fuel cell's state of health will be thoroughly investigated. Additionally, by updating the aging parameters, the system's dynamic behavior can also be predicted.

To enhance performance while ensuring component durability. This involves for-

mulating the durability enhancement control problem, which includes developing control hypotheses and defining the objective function that integrates the degradation state of the MEA components. This approach will determine optimal parameters, initially represented by the fuel cell temperature, to validate the framework. Recent designs often assume conventional materials with consistent characteristics and rely on static performance models that do not account for time-dependent changes or the fuel cell's health state. Therefore, control systems must be carefully synthesized to effectively address performance, durability, and service life under dynamic conditions.

Finally, the dissertation utilizes a version of the proposed model to develop a model-predictive control (MPC) framework aimed at enhancing the performance and durability of PEM fuel cell systems. The developed model will be tested in scenarios involving thermal management to assess the framework's effectiveness in extending fuel cell lifespan by optimizing operating temperatures. A range of simulation case studies will be conducted to compare the predictions of the developed model with experimental tests and literature data, evaluating its overall utility and accuracy.
The thesis is organized as follows:

— **Chapter 1** provides a comprehensive literature review on the aging and degradation mechanisms of PEM fuel cells, along with modeling approaches and strategies aimed at improving their lifespan and durability.

— **Chapter 2** presents a micro-scale model of the membrane electrode assembly (MEA) that focuses on the catalyst layer and proton exchange membrane, addressing their degradation mechanisms.

— **Chapter 3** introduces a framework for integrating a degradation model into a dynamic PEM fuel cell system for predictions, validated against experimental data, ensuring accurate real-world applications.

— **Chapter 4** presents a health management strategy based on MPC that addresses both membrane and catalyst degradation by actively adjusting the temperature to enhance system efficiency and durability.

— **Chapter 5** presents overarching concluding remarks and explores potential avenues for future research.

1 Introduction

Sommaire

1.1 Motivation . . . 17
1.2 Principles and Structure of PEM Fuel Cells . . . 19
1.3 Literature Review on Degradation Mechanisms in PEM Fuel Cells . . . 22
1.3.1 Pt Catalyst Degradation Mechanism . . . 22
1.3.2 Proton Exchange Membrane Degradation Mechanism . . . 24
1.3.3 Reversible Degradation of PEMFC . . . 26
1.3.3.1 Fuel Cell Flooding . . . 26
1.3.3.2 Membrane Dehydration . . . 26
1.3.3.3 Fuel or Oxidant Starvation . . . 26
1.4 Literature Review on Operating Condition Effects . . . 27
1.5 Literature Review on PEMFC Degradation Modeling . . . 30
1.5.1 Pt Catalyst Degradation Modeling . . . 30
1.5.2 Membrane Degradation Modeling . . . 31
1.5.3 System Level Degradation Model . . . 34
1.6 Literature Review on PEM Fuel Cell Modeling Approaches . . . 35
1.7 Literature Review on Control Strategies for PEMFC . . . 37
1.8 Summary and Conclusion . . . 40

1.1 Motivation

The European Union faces limited petroleum resources, and gasoline prices are projected to rise significantly in the future. In light of the urgent challenges posed by global warming [9], the need to reduce emissions, and constraints on energy resources, car manufacturers are increasingly motivated to explore advanced technologies that enhance vehicle energy efficiency and environmental friendliness [10]. In 2020, road transport was responsible for 23.2% of total greenhouse gas emissions in the European Union [11]. To tackle this issue, widespread adoption of electric vehicles is considered a promising solution [12]. Fuel cell electric vehicles (FCEVs), which rely on fuel cells (FCs) as their primary energy source, are gaining attention due to their high power and energy densities, zero CO2 emissions, and superior efficiency [13].

Hydrogen is widely recognized as a leading alternative fuel to complement fossil fuels, owing to its high energy density and potential for zero local emissions [14]. Proton exchange membrane (PEM) fuel cells, also known as polymer electrolyte membrane fuel cells, utilize hydrogen and are increasingly being considered for vehicular

power applications [15]. A PEM fuel cell is an electrochemical device that transforms hydrogen into electricity, water, and heat via electrochemical reactions. Its advantages, including high energy density, rapid response times, and zero tailpipe emissions, make it a compelling choice for automotive applications [16].

The primary challenges that impede the commercialization of FCEVs are cost and durability concerns. These issues stem largely from the use of platinum (Pt) as a catalyst and the polymer membrane as an ion exchanger. Degradation of these components threatens the overall reliability and efficiency of the system [1, 4]. Specifically, the loss of the active Pt catalyst significantly impacts PEMFC performance, while damage to the PEM can cause severe cell damage. In harsh operating conditions, such as those found in transportation, the degradation of the Pt catalyst and the membrane often has more detrimental effects on fuel cell performance than other components [1–4].

To address the degradation of PEMFCs, as depicted in figure 1.1, researchers are exploring various strategies. These approaches aim to enhance the durability and performance of PEMFCs under challenging operating conditions. One key approach is material design, which focuses on developing more durable materials to withstand harsh operating conditions across all fuel cell components. For instance, recent studies on Pt catalysts have examined different alloy compositions, surface treatments, and protective coatings to enhance their stability [17–19]. Similarly, advancements in membrane technology, such as incorporating expanded Polytetrafluoroethylene (ePTFE) reinforcement layers, have been shown to significantly reduce mechanical degradation [2]. Another approach involves optimal control, which aims to refine the operating conditions of the fuel cell [20]. This strategy includes managing load dynamics, reactant relative humidities, temperatures, and reactant supplies to minimize component degradation.

Optimizing the operating conditions to mitigate the degradation of the PEMFC involves developing strategies and addressing specific challenges in control design. An efficient way to achieve this is through the model predictive control (MPC) paradigm [21]. A reliable predictive model is essential for making control decisions aimed at optimizing a set of inputs. Consequently, there is a growing need to establish robust degradation models that can accurately predict fuel cell durability under various operating conditions. These degradation models are crucial for developing advanced monitoring and control strategies, ultimately leading to enhanced performance and extended lifetimes of fuel cells [22].

Developing advanced control strategies to enhance fuel cell longevity requires a precise degradation model that accurately predicts performance declines under real-world conditions. In this study, we present a novel modeling framework that integrates a multiphysics model with a fuel cell degradation model. This degradation model focuses on the catalyst layer and the membrane, two critical components of PEM fuel cells. For the catalyst, the model considers various factors affecting the electrochemical surface area, while for the membrane, it tracks the remaining membrane thickness over time. The multiphysics model, based on a 1D through-membrane PEMFC framework, provides valuable insights into the internal states of fuel cells. This is crucial

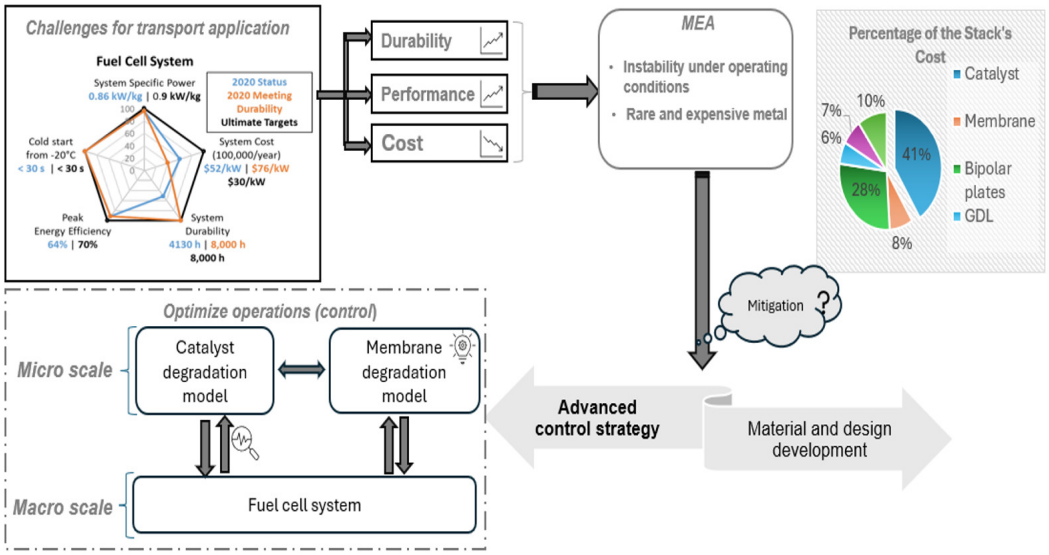

Figure 1.1 – Comprehensive Overview of Degradation Mitigation Techniques in PEMFCs

for evaluating degradation trends and continuously updating fuel cell performance based on feedback from the degradation model. The interaction between these two models enables the prediction of multiple degradation processes, including the losses attributed to each component under different operating conditions.

1.2 Principles and Structure of PEM Fuel Cells

In a PEMFC, hydrogen is introduced into the anode channel, while air or pure oxygen is supplied to the cathode channel. The membrane electrode assembly (MEA), which includes the membrane, catalyst layer (CL), and gas diffusion layer (GDL), is crucial to the fuel cell's performance. The operating conditions impact the durability of the MEA, as they contribute to its degradation over time. The proton exchange membrane allows only protons (H^+ ions) to pass through, while effectively blocking the flow of electrons. At the anode catalyst layer, hydrogen undergoes the hydrogen oxidation reaction (HOR), where it splits into protons and electrons. Since the electrons cannot traverse the electrolyte, they are forced to flow through an external circuit, generating an electric current that can be harnessed to power devices, as shown in figure 1.2.

At the cathode catalyst layer, the protons recombine with oxygen through the oxygen reduction reaction (ORR), producing water and releasing heat. The catalysts used at both the anode and cathode, typically platinum, play a critical role in facilitating these reactions. The HOR and ORR half-reactions are as follows:

$$\text{Anode (HOR):} \quad \mathrm{H_2} \rightarrow 2\mathrm{H^+} + 2e^-$$
$$\text{Cathode (ORR):} \quad \mathrm{O_2} + 4\mathrm{H^+} + 4e^- \rightarrow 2\mathrm{H_2O}$$

The overall reaction is the electrochemical combustion of hydrogen:

$$2\mathrm{H_2} + \mathrm{O_2} \rightarrow 2\mathrm{H_2O}$$

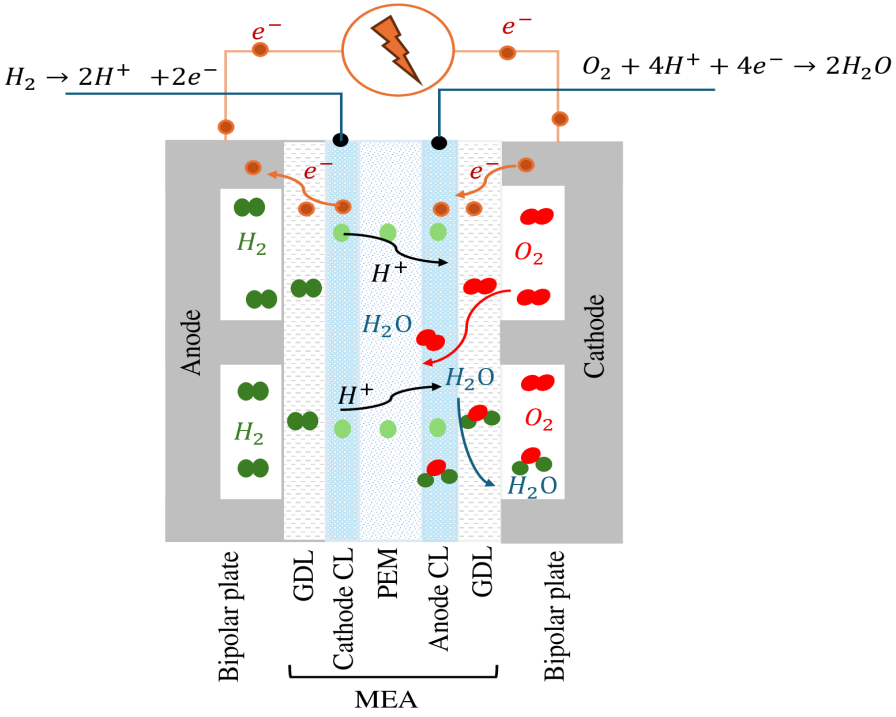

Figure 1.2 – PEM fuel cell operational principle

The catalyst layer typically consists of platinum nanoparticles, as illustrated in figure 1.3, which are dispersed on a high-surface-area carbon support. This setup maximizes the available surface area for catalytic activity, thereby enhancing the overall reaction rate. The dispersion of platinum nanoparticles on carbon not only increases the utilization of platinum, reducing the platinium amount required, but also helps to distribute the reactants more evenly across the electrode [3, 23]. The anode catalyst facilitates hydrogen oxidation, and due to the low potential at the anode, the degradation of the catalyst material is relatively minimal compared to the cathode. This results in a generally more stable performance at the anode side over the lifespan of the fuel cell [24].

A proton exchange membrane made of perfluorosulfonic acid (PFSA) ensures efficient proton transport. A widely used example is Nafion, which features long side

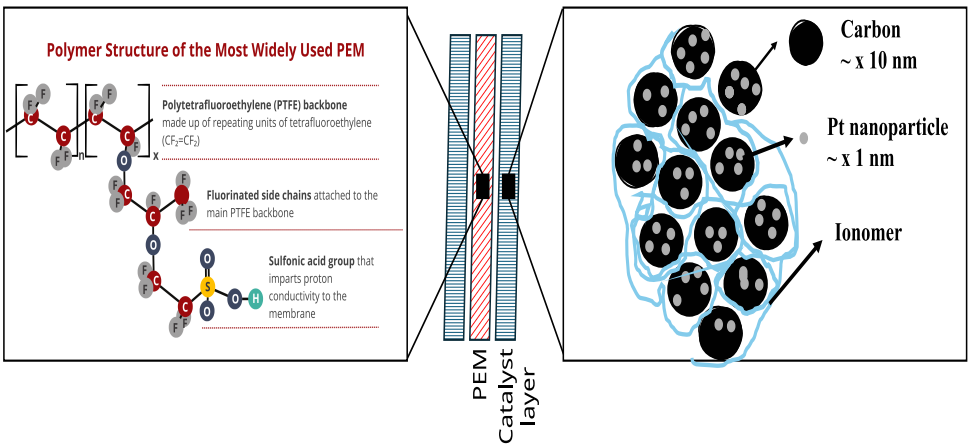

Figure 1.3 – PEM fuel cell structure

chains[25]. The PFSA membrane has a distinct molecular structure composed of a fluoropolymer backbone and sulfonic acid groups [26], as shown in figure 1.3. The backbone, typically polytetrafluoroethylene (PTFE), provides chemical stability and mechanical durability. Attached to this backbone are sulfonic acid groups ($–SO_3H$), which are pivotal for proton conductivity. When hydrated, these groups dissociate into sulfonate ions ($–SO_3^-$), facilitating proton conduction through the membrane. Additionally, the fluorinated side chains, which may include groups such as $–CF_3$ or $–C_6F_{12}$, enhance the membrane's hydrophobic properties, chemical stability, and mechanical strength. Hydration of the membrane is crucial, as it interacts with the sulfonic acid groups to create a proton-conducting phase, thereby maintaining high ionic conductivity essential for fuel cell performance [26, 27].

Understanding the degradation mechanisms of each component and the impact of operational conditions on degradation is crucial for developing a robust model to predict it. The performance and longevity of the PEMFC are significantly influenced by the degradation of its components. For the membrane, degradation can result from chemical attack by radicals or mechanical wear, leading to reduced proton conductivity, gas crossover, or even physical failure. In the electrodes, particularly the cathode, platinum catalyst degradation through mechanisms such as dissolution of Pt or detachment from the carbon support can cause a loss of catalytic activity. Additionally, the carbon support may corrode under high potentials, especially during start-stop cycles or dynamic operating conditions, further degrading the electrode structure.

1.3 Literature Review on Degradation Mechanisms in PEM Fuel Cells

The performance and longevity of a fuel cell are heavily dependent on the state of the membrane electrode assembly. Degradation is characterized by material aging, and changes in the morphology and microstructure of the components. In automotive applications, the harsh conditions accelerate fuel cell aging, resulting in multiple degradation mechanisms that require a comprehensive and detailed understanding.

In general, the degradation of PEM fuel cells can be attributed to various causes, which are categorized into two main classes: reversible and irreversible degradation. Reversible degradation includes issues such as fuel and oxidant starvation, water flooding, and localized overheating [28–30]. This type of degradation involves temporary changes in the internal state, which can typically be mitigated through effective control of subsystems, including water management, reactant supply, and thermal regulation [31, 32].

The second category encompasses irreversible degradation, which refers to the permanent aging and damage of the MEA materials due to the operating environment. This includes factors such as temperature, humidity, and load cycling [33]. Irreversible degradation progresses gradually over the cell's lifespan and leads to damage that cannot be recovered. To mitigate this, optimizing operating conditions over time through advanced control strategies is essential. Effective control can help define appropriate input systems, thereby extending the PEM fuel cell's lifetime. Despite the use of advanced materials and stringent performance requirements, limited understanding of health status evolution can still lead to unexpected failures and significant reductions in the fuel cell's service life.

1.3.1 Pt Catalyst Degradation Mechanism

Pt catalysts are susceptible to a range of degradation mechanisms that can significantly affect both their performance and lifespan. In this context, understanding these diverse degradation phenomena is crucial for accurate modeling and effective management of Pt catalysts degradation within PEM fuel cells.

Experimental studies have been conducted to examine the stability of Pt at the cathode in order to gain insights into the various degradation mechanisms and develop strategies for mitigation [34–37]. Several recent reviews have highlighted the four primary degradation modes of a Pt catalyst as shown in figure 1.4, which include [38, 39]: (1) platinum dissolution are the primary degradation mechanisms, which can initiate secondary degradation processes such as (2) Ostwald ripening , (3) particle migration and agglomeration, and (4) detachment.

Platinum dissolution and redeposition (Ostwald Ripening) represents a phenomenon that occurs with dissolved platinum particles. We observe a preferential dissolution of smaller platinum particles because these smaller particles have a higher chemical potential compared to their larger platinum counterparts. The dissolved platinum

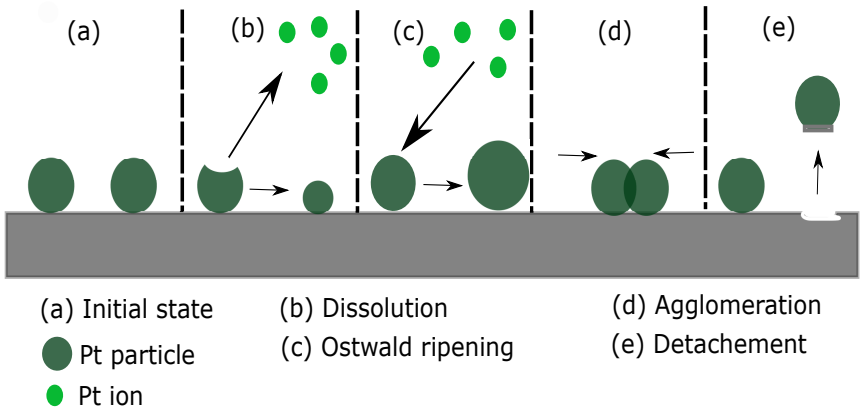

Figure 1.4 – Pt catalyst degradation mechanism

species then move through the electrolyte or ionomer and eventually accumulate on the surfaces of larger platinum particles. As a result, platinum is redeposited, leading to an enrichment of platinum on these larger particle surfaces. This process becomes more pronounced as particle size decreases, which increases the chemical potential and consequently accelerates the dissolution process. Consequently, larger particles grow more prominently at the expense of smaller ones, resulting in a loss of active Pt surface area, thereby diminishing the catalyst's effectiveness [34].

As particle size increases, the ratio of surface area to volume decreases. This results in a larger available surface area for electrochemical reactions when using smaller catalyst particles with the same amount of material. However, it's essential to note that excessively small catalyst particles may be susceptible to reduced long-term stability. Researchers and engineers in materials and structures must strike a balance between particle size and electrochemical surface area (ECSA) to attain the desired durability. In our context, our focus is primarily on limiting the operating conditions to mitigate this degradation process, rather than fine-tuning the particle size.

Platinum dissolution and precipitation within the fuel cell membrane represent a second critical process occurring with platinum ions dissolved in the cathode. A portion of these ions migrates from the cathode to the anode region by diffusion due to concentration gradients [40]. Inside the membrane, they engage in chemical interactions with hydrogen molecules permeating through the membrane from the anode. This leads to the formation of a platinum band within the membrane [39, 41]. Combining experimental data with mathematical models, some studies have revealed that the position of the platinum band within the membrane, under conditions of open circuit voltage (OCV) and cycling, is influenced by factors such as the partial pressure of hydrogen and oxygen, as well as the permeability of these gases and the platinum ions concentration [42, 43]. Nevertheless, the significance of the platinum band's effect on degradation is currently a topic of debate among researchers due to conflicting findings in the available literature [44, 45].

Coalescence is the process where platinum nanoparticles on the carbon support

move and merge together, resulting in the formation of larger particles without any platinum dissolution occurring. This phenomenon has significant implications. The driving force behind coalescence is the desire to minimize the overall surface energy. As the nanosized particles grow, their surface energy decreases. Consequently, this mechanism of particle growth gives rise to a distinct particle size distribution.

Differentiating between coalescence and Ostwald ripening remains unclear, and understanding their specific roles in the loss of electrochemical active area remains challenging [46, 47]. Honji et al. [48] demonstrated that the primary mechanism responsible for particle growth at higher potentials is likely platinum dissolution followed by subsequent redeposition. However, the merging of Pt particles was observed at potentials below 0.8 V. At this threshold, the solubility of platinum is minimal, suggesting that agglomeration plays a significant role as a degradation factor at these relatively lower potentials.

Detachment is a prominent outcome of catalyst layer deterioration caused by the carbon corrosion process, as shown in figure 1.4. It occurs when the carbon support undergoes electrochemical oxidation. This oxidation of carbon not only causes electrical insulation but also leads to the detachment of the platinum catalyst, loss of catalyst layer porosity, and increased performance losses due to mass transport limitations [49]. During quick jumps to higher potentials, like those experienced during the start-stop operation of a vehicle, significant carbon corrosion is known to happen[49]. Moreover, it's possible that even prolonged operation at normal operating cycle potential can harm the carbon support [49].

These various degradation mechanisms are regarded as irreversible losses occurring inside PEM fuel cells during operation. Alongside the material structure of the Pt catalyst and the fabrication process, operating conditions play a crucial role in amplifying these mechanisms, which will be discussed in the next section.

1.3.2 Proton Exchange Membrane Degradation Mechanism

Generally, the membrane can experience aging due to thermal, mechanical, and chemical effects [50], leading to a gradual decline in its properties. Thermal stress accelerates the decomposition of the molecular structure, with degradation often exacerbated by hot spots. Mechanical aging involves the formation of cracks and pinholes in the membrane caused by factors such as frequent shrinkage and swelling during dry-wet cycles. Chemical degradation is primarily driven by attack from free radicals [50, 51]. As the membrane degrades, hydrogen permeability increases, and ionic conductivity decreases. Even tiny pinholes in the PEM can act as conduits for gas transport, allowing direct contact between reactants and potentially leading to complete fuel cell failure [52]. The incorporation of expanded Polytetrafluoroethylene reinforcement layers has proven effective in mitigating mechanical degradation [2]. Despite these advancements, resistance to chemical degradation remains a significant challenge for the long-term operation of PEMFCs [51].

The chemical degradation process in PFSA membranes during fuel cell operation unfolds in three sequential steps. Initially, gas crossover poses a challenge, wherein

oxygen reaching the anode catalyst layer reacts with hydrogen, giving rise to peroxide species (H_2O_2). This process sets off a cascade of chemical reactions that gradually degrade the membrane, contributing to its overall deterioration during operation.

The anode is identified as the primary source of H_2O_2 generation in fuel cells due to its lower potential, which creates favorable conditions for H_2O_2 formation. The key reactants involved are hydrogen at the anode and crossover oxygen [33, 53]. Consequently, gas permeation significantly impacts the chemical stability of the membrane. Researchers have explored the relationship between membrane thickness and gas permeation rates, observing a disproportionate decrease in the thickness of thinner membranes and a marked increase in hydrogen crossover. While reducing membrane thickness can lower ionic resistance, it ultimately shortens the operational lifespan of the PEM fuel cell [50].

Following the formation of peroxides, these species decompose into radicals, specifically hydroxyl (OH) and hydroperoxyl (OOH) radicals. This decomposition process is facilitated by the presence of metal impurities [54]. Radical generation resembles the process that occurs in Fenton's reagent (H_2O_2/Fe^{2+}), where transition metal ions (represented by M^{2+}, such as Fe^{2+}, Co^{2+}, and Cu^{2+}) participate in a series of reactions. Metal ions may be introduced during the manufacture of the MEA and stack, derived from components in the fuel cell system [33, 53], or released from the metal bipolar plates once they are used [33, 53].

Radical attacks on the polymer structure can occur at different locations, with carboxylic acid groups on the polymer backbones recognized as vulnerable sites. This degradation process follows the so-called unzipping mechanism [55]. Additionally, radicals may target the sulfonic acid groups or the ether linkages on the side chain. The result of free radical attack on PFSA membranes includes thinning, surface roughness, cracks, and pinholes. These morphological changes affect proton conductivity, gas crossover, and ultimate membrane stability. The basic molecular structure of a PFSA membrane consists of a main chain and side chains. The main chain determines the mechanical properties, and the side chain determines proton conductivity via a terminal sulfonic acid group [54, 55]. The primary unzipping mechanisms that occur during the chemical degradation of the membrane involve the main chain and side chains being attacked at weak points accompanied by fluorine release. This process illustrates how the main chain is attacked at a terminal carboxyl group, leading to continuous unzipping and shortening of the main chain [55].

In addition, improper fabrication of MEAs can lead to issues such as perforations, cracks, tears, pinholes, and contamination by foreign materials. Localized stresses at the interface between lands and channels can cause small perforations, while inadequate humidification can result in membrane shrinkage and swelling, creating stress and tension. Additionally, degradation of other components and particle accumulation can significantly impair membrane performance and lead to failure. Research has highlighted the challenges of thermal stability and degradation in Nafion membranes, with conventional proton exchange membranes experiencing severe breakdown at elevated temperatures[3].

1.3.3 Reversible Degradation of PEMFC

Reversible degradation refers to temporary changes in the internal state of a fuel cell, where voltage loss can be addressed through appropriate corrective measures, enabling the restoration of performance to pre-degradation levels [56]. This type of degradation is primarily attributed to mass transfer issues stemming from improper reactant supply, water accumulation, or drying, as well as the temporary reduction of the electrochemically active surface area due to the oxidation of platinum particles.

1.3.3.1 Fuel Cell Flooding

Fuel cell flooding occurs when excess water accumulates inside the fuel cell, a phenomenon that significantly impacts fuel cell performance [57]. This excess water impedes the mass transport of reactants to the electrocatalyst sites, particularly on the cathode side. Moreover, water-blocked pores in the gas diffusion layer can lead to gas starvation and a reduction in cell potential [58]. Research by W. He and G. Lin [59] demonstrates that cathode flooding exacerbates the drop in partial gas pressure at higher current densities, adversely affecting fuel cell performance. Prolonged operation in such a compromised state can lead to irreversible damage, including accelerated corrosion of electrodes, catalyst layers, gas diffusion media, and the membrane due to excessive water [33]. Corrosion products may deposit on catalysts, replacing H^+ ions in the membrane and contributing to cell failure [60].

1.3.3.2 Membrane Dehydration

Dehydration of the proton exchange membrane causes both immediate and long-term damage. Reduced water content decreases membrane conductivity, leading to increased ionic resistance and ohmic losses [57, 61]. Sone et al. [61] used alternating current impedance spectroscopy methods to measure the conductivity of Nafion 117 membranes as a function of relative humidity (RH). Le Canut et al. [57] found that exposing a cell to drying conditions for approximately 12 minutes caused the cell voltage to drop from around 0.8 V to 0.75 V. However, this degradation was reversible, with the voltage recovering after 15–20 minutes of rehumidification. Huang et al. [62] further showed that extended exposure to dry conditions can make membranes brittle, leading to the development of cracks or crazes. This brittleness facilitates gas crossover and uncontrolled reactions between H_2 and O_2, creating hot spots and increasing the risk of pinholes and further gas crossover.

1.3.3.3 Fuel or Oxidant Starvation

Fuel or oxidant starvation occurs when fuel cells operate under sub-stoichiometric reaction conditions [33]. Liu et al. [63] studied polarization curves of segmented single fuel cells under conditions of anode and cathode starvation. Their findings indicate that starvation of oxygen at the anode or hydrogen at the cathode can lead to the production of hydrogen or oxygen in the opposite electrode. This reversal in

cell potential increases the corrosion of carbon components, such as backing layers, which in turn accelerates the corrosion of electrocatalysts and results in component damage [64, 65].

In recent years, researchers have focused on mitigating reversible degradation in fuel cells through various control design approaches, including the development of improved water and thermal management systems, as well as optimized reactant supply management. Despite these advancements, the challenge of reversible degradation remains significant, particularly in models oriented towards control and design, as there is a lack of problem formulations that consider the microstructural changes in fuel cell components.

Addressing reversible performance decay is crucial during durability testing, as it can skew degradation assessments and lead to inaccurate aging estimates. For example, Kundu et al. [66] found that reversible degradation in open circuit voltage testing significantly surpassed irreversible degradation. They reported an irreversible OCV decay rate of only 0.089 $mV \cdot h^{-1}$, while reversible decay reached 5.8 $mV \cdot h^{-1}$ within the first 20 hours. Similarly, Jouin et al. [4] noted clear reversible effects in fuel cells operating at 600 $mA \cdot cm^{-2}$ and various current densities up to 1000 $mA \cdot cm^{-2}$.

1.4 Literature Review on Operating Condition Effects

When examining fuel cell components, it is crucial to study the operating conditions to understand their influence and the severity of their impact on various fuel cell components. Key parameters to consider include temperature, humidity, potential, pressure, and flow rate, as well as their combinations [55].

The degradation of automotive fuel cells can be significant, primarily due to the complex and demanding operational environments they endure. Various factors within these conditions accelerate the aging process of fuel cells, leading to component deterioration, morphological changes, parameter degradation, and ultimately a decline in performance, as shown in Fig.1.5. Understanding these degradation mechanisms under standard operating conditions is essential for effective management. Extensive research has been conducted to explore the effects of fuel cells under typical automotive operating conditions, as evidenced by numerous experimental studies [55].

In automotive applications, the most severe degradation occurs during load transitions, such as open-circuit/idling conditions, dynamic loads, and startup-shutdown cycles. For PEM fuel cells, platinum starts dissolving at potentials around +0.6–0.7V, which is exacerbated by higher operating temperatures that thermodynamically favor Pt dissolution [55]. Studies show that platinum particles on carbon supports experience increased dissolution at potentials between 0.65 and 1.0 V in potentiostatic tests [67]. Moreover, at high cathode potentials during open-circuit or idling conditions, the platinum catalyst undergoes significant dissolution [68]. Elevated concentrations of dissolved platinum in these conditions enhance Ostwald ripening and promote Pt

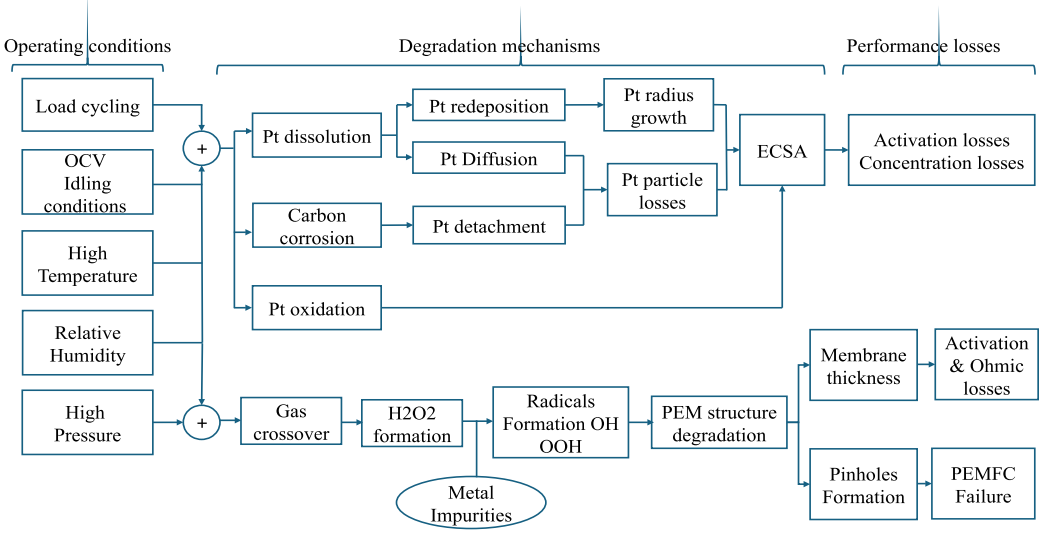

Figure 1.5 – Influence of different operating conditions on degradation

migration.

Additionally, carbon support corrosion is accelerated at high potentials, increasing the likelihood of Pt detachment, which leads to a decrease in Pt loading. Pt detachment after startup-shutdown cycles is widely documented in the literature. Carbon corrosion at relatively high potentials is influenced by several factors. Research indicates that increased gas humidity and higher operating temperatures accelerate both carbon corrosion and Pt catalyst degradation. The Pt catalyst's degradation is affected by various operating conditions, including potential, potential sweep rate, upper potential limit (UPL), lower potential limit (LPL), temperature, and relative humidity [69].

Open-circuit and idling conditions are considered the most critical for chemical degradation of the membrane due to two main factors: strong gas permeation, primarily oxygen, and high cathode potential. Increased fluorine emission and higher average ·OH density at low load currents further confirm the damaging impact of these conditions [70]. Gas permeation peaks under OCV conditions [71]. This occurs because the absence of gas consumption at OCV increases the partial pressure of the reactants in the electrode, while the lack of water production at OCV decreases the water content of the membrane and the partial pressure of water in the cathode [71]. Elevated cathode potential during idling and OCV conditions is recognized as a significant factor in the accelerated chemical degradation of the membrane. Consequently, performance degradation can be attributed to various factors [72]: load changes (56.5%), startup-shutdown cycles (33.0%), idling (4.7%), and high-power operation (5.8%).

The effect of the relative humidity of the supplied gas on the chemical degradation of the membrane has been extensively investigated. Results show that lower RH leads to greater fluorine release [73, 74]. Most studies on PEM fuel cells indicate that fuel cell

performance is significantly influenced by decreasing RH [75, 76]. Reducing RH from 100% to 25% significantly depresses fuel cell performance due to slower electrode kinetics, including reaction and mass diffusion rates, and higher membrane resistance [77].

In contrast, the Pt catalyst layer exhibits slower degradation at lower relative humidity levels due to decreased mobility of dissolved Pt ions under these conditions [78]. Various studies have explored the impact of relative humidity on catalyst deterioration. Wu Bi et al. [78] noted that reducing the humidity in the air from 100% to 50% results in a threefold reduction in Pt mass loss rate and a twofold decrease in the loss of active surface area, with no notable disparities in Pt surface oxide between the two humidity levels. The slower degradation at lower RH levels is attributed to decreased mobility of dissolved Pt ions under these conditions.. The impact of oxygen partial pressure on cathode degradation was found to be negligible.

High temperatures can accelerate the chemical degradation of the membrane material. For instance, in PEM fuel cells, the proton exchange membrane is often made from perfluorosulfonic acid polymers. These polymers can degrade more quickly at higher temperatures due to increased oxidative and hydrolytic stress. Operating a fuel cell at lower temperatures can increase mechanical durability due to enhanced mechanical strength, as lower temperatures shift strength curves toward longer lifetimes [79, 80]. However, lower temperatures increase the membrane modulus, thereby increasing the stress generated under these conditions. Despite this, the increased strength appears to outweigh the rise in stress, as evidenced by humidity cycling results for Gore-Select 57 membranes, which demonstrate longer lifetimes at lower temperatures [79, 80]. High temperatures can disrupt the water balance within the fuel cell, as the membrane must remain hydrated to sustain its ionic conductivity. Elevated temperatures lead to higher water evaporation, exacerbating membrane degradation.

Higher temperatures cause faster breakdown or detachment of Pt particles, leading to a decrease in the electrochemically active surface area of the Pt catalyst [81]. Significant carbon corrosion is attributed to high temperatures and high voltages during potential cycling. Higher temperatures lead to increased Pt atom loss into the membrane and greater changes in particle size [82]. Experiments involving high-temperature operation at 90°C and high-potential operation at 0.9 V indicate that Pt catalyst degradation, caused by dissolution and re-deposition processes, is accelerated by both increased operating potential and temperature [83].

In the same time, Operating PEM fuel cells at relatively low temperatures can reduce the electrochemical kinetics rates, and proton conductance in the ionomer, potentially causing a reversible drop in cell performance [84]. It is essential to identify the primary factors accelerating fuel cell component deterioration and to exercise caution in diagnosing the temperature's influence. This work aims to clarify the effects of different factors on Pt catalyst degradation.

1.5 Literature Review on PEMFC Degradation Modeling

Predicting fuel cell durability presents a range of technical challenges, including issues related to material degradation, catalyst efficiency, and performance. These challenges stem from the intricate chemical and physical interactions occurring at both the atomic level and within the entire stack system. Current research often features fragmented or inconsistent assumptions and guidelines, which complicates the understanding of these phenomena across various disciplines. To address these complexities, framework should aim to unify previous findings and address the multi-faceted nature of degradation processes to enhance our ability to predict and extend the lifespan of fuel cells.

The previous section describes the degradation phenomena occurring within the components of a PEM fuel cell, particularly in the membrane electrode assembly , which includes the Pt catalyst layer and the membrane. Operating conditions play a crucial role in the rate of degradation. To predict the degradation rate of the PEM fuel cell, modeling at the micro-scale level inside the cell allows for quantifying the degradation rate over the cell's lifespan.

1.5.1 Pt Catalyst Degradation Modeling

Research in this field is ongoing, and new models and methods are continuously being developed to improve the understanding and prediction of Pt catalyst degradation in PEM fuel cells [85]. Darling and Meyers [86, 87] put forward the initial degradation model for Pt catalysts. This model describes the dissolution of Pt and its subsequent electrochemical deposition on Pt nanoparticles located at the cathode, without accounting for carbon corrosion, Pt migration, and coalescence. Building upon their work, Wu Bi and Thomas F. Fuller [41] proposed a more comprehensive model, which includes novel features such as the mass loss of cathode Pt into the membrane, leading to the formation of a Pt band. However, both models rely on a simplified bimodal approach, considering only a two-particle size profile to simulate the loss of cathode active surface area due to Pt dissolution and deposition.

Rinaldo et al. [88] introduced a novel nanoparticle population dynamics model for a variety of catalysts. This advanced model not only predicts the changes in the distribution of particle radii over time but also estimates the loss of electrochemically active surface area. It takes into consideration the initial distribution of particle radii and incorporates various kinetic processes such as Pt dissolution, platinium oxide (PtO) formation, and PtO chemical dissolution. Furthermore, the authors extended their research by developing a dynamic model that encompasses the phenomena of surface area loss [89]. They utilized population balance equations in particle space to account for nanoparticle dissolution, redeposition, coagulation, and detachment, providing a comprehensive understanding of the complex dynamics involved [89].

To apply the developed catalyst degradation models in practical situations, Mayur

et al. [90] developed a lifetime prediction model that separates the fuel cell's performance and degradation mechanism using a first-order approximation. This multi-scale model links a fuel cell car model with a cell level catalyst degradation model that can be customized by applying real-time drive data. Nonetheless, there are some limitations to the degradation model. For instance, the model doesn't account for the direct impacts of voltage cycling on platinum degradation. In addition, the model employs a degradation factor that appears empirical which makes the model lack of generalization consideration. Similarly, Kneer et al. [91] developed a semi empirical model to predict how platinum surface area will decrease after being subjected to voltage cycling based on the accelerated stress test (AST) data, then coupled to an analytical polarization curve model to estimate the MEA performance. However, this model remains effective only when the primary causes of degradation are Pt dissolution and Pt particle growth. Furthermore, different-sized particles within an electrode may undergo specific aging or degradation mechanisms. Therefore, establishing the correlation between particle size distribution and ECSA enables precise predictions and the seamless incorporation of various degradation mechanisms within the Pt catalyst.

The majority of current degradation model, exhibits a limitation in its scope by concentrating on just one degradation process. Even the dynamic population model, although it attempts to describe various degradation mechanisms, fails to provide a clear understanding the effects of different internal physical states (temperatures, relative humidities, etc.). Moreover, these initial models have not been seamlessly integrated into dynamic or multiphysics fuel cell models which limits the interpretation of the model output at stack and system level and the model prediciton accuracy since the dynamic internal states can hardly be estimated.

On the other side, empirical degradation models offer the advantage of often being examined in conjunction with multiphysics models. However, they fall short in terms of explaining the impact of a specific degradation on the catalyst functionnality. The use of aggregated degradation models, where a simplified empirical model replaces the entire sequence of degradation mechanisms, severely limits their effectiveness in widely varied operating conditions.

1.5.2 Membrane Degradation Modeling

First, M. Chandesris et al.[92] introduce a one-dimensional performance model for a polymer electrolyte membrane water electrolyzer, incorporating chemical membrane degradation. This model accounts for electronic and ionic transport through the cell components, as well as the electrochemical behavior of both the anodic and cathodic catalyst layers. Subsequently, in [51], the same authors investigate the degradation of proton exchange membranes reinforced with expanded polytetrafluoroethylene under various operating conditions. Researchers utilized electrochemical analysis, post-mortem analysis, and fluoride release measurements to track membrane degradation. Key findings from this research highlight several critical aspects of membrane degradation in PEMFCs. Notably, the fluoride release rate (FRR) exhibits a strong

dependence on cell potential, indicating that variations in operational voltage can significantly influence degradation processes. Additionally, a linear correlation has been established between the FRR and the average OCV drop, particularly under conditions of increased cathode oxygen partial pressure.

The study reveals that humidity has a limited impact on the FRR, indicating that factors such as temperature and voltage may play a more substantial role in membrane degradation. To further quantify these complex relationships, the authors have developed semi-empirical models that effectively capture the effects of various operating conditions on membrane degradation. These models provide valuable insights for predicting the impact of operating conditions on membrane performance and longevity.

A detailed and comprehensive analysis of chemical membrane degradation in a PEMFC and its impact on cell performance is provided in [71]. The paper discusses assumptions about the chemical degradation of the PFSA-based membrane and emphasizes the alignment between simulated degradation rates and those reported in the literature. The model encompasses various aspects of membrane chemical degradation, including radical formation and chemical reactions leading to degradation. The study concludes by outlining future research directions for understanding and predicting the chemical degradation of polymer electrolyte membrane fuel cells.

The work presented in [93] introduces a comprehensive model of PEMFC degradation, focusing on the chemical degradation of perfluorinated sulfonic acid membranes. The model, grounded in conservation principles, details transport phenomena and includes a degradation submodel that describes the formation of hydrogen peroxide. This is followed by the production of radicals through Fenton reactions involving metal-ion impurities, which decompose reactive end groups into carboxylic acid, hydrogen fluoride, and carbon dioxide through unzipping of the polymer backbone and cleavage of side chains. Simulation results validate the numerical model, capturing degradation trends under various conditions and highlighting key factors such as temperature, water activity, and impurities that accelerate degradation. The findings emphasize that degradation of the membrane preferentially occurs on the anode side due to increased production of hydrogen peroxide and free radicals. Furthermore, the study highlights the limitations of using hydrofluoric acid emission rates as a diagnostic tool for assessing degradation. The model provides valuable insights into the complex chemical processes driving membrane degradation in PEM fuel cells.

Futter et al. [2] investigate the impact of chemical membrane degradation on PEMFCs by integrating a physics-based degradation model into a numerical framework and expanding a 2D PEMFC model. It considers key mechanisms such as hydrogen peroxide formation, iron contaminant redox cycles, radical formation, and polymer degradation. The model is validated against experimental data from accelerated stress tests, highlighting the influence of operating conditions such as pressure, relative humidity, and cell voltage, on degradation kinetics and spatial distribution. The study identifies hydrogen peroxide production as a primary driver of chemical degradation, influenced by operating conditions. It also explores the role of iron ions, their chemical reactions, transport, and the kinetics of radical formation within the membrane.

However, due to the model's complexity and 2D nature, simplifications are needed for it to be applicable to control objectives.

In [94], the model includes a semi-empirical approach for the physico-chemical properties of the PEM and a computational fluid dynamics model for the cell's 3D performance. It accounts for degradation rates of membrane thickness and conductivity, acid group concentration, and gas diffusion coefficients as functions of membrane thickness. When coupled with the computational fluid dynamics model, the degradation model shows that cell current density decreases faster with lower humidity and higher temperature. It also reveals non-uniform in plane membrane degradation dependent on local operating conditions. The paper extensively discusses the development and application of the degradation model, including its validation through experimental data comparisons, demonstrating its potential for simulating and analyzing PEMFC performance over time [40].

Xie et al.[95] review two possible initiation points for PFSA degradation: weak polymer end groups versus side chain cleavage. They developed a kinetic model that calculates the relative contributions of these two degradation initiation pathways under different conditions. The authors analyzed degraded PFSA samples using infrared spectroscopy to measure the concentration of carboxylic acid end groups on the polymer chains. This data, coupled with fluoride loss measurements, was used to validate the kinetic model and calculate the corresponding kinetic constants that distinguish the two degradation mechanisms.

A modeling approach to simulate pinhole defects in polymer membranes during chemical degradation in fuel cells presented in [96]. It outlines key objectives and methods, including the development of a dynamic chemical degradation model that incorporates the formation of pinholes. The model also considers the reduction in membrane thickness and is validated against experimental results. Additionally, it examines the effects of temperature, pressure, and relative humidity on chemical degradation. The proposed method enhances the accuracy of the chemical degradation model and has significant implications for fuel cell durability.

An empirical model was developed to predict the lifespan of membranes in heavy-duty fuel cell systems, such as those used in transit buses [53]. Researchers conducted accelerated membrane durability tests to gather lifetime data, taking into account factors such as cell voltage, temperature, oxygen concentration, humidity cycling, and platinum presence [53]. The model utilizes inverse power law and exponential relationships within a log-linear Weibull distribution to extrapolate membrane lifespan from test conditions to real-world scenarios.

In [97], an experimental and modeling investigation explores membrane degradation behaviors in PEMFCs. The study reveals that degradation is significantly influenced by the oxygen partial pressure of the supplying gas. Under H_2-O_2 supply, degradation is more pronounced on the anode side, whereas under H_2-air supply, it is more pronounced on the cathode side. The research quantitatively characterizes oxygen crossover and develops a model for membrane thinning based on a first-order reaction with partial pressure effects. Additionally, the study highlights the correlation between oxygen partial pressure and membrane thinning behaviors, discussing the

impact of gas crossover and the role of oxygen dissolution and diffusion in membrane degradation. It proposes a simplified reaction rate equation to model membrane thinning behaviors and demonstrates that the calculated values are consistent with experimental results.

The prediction models referenced in the literature primarily concentrate on degradation at the component level within PEMFCs. These models typically analyze how individual components, such as catalysts and membranes, deteriorate over time due to various operational and environmental factors. However, this component level focus, while valuable, is somewhat limited in its scope. To gain a comprehensive understanding of PEMFC performance and longevity, it is essential to integrate component level degradation insights with a broader perspective on overall fuel cell degradation. This integration involves not only assessing the degradation of individual components but also understanding how these components interact and contribute to the overall decline in the fuel cell's performance.

1.5.3 System Level Degradation Model

In many current PEM fuel cells degradation prediction models, stack voltage and power derived from monitoring data are key indicators used to assess the aging status of PEMFCs [98–100]. These metrics are valuable because they provide direct measurements of fuel cell performance and can be monitored in real time. However, their reliability is significantly compromised under non stable or varying operating conditions. For instance, the operational environment of a PEMFC in a vehicle, which involves fluctuating loads, temperatures, and driving conditions, can lead to substantial deviations from stable operational states. Under such dynamic conditions, the accuracy and usefulness of stack voltage and power as indicators of degradation decline. This limitation arises because these indicators are often calibrated for stable, controlled environments and may not account for the complex, real-world factors affecting fuel cell performance.

Pei et al. [101] introduced a rapid lifetime evaluation method inspired by cumulative fatigue damage theory, where the overall decay rate is considered a linear combination of decay rates under various conditions. The proposed lifetime formula is:

$$T_f = \frac{\Delta P}{k_p \left(P_1' n_1 + P_2' n_2 + P_3' t_3 + P_4' t_4 \right)} \tag{1.1}$$

In this context, T_f signifies the operational lifetime of the fuel cell, while P denotes the rate of performance degradation as the fuel cell approaches the end of its lifespan. The parameter k_p serves as an acceleration coefficient, which is affected by various factors, including differences in gas quality. The decay rates represented by P_1', P_2', P_3', and P_4' correspond to specific conditions: load changes, startup-shutdown cycles, idling, and high-power operation, respectively. Additionally, n_1 and n_2 represent the number of cycles associated with these conditions, while t_3 and t_4 indicate the durations of operation under each specific scenario. Therefore, while this indicator provides valuable insights, it is insufficient for a comprehensive understanding of the

fuel cell's health under varying conditions.

Moreover, relying solely on these health state indicators for control strategies is inadequate for optimizing performance and extending the fuel cell's lifespan. Effective optimization requires a more nuanced understanding of how different operating parameters interact with degradation rates. This involves considering factors such as temperature fluctuations, load variations, and transient operating conditions that impact the overall health of the fuel cell. A more integrated approach, which combines these performance indicators with a detailed analysis of operating conditions and their effects on degradation, is essential for developing robust control strategies and achieving optimization goals.

1.6 Literature Review on PEM Fuel Cell Modeling Approaches

The previous section examined critical aspects of degradation mechanisms and modeling in fuel cell components. However, the primary objective of this model development is to effectively control and mitigate degradation by incorporating the aging effects of the components into the fuel cell system model. This integration aims to optimize the operating conditions in PEM fuel cells to enhance their longevity.

When examining transport phenomena, many models focus on the specific layers within the fuel cell. Notably, extensive research has been dedicated to water transport in the proton exchange membrane (PEM), exploring mechanisms such as electro-osmotic drag, diffusion, thermo-osmosis, and hydraulic permeation [102]. Interest in the modeling of transport phenomena in fuel cells has significantly increased since the pioneering studies by Springer et al. [103] and Bernardi et al. [104] in the early 1990s. Their foundational models for membrane water transport remain highly relevant today and have provided a robust framework for ongoing research in this field.

Over the past two decades, a variety of models have been developed to investigate different transport phenomena in PEMFCs. These models can be classified based on their application domains, spatial dimensions, and temporal characteristics. Moreover, specific models have been created to examine transport processes within the gas flow channels [105]. These initiatives significantly enhance our comprehension of the intricate transport dynamics within PEMFC, thereby facilitating the optimization of their performance and durability. In addition to component-specific models that examine the transport and material properties of individual components, there has been an increasing interest in holistic multiphysics models in recent years [106, 107].

Furthermore, for effective control implementation, it is essential to incorporate system-level models that unify various submodels representing different actuators, such as compressors, humidifiers, and cooling systems, while avoiding detailed examinations of transport phenomena within a single cell. These system-level models aim to encapsulate the entire fuel cell stack, which is crucial for developing effective control strategies [108, 109]. It is also important to recognize that transport phenomena within the stack can have varied impacts on individual cells, ultimately affecting

overall performance and control methodologies.

Cell models for PEM fuel cells encompass a wide spectrum of spatial dimensions, including 0D, 1D, pseudo-2D, 2D, pseudo-3D, and 3D. In 0D models, spatial distributions of variables are disregarded, resulting in a simplified representation of the system [109]. Typically, 1D models focus on transport phenomena through the membrane [110, 111], although some are specifically designed to analyze transport within the flow channels.

Pseudo-2D models expand this approach by investigating transport in two dimensions without fully solving a coupled problem across both spatial directions [112]. Instead, they decouple transport in the through-membrane and along-channel directions, with interactions primarily occurring through boundary conditions. This methodology strikes a balance between complexity and computational efficiency, making it a popular choice for modeling transport phenomena in PEM fuel cells [112].

A variety of 2D models have been developed for PEM fuel cells, differing mainly in the spatial dimensions they address. Some 2D models simulate transport through the membrane and along the flow channels, while others focus exclusively on through-the-membrane transport, incorporating channel-to-channel variations and land effects in the third (in-plane) direction [113]. In certain cases, these models can be simplified to 1D through conformal mapping of the domain [114]. An alternative approach, known as bi-domain modeling, was introduced by Zaglio et al.[111], wherein the transport problem is divided into two separate 1D problems: one under the channel and another under the land [112].

Pseudo-3D models have also been developed to strike a balance between model accuracy and computational efficiency. These models treat membrane transport as a 2D problem coupled with a 1D channel model via boundary conditions [115]. In contrast, full 3D models capture transport phenomena in all spatial directions, providing the highest fidelity but at a significantly increased computational cost [116].

Initially, most PEM fuel cell models focused on steady-state conditions [103]. However, with growing interest in understanding the dynamic behavior of fuel cells, more dynamic models have been developed in recent years [108, 117]. Despite this shift, steady-state models remain relevant as they offer valuable insights into performance limitations by detailing thermal and mass transport within the complex structure of PEM fuel cells [118].

Real-time modeling of PEM fuel cells is increasingly important for obtaining state information, especially to reduce reliance on sensors and address the challenges of measuring mass and temperature distributions within cell components. Advances in imaging and measurement technologies, and novel methods for gas transport resistance, have enhanced our understanding of transport mechanisms, including complex two-phase flow in porous layers [119–121]. However, these techniques are not feasible for on-board vehicle use, making real-time modeling the primary tool for monitoring temperature and water states within the cell.

One widely used real-time model in the controls community is the lumped-parameter 0D system-level model developed by Pukrushpan et al. [108]. This model simplifies PEM fuel cell behavior by excluding spatial variations and relying heavily on empirical

relationships derived from curve fitting, without incorporating key physical phenomena such as two-phase flow within the cell. As a result, its ability to estimate internal states in real-time is limited and lacks robustness.

Additionally, data-driven and black-box models like neural networks have been applied for real-time simulations [122]. While these models are computationally efficient, their reliance on extensive experimental data for accuracy and their focus on input output mappings without insight into internal states limit their broader adoption.

A multiphysical model of a PEMFC system that illustrates the evolution of system states and the interplay between inputs and outputs is essential for effective control design. Over the past few decades, numerous studies have been conducted on fuel cell system modeling, examining various perspectives and addressing diverse objectives [108, 109, 123]. However, the available FC dynamic models, either analytical ones or black-box ones, are usually built with fixed structure, and structures parameters without consider the aging effect. The model validation is restricted to a short-term interval. Due to FC degradation, the FC dynamics can change between operating instances over the FC life cycle. Moreover, the FC system models are usually built in predefined and limited operating conditions. The models may lose their effectiveness when the practical operating condition varies to an unseen one, which is often the case in practice.

1.7 Literature Review on Control Strategies for PEMFC

Effective control of fuel cell power systems is essential for ensuring reliable and optimal power delivery. Consequently, most current approaches emphasize system-level performance to efficiently regulate power output [108, 124]. However, some studies have also concentrated on cell-level performance to mitigate specific issues, such as flooding, membrane dehydration, and local reactant starvation [125]. To prevent reactant starvation, it is crucial to achieve effective distribution of reactants throughout the cell. This requires the implementation of a robust monitoring system equipped with precise sensors and indicators.

The efficient operation of PEM fuel cells is fundamentally dependent on effective water management, which has become a key area of research. Proper water management entails striking a balance between maintaining adequate membrane hydration and preventing excessive water accumulation in critical components such as the catalyst layers, gas diffusion layers, and gas flow channels. When water is over-accumulated, it can significantly impair both the performance and durability of the fuel cell. To achieve optimal membrane hydration, reactants are typically humidified prior to entering the cell. However, challenges can arise during high-load cycles or in cold, humid environments, where oversaturation of water vapor may result in condensation on both the anode and cathode, subsequently reducing performance [126].

Thermal management is essential for the optimal performance of PEM fuel cells, particularly when operating under extreme temperature conditions, either below 0°C or above 80°C. Research has shown that insufficient thermal management, which allows the cell to reach elevated temperatures, can significantly accelerate the degradation of both the membrane and the catalyst. High temperatures facilitate the formation of radicals and decrease the electrochemical surface area, ultimately compromising the durability of the cell. To effectively address these thermal challenges, various cooling techniques are implemented [127].

Challenges impacting the performance, reliability, and longevity of PEM fuel cells include control strategies for reactant gas supply, thermal management, and water management. Researchers in this field have made significant strides in developing robust control systems to prevent faulty operations. However, the degradation that occurs over the cell's lifespan due to aging has received limited attention.

Researchers have developed robust control systems to prevent faulty operations through effective management of water, thermal conditions, and reactant supply. These efforts often prioritize the mitigation of irreversible degradation and the prevention of faulty operating conditions, with limited focus on the effects of aging degradation. This gap needs to be well-defined and formulated to design a comprehensive architecture that ensures the optimal functionality of fuel cells and extends their durability. On the other hand, research on fuel cell degradation has highlighted the crucial role of local environmental conditions in component deterioration. Consequently, the existing control strategies, which focus on system-level dynamics, often miss the opportunity to leverage a deeper understanding of degradation processes at the stack level, leaving significant potential for improvement.

While operational control strategies have received significant attention, addressing the long-term effects of degradation remains a key challenge. In the literature on degradation control, techniques such as life-extending control or damage-mitigating control could be proposed to enhance the lifespan of PEM fuel cells [6, 128]. These control methods consider degradation as part of their strategy but require a deep understanding of system behavior to ensure reliable operation over time. Control systems aimed at mitigating degradation typically rely on a factor-based model incorporated into the controller or use predictive models to support decision-making within the optimization layer of the automation hierarchy. Common approaches, such as linear-quadratic or model-predictive control, enable the integration of degradation models, either as constraints or directly within the objective function [7].

These approaches allow the incorporation of degradation models into control strategies, enabling a balance between performance and longevity. They often rely on factor-based degradation models to develop algorithms that keep degradation within acceptable limits. Control scheduling, particularly at a high operational level, is another key application area. By understanding the relationship between influencing factors and degradation, it becomes possible to mitigate detrimental changes by adjusting operating conditions [7]. Fuller's patent [129] introduced a comprehensive framework for life-extending control through model predictive control, where degradation constraints were integrated using factor-based models. This innovative

approach has been applied in various industries, such as in the work of [130], who developed a control system for a power plant, modeling structural degradation as a key state variable. Their MPC strategy effectively incorporated degradation within both the objective function and system constraints to enhance reliability and lifespan. Similarly, in [131] applied MPC in a gas turbine, embedding degradation parameters into the constraints to successfully limit wear and extend operational durability.

The application of this approach to PEM fuel cells has the potential to introduce a novel method for extending their operational lifetime. However, a significant challenge remains in understanding the degradation processes and developing an accurate model to represent them. This work will introduce a framework for predicting the degradation of PEM fuel cells, and we will explore the application of temperature optimal control, which is crucial for enhancing both performance and longevity.

1.8 Summary and Conclusion

The degradation due to PEMFC aging presents significant challenges to their performance and dynamic behaviour over time. These degradation processes can cause substantial reductions in efficiency and operational reliability, underscoring the need for control strategies that address these issues in a comprehensive manner. It is important to prevent irreversible degradation caused by operating conditions through material improvements and optimal control strategies that consider the aging effect.

To improve PMEFCs health state, new control approaches should focus on anticipating and mitigating the effects of aging degradation, rather than merely responding to them after they occur. Consequently, there is a growing need to establish robust degradation models capable of accurately predicting fuel cell durability under various operating conditions and serving as health state indicators. These degradation models play a pivotal role in relating aging losses to the operating conditions. This helps avoid harsh conditions in the fuel cell control system, ultimately resulting in enhanced performance and extended lifetimes of fuel cells.

Relying solely on stack voltage and power as state-of-health indicators is limited to stable operating conditions and fails to accurately predict aging effects. These indicators become less reliable for assessing PEMFC aging under dynamic conditions, such as those encountered in vehicle operations. Therefore, it is essential to consider degradation at the component level. In PEMFCs, catalyst degradation is the primary contributor to performance loss, while the membrane also plays a vital role in overall performance. The degradation of both components is highly sensitive to operating factors. This highlights the importance of a novel predictive multiscale modeling approach, which is crucial for enhancing the durability of PEMFCs.

Such an approach not only enables a deeper understanding of the aging mechanisms at different scales but also supports the development of effective health management strategies. By integrating microscale and macroscale degradation models, this approach can more accurately predict the fuel cell's performance over time, providing valuable insights for optimizing operation and maintenance strategies. Ultimately, it facilitates the design of more robust and long-lasting PEMFC systems, ensuring their reliability in diverse applications. By addressing aging degradation through a proactive management strategy, we can pave the way for more sustainable and efficient hydrogen fuel cell technologies, making a significant contribution to the advancement of clean energy solutions.

2 Micro-Scale Model : PEM Fuel Cell Degradation Model

Sommaire

2.1 Inroduction . . . 41
2.2 Development of a Pt Catalyst Degradation Model . . . 42
2.2.1 Pt degradation processes and kinetics . . . 44
2.2.2 Physical Pt catalyst degradation model . . . 48
2.2.2.1 PRD evolution equation . . . 48
2.2.2.2 Mass balance . . . 49
2.2.2.3 Microstructure Evolution . . . 50
2.3 Results and Discussion . . . 51
2.3.0.1 Microscale Examination of Degradation . . . 53
2.3.0.2 Catalyst Microstructure Evolution Analysis . . . 58
2.4 PEM Model Development . . . 61
2.4.1 Hydrogen peroxide formation . . . 62
2.4.2 Fluoride release rate . . . 63
2.4.3 Membrane thinning . . . 64
2.4.4 Results and Discussion . . . 66
2.5 Summary and Conclusion . . . 69

2.1 Inroduction

Typically, lifetime prediction relies on data-driven methods to forecast voltage or power decay [132, 133]. However, these approaches lack detailed information about the component level state of health, limiting their ability to accurately predict system longevity [31]. Moreover, the stack voltage and power indexes can only be utilized under constant operating conditions. For complex operating conditions such as vehicle operating conditions, the aging characteristics of PEMFCs characterized by them are no longer significant and accurate. As a result, component specific lifetime prediction and the optimization of operating strategies to control degradation and meet lifetime requirements are significantly constrained. To address this gap, this study provides valuable insights into the degradation mechanisms of key components, enabling more precise lifetime predictions and informed decision-making for durability improvements.

Aging indicators for individual components can be used to assess PEMFC degradation effectively. These component specific degradation indices provide an accurate representation of the aging states of different PEMFC parts and are suitable for real-time application. Integrating operational parameters monitored during PEMFC operation into component degradation models enhances this accuracy. Additionally, because no single component can fully represent the overall aging of PEMFC stacks, it is essential to develop a component level framework that combines the degradation of the most critical elements, enabling a more precise depiction of the system's aging state [134, 135].

This chapter presents a detailed micro-scale model of the membrane electrode assembly, focusing on its two most critical components: the catalyst layer and the proton exchange membrane, which are among the primary contributors to the performance degradation of PEMFCs. A comprehensive degradation model has been developed using physics-based mathematical equations to capture the microstructural evolution of the MEA under various operational conditions. The primary goal is to create a computationally efficient and robust model that strikes a balance between detail and speed. The robustness of the model lies in its ability to accurately simulate the degradation of MEA materials across a wide range of operating conditions, including variations in voltage signal amplitude, dwell time at higher potentials, temperature, humidity, and reactant supply. This model serves as a valuable tool for optimizing fuel cell performance and longevity by providing predictive capabilities under diverse conditions.

While these models provide valuable insights into component-level degradation, they are intended to be integrated into a macro-scale performance model as shown in figure 2.1, allowing for a comprehensive assessment of overall PEMFC performance. This integrated approach not only enhances predictive capabilities but also aids in optimizing operational strategies to prolong fuel cell lifespan.

To calibrate the model and evaluate its predictive ability, the validation process will first utilize Accelerated Stress Test data from the literature. Following this, the microstructural evolution of the model will be analyzed to assess its applicability in real-world scenarios.

2.2 Development of a Pt Catalyst Degradation Model

The developed platinum catalyst model is designed to simulate the dynamic behavior of platinum particles within the catalyst layer of a PEMFC. By tracking the temporal evolution of key micro-scale parameters, the model offers valuable insights into how degradation mechanisms influence the long-term performance of the fuel cell. Additionally, it quantifies the impact of electrode degradation on PEMFC aging across a range of operating conditions, providing a comprehensive understanding of the factors affecting durability.

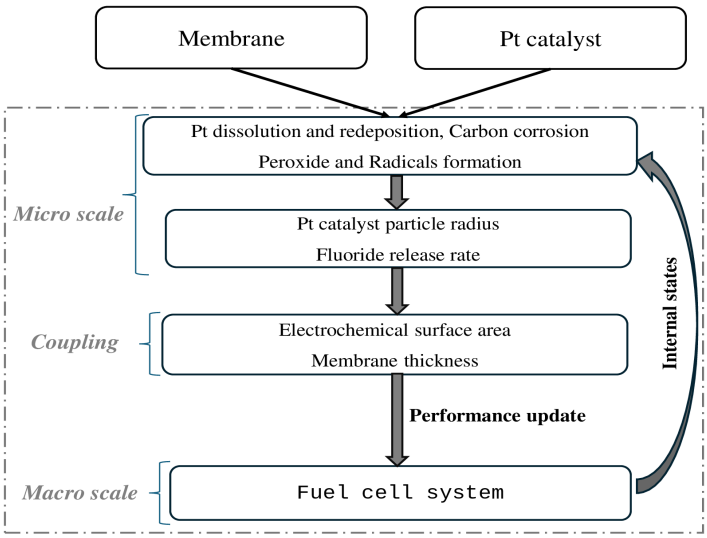

Figure 2.1 – Micro scale modeling structure

The platinum catalyst model monitors several key parameters essential for understanding its degradation behavior. These parameters include particle radius density, particle size evolution, and the concentration of platinum ions in the electrolyte, all of which significantly influence the electrochemical activity and long-term performance of the fuel cell. Additionally, the model tracks oxide coverage, changes in the platinum band structure, and the mass of active platinum, providing critical insights into the reduction of catalytic efficiency. The ECSA also serves as a vital indicator of the catalyst's health, directly linking degradation mechanisms to overall fuel cell performance. This comprehensive approach not only enhances the accuracy of lifetime predictions but also informs operating strategies aimed at improving durability.

This detailed modeling approach enables a more accurate prediction of catalyst degradation by simulating the micro-scale mechanisms. Furthermore, this model can be used to assess the impact of different operating conditions (e.g., temperature, humidity, load cycling) on the degradation rates of the catalyst, helping to optimize operating strategies and mitigate performance losses. It also serves as a foundation for developing control strategies aimed at minimizing degradation and extending the fuel cell's lifespan.

The proposed degradation model for the platinum catalyst considers various degradation mechanisms influencing the platinum particle size distribution, such as platinum oxidation, dissolution, re-deposition, detachment, and agglomeration, and its results are compared and analysed based on experimental data. Initially, a kinetic model describes the electrochemical reactions occurring at the nanoparticle level within the catalyst layer [38]. Platinum dissolution and re-deposition are identified as the most prominent degradation phenomena under different operating conditions, particularly within the voltage range of 0.6-0.9 V [39, 41]. Additionally, carbon support

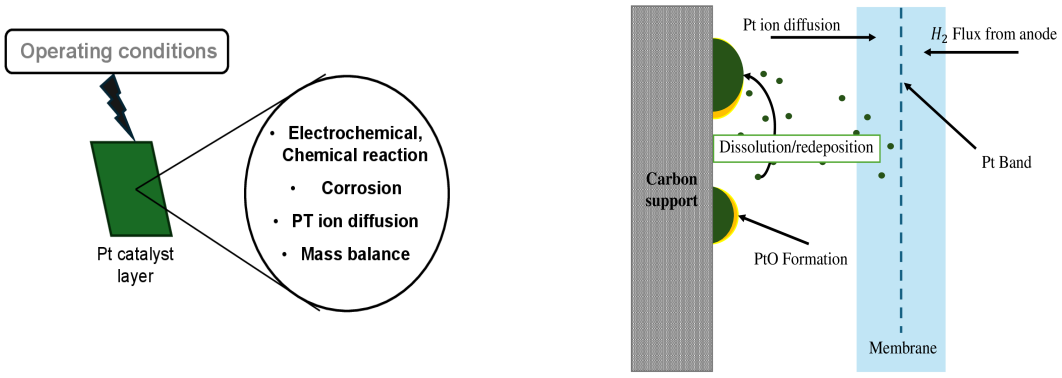

(a) (b)

Figure 2.2 – Schematic Presentation of Catalyst Degradation

corrosion is notable during idling and start-stop conditions, especially near 1 V [49, 136]. This kinetic model is then integrated into a physical model of platinum catalyst degradation, which will be presented and discussed in detail. The initial kinetic rate parameters were refined based on several accelerated stress test experimental data sets, allowing for a more accurate representation of the degradation processes.

2.2.1 Pt degradation processes and kinetics

Although platinum is generally considered a noble metal with higher resistance to oxidation in the presence of air compared to other materials [137], thermodynamic analysis based on the Pourbaix diagram suggests that platinum can still undergo oxidation and even dissolve under relevant conditions of potential and pH in fuel cells [138]. This behavior, known as Pt dissolution, arises from the electrochemical instability exhibited by platinum particles when subjected to an applied potential. Two primary mechanisms contribute to the loss of Pt particles. The first mechanism involves the electrochemical dissolution of Pt, resulting in the formation of platinum ion (Pt^{2+}) as described in reaction 2.1. The second mechanism entails the chemical dissolution of the PtO film, which forms due to the oxidation of platinum, as indicated in reactions 2.2 and 2.3 [41, 139]. The platinum degradation related reactions assumed in this model are presented as follows:

1. Electrochemical dissolution and redeposition of platinum:

$$Pt \leftrightarrow Pt^{2+} + 2e^-, \quad U_1^0 = 1.188\,V \text{ vs. SHE} \tag{2.1}$$

2. Electrochemical reaction for platinum oxide formation

$$Pt + H_2O \leftrightarrow Pt\text{-}O + 2H^+ + 2e^-, \quad U_2^0 = 0.98\,V \text{ vs. SHE} \tag{2.2}$$

3. Chemical dissolution of platinum oxide:

$$\text{Pt-O} + 2\text{H}^+ \leftrightarrow \text{Pt}^{2+} + \text{H}_2\text{O} \tag{2.3}$$

The rates of the electrochemical reactions, namely the dissolution and oxidation rates of Pt, are described by the modified Butler-Volmer equations. These equations, initially developed by Darling and Meyers [86], consider the electrochemical potentials of the Pt particles in relation to their radius. The Pt dissolution rate, relating to (reaction.2.1), where the first term describes the dissolution of Pt and the second term defines the re-deposition of dissolved Pt^{2+} ions, is given by:

$$\begin{aligned} R_1(r,t) = k_1(T,RH)\,(1-\theta(r,t)) \Bigg[\exp\left(\frac{\alpha_1 F}{RT}(U(t) - U_1^{eq}(r))\right) \\ - \frac{c_{Pt^{2+}}(t)}{c_{Pt^{2+}}^{ref}} \exp\left(\frac{-(1-\alpha_1)F}{RT}(U(t) - U_1^{eq}(r))\right) \Bigg] \end{aligned} \tag{2.4}$$

The rate of platinum oxidation (reaction.2.2) employed in this study is adapted from the models originally developed by Harrington et al. [140–142], with further modifications and adjustments made by Darling et al.[86].

$$\begin{aligned} R_2(r,t) = k_2(T,\text{RH}) \Bigg[\exp\left(-\frac{\omega\theta(r,t)}{RT}\right) \exp\left(\frac{\alpha_2 F}{RT}(U(t) - U_2^{\text{eq}}(r))\right) \\ - \theta(r,t) \left(\frac{c_{H^+}}{c_{H^+}^{\text{ref}}}\right)^2 \exp\left(-\frac{(1-\alpha_2)F}{RT}(U(t) - U_2^{\text{eq}}(r))\right) \Bigg] \end{aligned} \tag{2.5}$$

The reaction constant rates, denoted as k_i, are k_1 for the Pt dissolution reaction and k_2 for the Pt oxidation reaction. The applied potential, $U(t)$, refers to the external voltage applied to the fuel cell. The concentrations of dissolved Pt and protons (H^+) are denoted as $c_{\text{Pt}^{2+}}$ and c_{H^+}, with corresponding reference concentrations $c_{\text{Pt}^{2+}}^{\text{ref}}$ and $c_{\text{H}^+}^{\text{ref}}$. The surface coverage of Pt particles covered with oxides is described by $\theta(r,t)$, which ranges between 0 and 1. It serves as an insulating layer, inhibiting the electrochemical dissolution of platinum. The equilibrium potential for the electrochemical reactions ($i = 1,2$), denoted as $U_i^{\text{eq}}(r)$, depends on the particle radius. The parameters α_i, R, F, T, and ω represent the electron transfer coefficient in reaction ($i = 1,2$), the universal gas constant, Faraday's constant, temperature, and PtO–PtO interaction energy, respectively.

Since the catalyst exists in the form of nanoparticles, it is necessary to modify the standard equilibrium potentials to account for the nanospherical structure [86], as illustrated in figure 2.3. This adaptation involves applying the Gibbs-Thomson correction. Consequently, the adjusted thermodynamic dissolution potential $U_1^{eq}(r)$, and thermodynamic oxidation potential $U_2^{eq}(r)$ are as follows:

$$U_1^{eq}(r) = U_1^0 - \frac{\Delta\mu_{Pt}(r)}{2F} \tag{2.6}$$

$$U_2^{eq}(r) = U_2^0 - \frac{\Delta\mu_{Pt}(r)}{2F} + \frac{\Delta\mu_{PtO}(r)}{2F} \tag{2.7}$$

where the Gibbs-Thomson correction terms $\Delta\mu_{Pt}(r)$ and $\Delta\mu_{PtO}(r)$ are given by

$$\Delta\mu_{Pt}(r) = \frac{\sigma_{Pt} M_{Pt}}{\rho_{Pt}} \frac{1}{r} \tag{2.8}$$

$$\Delta\mu_{PtO}(r) = \Delta\mu_{PtO}^{ref} + \frac{\sigma_{PtO} M_{PtO}}{\rho_{PtO}} \frac{1}{r} \tag{2.9}$$

These terms describe the correlation between the particle radius r and the surface tensions of Pt (σ_{Pt}) and PtO (σ_{PtO}). Here, ρ_{Pt} and ρ_{PtO} denote the densities of platinum and platinum oxide, respectively, while U_1^0 and U_2^0 represent the standard equilibrium potentials for dissolution and oxidation.

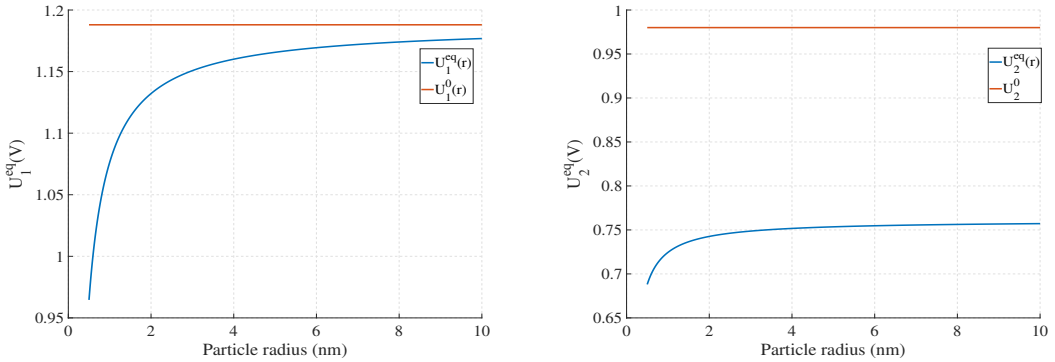

(a) Thermodynamic dissolution potential (b) Thermodynamic oxidation potential

Figure 2.3 – Adjusted thermodynamic potentials

Finally, the rate of the chemical dissolution of PtO (Reaction.2.3) is given by [143]

$$R_3(r,t) = k_3^{ref}\theta(r,t)c_{H^+}^2 \tag{2.10}$$

The chemical dissolution rate, denoted as k_3, represents the rate at which the chemical dissolution process occurs. c_{H^+} denotes the concentration of protons.

In addition to the change in radius of each particle, particles can be permanently detached from carbon support due to carbon corrosion, causing a change in the amount of particles. At high voltage, the catalyst support material undergoes degradation due to reaction 2.11, diminishing the adhesion of Pt and resulting in particle loss. This corrosion process unfolds in aqueous solutions as outlined by Schneider et al[144].

$$C + 2H_2O \leftrightarrow CO_2 + 4H^+ + 4e^- \tag{2.11}$$

The detachment mechanism is directly linked to the corrosion rate, which is incorporated into the model using the following equation:

$$R_4(r,t) = k_4(T,RH)\frac{M_{cc}}{\rho_{cc}}\exp\left(\frac{\alpha_4 F}{RT}(U(t) - U_4^{eq})\right)\frac{1}{r} \tag{2.12}$$

Here, k_4 represents the corrosion reaction rate, α_4 describes the charge transfer coefficient, and U_4^{eq} signifies the equilibrium constant of the corrosion reaction. $M_c c$ and $\rho_c c$ are the carbon molar mass and density, respectively. The ratio $\frac{1}{r}$ accounts for the effect that smaller Pt particles have a reduced contact surface, which leads to decreased adhesion.

Temperature significantly influences the electrochemical reactions associated with platinum dissolution in multiple ways. First, it affects the Tafel slope $\left(\frac{RT}{F}\right)$ present in the exponential terms of equations (2.4), (2.5), and (2.12). Additionally, temperature alters the equilibrium potentials of the reactions described in equation (2.6) and (2.7). However, as demonstrated in [145, 146], the shift in equilibrium potential resulting from temperature variations is minimal and can be regarded as negligible; thus, it is not considered in this study. More importantly, temperature plays a crucial role in determining the reaction rate constants for platinum dissolution, oxidation, and carbon corrosion. In this work, we employ the Arrhenius equation to quantify the impact of temperature on these rate constants.

Given that increased humidification and temperature of the electrode enhance the electrochemical and chemical reactions (i = 1, 2, 4) [146, 147], both relative humidity (RH) and temperature are taken into account to reflect their effects on the reaction rates as follows:

$$k_i(T,RH) = k_i^{ref}\left(\frac{RH}{RH_0}\right)T \cdot \exp\left(-\frac{G_\mathrm{i}}{k_B \cdot T}\right) \tag{2.13}$$

where k_b denotes the Boltzmann constant, T is the temperature. k_i^{ref} represents the reference rate constants for dissolution ($i = 1$), oxidation ($i = 2$) and carbon corrosion ($i = 4$), respectively. Gibbs free energy G_i defines activation energy barrier influence [146].

The kinetic model provides the reaction rates of platinum losses process (R_1, R_2 , R_3 and R_4) as functions of the applied potential, particle radius, and operation dependent variables such as relative humidity, temperature, and proton concentration. Integrating the kinetic models of platinum dissolution into the physical catalyst degradation model is crucial. This integration allows us to assess the effect of platinum dissolution on particle distribution and predict the electrochemical surface area over time and under time varying operations.

The kinetic model of the platinum degradation process involves several constants and parameters that govern the behavior of the degradation mechanisms. These

parameters are critical for accurately modeling the dissolution, redeposition, and agglomeration processes of platinum particles in the catalyst layer. The table 2.3 defines the key parameters used in the kinetic model [86, 148].

2.2.2 Physical Pt catalyst degradation model

In our model, we represent the initial state of the platinum catalyst using an initial particle radius distribution (PRD), which is typically characterized by a log-normal distribution, $f_N(r,t)$. This distribution is normalized to the total number of particles in the initial set, as outlined by Rinaldo et al. (2014) [149]. By utilizing the average particle size and the Beginning of Life (BOL) of the ECSA, we can effectively determine the distribution, even though comprehensive measurements of particle radius distributions are not commonly found in the literature.

The initial PRD is essential for characterizing the pristine state of the catalyst layer. This characterization can be performed through techniques such as Transmission Electron Microscopy image analysis or X-Ray Diffraction measurements [89].

2.2.2.1 PRD evolution equation

During aging and under potential load, the PRD undergoes noticeable changes that indicate the level of degradation [150]. The increase in particle size is thought to result from coagulation and redeposition mechanisms. The loss of platinum mass from the support can be attributed to detachment or dissolution. The dissolved platinum in the electrolyte may either be redeposited or migrate into the membrane, where it can form platinum bands within the membrane [151].

A governing equation was developed based on the theories of Wagner, Lifshitz, and Slyozov [152], to incorporate the changes in the particle radius distribution, $f_N(r,t)$. This equation accounts for the contributions from each mechanism and allows for the evolution of the PRD over time, assuming that all processes are spatially invariant on the catalyst surface. The evolution of the PRD over time is given by:

$$\frac{\partial f_N(r,t)}{\partial t} = -\frac{\partial}{\partial r}\left[f_N(r,t)\frac{dr}{dt}\right] + J^+ - J^- - R_4(r,t)f_N(r,t) \tag{2.14}$$

The first term presented in equation (2.14) represents the process of dissolution and redeposition via the rate of particle radius change, $\frac{dr}{dt}$. The second term accounts for the coagulation mechanism, where random collisions are assumed. The terms J^+ and J^- describe the coagulation process, representing particle creation and extinction, respectively. The detachment mechanism is described in the last term of equation (2.14) by the detachment rate $R_4(r,t)$, which is dependent on the particle radius.

The phenomenon of coagulation, which involves the physical merging of particles, is characterized by the radius-scaled Smoluchowski creation and extinction terms, as described in [152, 153]

$$J^{+} = \frac{1}{2} k_5^{ref} \int_{r_{\min}}^{r_{\max}} \frac{r^2}{(r^3 - \hat{r}^3)^{\frac{2}{3}}} f_N\left((r^3 - \hat{r}^3)^{\frac{1}{3}}, t\right) f_N(\hat{r}, t)\, d\hat{r} \tag{2.15}$$

$$J^{-} = k_5 \int_{r_{\min}}^{r_{\max}} f_N(r, t)\, f_N(\hat{r}, t)\, d\hat{r} \tag{2.16}$$

where k_5^{ref} is the coagulation rate constant. and $\hat{r}$ is the radius of the merging particle.

2.2.2.2 Mass balance

To incorporate the influence of dissolution and redeposition, the rate of change in particle radius r for individual particles is linked to the rates of platinum dissolution, oxidation and detachment, as well as the rate at which particles redeposit [86]. This relationship can be expressed as follows:

$$\frac{dr}{dt} = -\frac{M_{Pt}}{\rho_{Pt}} \left(R_1(r, t) + R_3(r, t)\right) \tag{2.17}$$

The dissolved platinum is not solely restricted to redeposition; it may also be lost to the membrane. The mass balance equation governing the concentration of Pt^{2+} ions, denoted as $c_{Pt^{2+}}$, in the electrolyte can be expressed as follows:

$$\frac{dc_{Pt^{2+}}}{dt} = S_{Pt} + q_{Pt,loss} \tag{2.18}$$

The net generation of Pt^{2+} ions through dissolution and redeposition is given by:

$$S_{Pt} = 4\pi \int_{r_{\min}}^{r_{\max}} r^2 f_N(r, t) \left(R_1(r, t) + R_3(r, t)\right) dr \tag{2.19}$$

The loss of platinum into the membrane is incorporated into the total mass balance equation. The loss of platinum ions, denoted as q_{Pt}, is calculated based on the diffusion of Pt into the membrane and the concentration difference between the catalyst layer and the membrane, assuming zero concentration in the membrane. The rate of Pt loss associated with the formation of Pt bands is expressed as:

$$q_{Pt,loss} = -D_{Pt}^{eff} \frac{c_{Pt^{2+}}(t)}{\delta_{CL}\delta_{band}} \tag{2.20}$$

where D_{Pt}^{eff} is the effective diffusion coefficient of Pt ions in the membrane, and δ_{band} is the diffusion length to the platinum band [42]. The diffusion length can be estimated by:

$$\delta_{band} = \frac{\delta_{CL}}{2} + \frac{2\psi_{O_2} P_{O_2}}{\psi_{H_2} P_{H_2} + 2\psi_{O_2} P_{O_2}} \delta_{mb} \tag{2.21}$$

where the partial pressures and permeabilities of H_2 and O_2 are denoted by P_{H_2}, P_{O_2},

ψ_{H_2}, and ψ_{O_2}, respectively. The catalyst and membrane thicknesses are represented by δ_{CL} and δ_{mb}, respectively.

The diffusivity of Pt ion is related to the volume fraction of water in the ionomer and dependence on temperature. The effective diffusion coefficient of platinum ions in the presence of water can be expressed as:

$$D_{Pt}^{eff} = D_{Pt} f(\lambda) \left(\frac{T}{T_0} \right)^{1.5} \tag{2.22}$$

where D_{Pt}^{eff} represents the effective diffusion coefficient, D_{Pt} is the intrinsic diffusion coefficient of platinum ions, and $f(\lambda)$ is a parameter that accounts for the influence of water on diffusion, representing the volume fraction of water in the ionomer. This parameter can be further defined as:

$$f(\lambda) = \frac{\lambda V_{H_2O}}{V_{mb} + \lambda V_{H_2O}} \tag{2.23}$$

where V_{H_2O} is the molar volume of liquid water under typical PEMFC operating conditions, and V_m represents the equivalent volume of the dry membrane, defined as:

$$V_{mb} = \frac{EW}{\rho_{ion}} \tag{2.24}$$

Here, EW is the ionomer equivalent weight, and ρ_{ion} is the ionomer density.

In this equation, λ represents the membrane's water content as a function of RH.

$$\lambda = 0.043 + 17.81RH - 39.85RH^2 + 36RH^3 \tag{2.25}$$

Finally, assuming spherical platinum crystallites [86], the evolution of the oxide coverage, θ , of the catalyst layer is defined by

$$\frac{d\theta}{dt} = \left(\frac{R_2(r,t) - R_3(r,t)}{\Gamma_{max}} \right) - \left(\frac{2\theta(r,t)}{r} \right) \frac{dr}{dt} \tag{2.26}$$

The right side explains oxide formation/reduction via reaction paths and how varying particle size affects oxide coverage. Here, Γ_{max} represents the active site quantity in moles per platinum area.

2.2.2.3 Microstructure Evolution

The evolution of the particle radius distribution, $f_N(r,t)$, over time forms the basis for calculating the time-dependent electrochemical surface area, $S(t)$, which serves as a key indicator of catalytic activity. This is expressed as:

$$S(t) = 4\pi \int_{r_{min}}^{r_{max}} r^2 f_N(r,t)\, dr \tag{2.27}$$

where $S(t)$ represents the total electrochemical surface area, integrating the sur-

face areas of particles within the range $[r_{\min}, r_{\max}]$ and weighted by the distribution function $f_N(r,t)$.

The platinum mass loading, $L_{\mathrm{Pt}}(t)$, which quantifies the mass of platinum per unit active area of the cell in the catalyst layer, is calculated as:

$$L_{\mathrm{Pt}}(t) = \frac{4}{3}\pi\rho_{\mathrm{Pt}}\int_{r_{\min}}^{r_{\max}} r^3 f_N(r,t)\,dr \tag{2.28}$$

Similarly, the average particle radius, $r_{\mathrm{avg}}(t)$, representing the mean particle size in the distribution, is given by:

$$r_{\mathrm{avg}}(t) = \frac{\int_{r_{\min}}^{r_{\max}} r\, f_N(r,t)\,dr}{\int_{r_{\min}}^{r_{\max}} f_N(r,t)\,dr} \tag{2.29}$$

Lastly, the effective active site, $ECA(t)$ in $cm^2/cm^2_{/A_{fc}}$, which provides a measure of the catalyst's active sites per unit active area of the cell, is represented as:

$$ECA(t) = S(t)\cdot L_{\mathrm{Pt}}(t) \tag{2.30}$$

This framework enables the evaluation of the microstructural evolution of the catalyst layer over time, allowing assessment of how changes in the particle distribution impact performance and stability in PEM fuel cell applications.

The proposed Pt catalyst degradation model effectively illustrates the relationship between various operating conditions specifically potential, temperature, relative humidity, and species concentrations and enables the prediction of electrochemical surface area evolution over time.

2.3 Results and Discussion

The objective of this section is to analyze microscale degradation behavior, focusing on interactions between key processes affecting Pt catalyst performance. This includes examining Pt concentration changes, oxide coverage, particle radius distribution, and nanoparticle size evolution across different potential profiles to better understand catalyst degradation under varied operating conditions. The ECSA is also evaluated as an indicator of Pt microstructural changes. The degradation model's reliability and accuracy are assessed using AST data to confirm its predictive capability and suitability for real-time applications, with simulations illustrating microstructural aging across operating scenarios.

Load cycling profile

The load cycle degradation test was conducted in accordance with the U.S. Department of Energy (DOE) [154] electrocatalyst degradation protocol, designed to simulate load cycling by alternating between a lower potential limit (LPL) and an upper potential limit (UPL). The experimental data captured two signal types: a triangular wave

(TW) that transitions between LPL and UPL with a specified scan rate in [mV/s], and a square wave (SW) with dwell times defined at both the UPL and LPL. These dwell times indicate the duration each potential is held, as illustrated in the voltage cycle profile in figure 2.4.

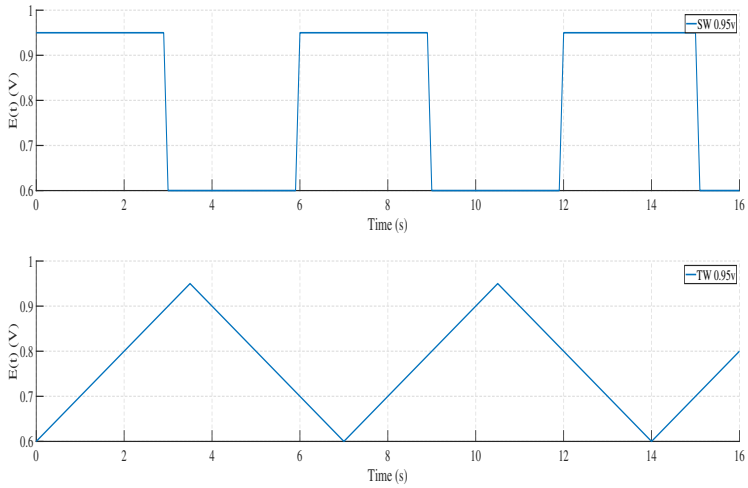

Figure 2.4 – Load cycling voltage profile

Initial distribution of catalyst particle sizes

We utilize an initial PRD, typically generated using a log-normal distribution $f_N(r,t)$ given by

$$f_N(r,0) = \frac{1}{\sigma\sqrt{2\pi}} \exp\left(-\frac{(\ln(r)-\mu)^2}{2\sigma^2}\right) \tag{2.31}$$

Our choice of utilizing a log-normal distribution is informed by its good alignment with experimental PRD data derived from various catalyst layers [88]. Where the standard deviation σ and the mean μ are fitted based on the available experimental PRD data. This distribution comprises a finite number of particle groups, each categorized by their particle radius and the number of particles contained within. Figure 2.5 visually represents the assumed PRD, divided into N distinct groups, with fresh catalyst specifications detailed in the following table 2.1.

AST experimental data

During this stage, degradation tests were conducted with variations in temperature, relative humidity, and potential range. This step is crucial for understanding the impact of different operating conditions on degradation and for validating the model's ability to predict degradation under diverse scenarios, thereby extending its applicability beyond focused AST to real-world driving conditions. The experimental

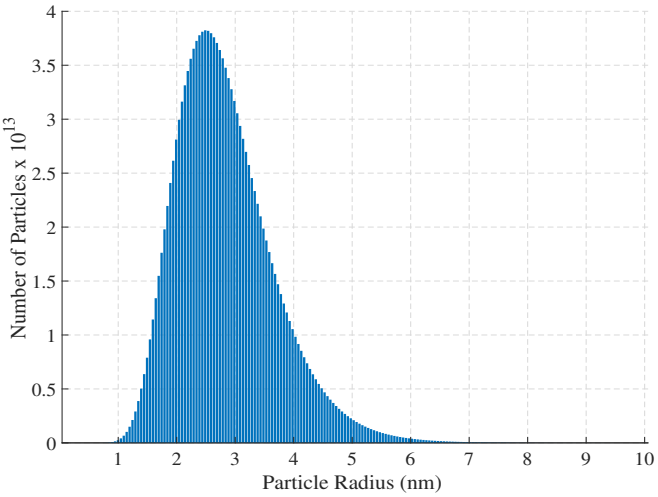

Figure 2.5 – Initial particle radius distribution

Parameter	Meaning	Value/unit
$S(0)$	Initial ECSA	[30 50] $m^2.g_{Pt}^{-1}$
$L_{pt}(0)$	Initial mass loading of Pt	[0.4 0.5] $mg_{Pt}.cm^{-2}$
r_{min}	Min particle radius	0.5 nm
r_{max}	Max particle radius	10 nm
r_{avg}	Initial radius mean	2 nm
σ	Standard deviation	0.549
μ	Mean in log space	0.538

Table 2.1 – Pt catalyst specification

data from the literature concerning ECSA losses is summarized in table 2.2, which is utilized to validate catalyst degradation in PEM fuel cells under AST by comparing ECSA evolution across various operating conditions.

The initial model simulation compared ECSA normalized loss over 30k load cycles under the conditions outlined in dataset (1), considering the experimental setup and the initial characteristics of the Pt catalyst, with full details provided in [155]. The simulation was performed on a standard desktop PC with an Intel Core i9 processor clocked at 2.6 GHz. It took approximately 15 minutes to complete for 50 particle radii groups. However, the computation time depends on the number of particle groups, with a minimum of 50 radii groups required to ensure reliable simulation results.

2.3.0.1 Microscale Examination of Degradation

At the nanoscale, we can examine how Pt dissolution and redeposition rates change in response to cyclic potential and assess how well the model aligns with prior knowledge from both experiences and the existing data regarding the degradation mechanisms. The results in nano, microscale in SW 0.98V are illustrated for the first three

Purpose	Dataset	Signal	UPL/LPL (V)	Hold time (s)	Cycles	Temp (°C)	RH (%)	Ref
Potential	(1)	SW 0.98V	0.98/0.6	3/3	30,000	80	85	[155]
	(2)	TW 0.9V	0.9/0.6	-	300,000	80	100	[144]
	(3)	SW 0.9V	0.9/0.6	3/3	300,000	80	100	[144]
	(4)	SW 0.95V	0.95/0.6	3/3	300,000	80	100	[144]
Relative Humidity	(5)	SW 0.95V	0.95/0.6	3/3	300,000	80	60	[144]
	(6)	SW 0.95V	0.95/0.6	3/3	300,000	80	30	[144]
Temperature	(7)	SW 0.95V	0.95/0.6	3/3	300,000	90	100	[144]
	(8)	SW 0.95V	0.95/0.6	3/3	300,000	60	100	[144]

Table 2.2 – Summary of experimental conditions used for validation purposes.

potential cycles between 0.6 and 0.98V, and have disccused and analysed in this part.

In figure 2.6a, the simulated evolution of Pt oxide coverage is shown for three particle sizes (2, 4, and 6 nm). It is evident that smaller particles display greater overall oxide coverage, which can be attributed to the shift in equilibrium potential, $E_2^{\mathrm{eq}}(r)$. After a dwell time of 3 seconds at 0.98 V, the oxide reaches a maximum partial coverage of 0.6 before the voltage decreases. The higher total coverage observed in smaller particles results from the shift in equilibrium potential, indicating that smaller radii promote increased oxide growth. This effect is reflected in the right-hand side of equation (2.26), where the radius appears in the denominator, meaning that as the particle radius increases, the rate of oxide coverage decreases.

In figure2.6b, the oxide coverage θ is compared as a function of the applied potentiostatic voltage, following a hold time at 80°C until the oxide coverage reaches its steady-state value. The model shows good agreement with the literature findings within the potential range of 0.75 V to 1.0 V [86, 88]. Normal fuel cell operating conditions should not exceed 1.0 V, as higher potentials lead to accelerated degradation. However, understanding the effects of high potential is crucial since specific cases, such as startup or shutdown, may be subject to these conditions and exhibit significantly greater oxide growth. This growth increases almost exponentially with the applied voltage. It is evident that as the potential increases, platinum oxidation progresses, forming an oxide layer on the catalyst surface. This oxide layer partially protects Pt particles from direct dissolution; however, chemical dissolution continues at a reduced rate. Meanwhile, this coverage leads to irreversible performance losses in the PEMFC by limiting the oxygen reduction reaction.

The dissolution rates for particles of three different sizes (0.5, 2, and 4 nm) are shown in figure 2.7. A comparison of the dissolution and redeposition rates across these sizes clearly indicates the occurrence of Ostwald ripening. Notably, smaller particles exhibit much higher dissolution rates than larger ones, which can be attributed to their lower equilibrium potential, $E_1^{\mathrm{eq}}(r)$. As dissolution proceeds, the concentration of Pt^{2+} ions in the catalyst layer's ionomer increases figure 2.8. For $r = 4\,\mathrm{nm}$, the redeposition rate (R_{dis}) quickly becomes negative, even at high potentials. This indicates a tendency for

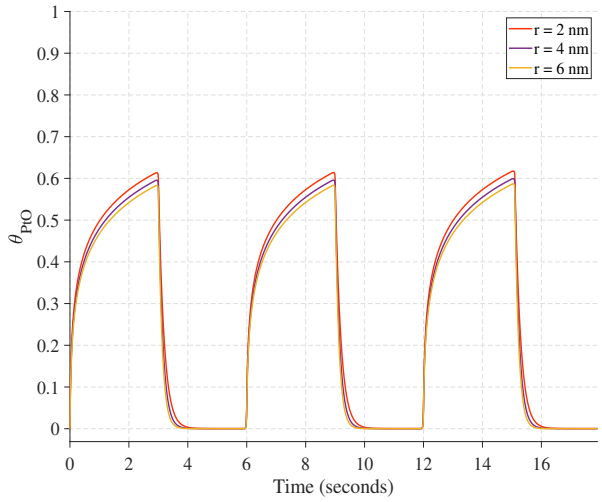

(a) Evolution of PtO for three radii $r = 2, 4, 6$ nm

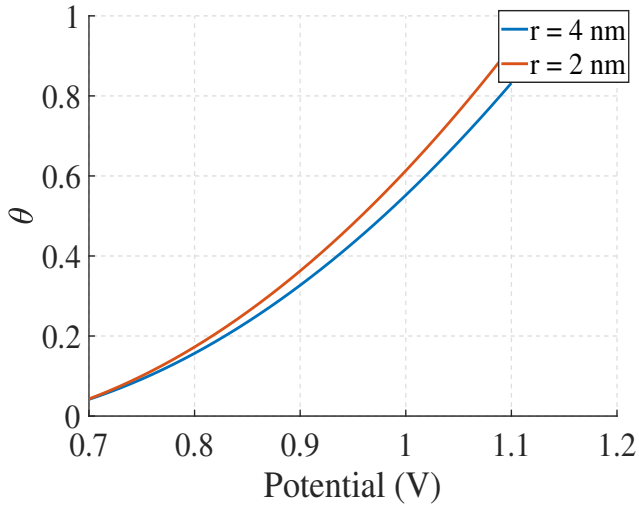

(b) Evolution of PtO Coverage with Voltage Potential

Figure 2.6 – Comparison of PtO evolution and coverage under varying conditions

larger particles to redeposit due to the high concentration of platinum ions generated from the dissolution of smaller particles, which primarily contribute to degradation. When the potential subsequently decreases, redeposition of dissolved Pt ions occurs rapidly for all particle size, causing a decline in ion concentration within a few time steps and leading to the preferential growth of larger particles. The combination of increased dissolution of smaller particles and the growth of larger ones ultimately results in a net loss of ECSA, known by Ostwald ripening.

The concentration of Pt^{2+} ions dissolved in the ionomer under different potential profiles, as illustrated in figure 2.8, is influenced by variations in the applied potential, oscillating between maximum and minimum values. Furthermore, as the potential

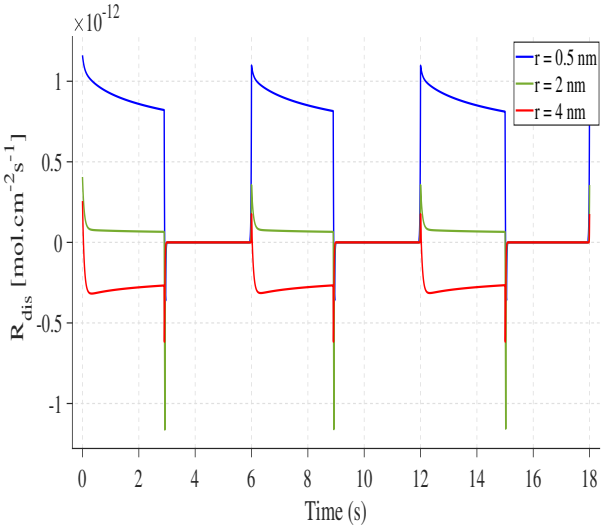

Figure 2.7 – Dissolution/redeposition rates for two radius

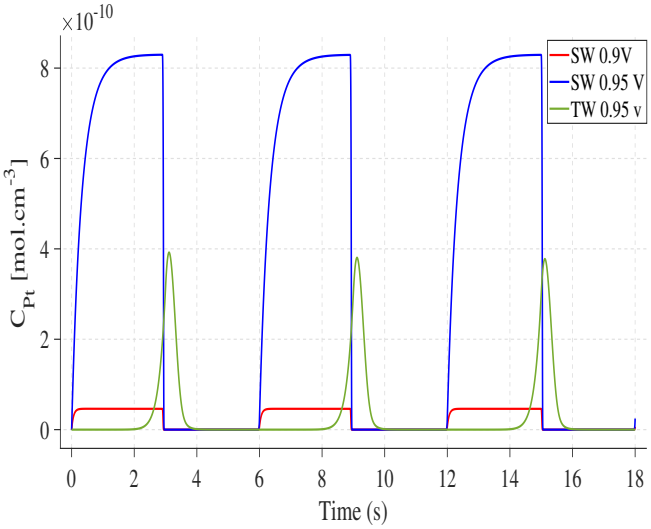

Figure 2.8 – Concentration of Pt^{2+} ions in the ionomer

increases from 0.6 to 0.95 V, we observe a rapid onset of Pt dissolution. Concurrently, as the dissolution process progresses, the concentration of Pt^{2+} ions within the catalyst layer's ionomer increases until it reaches saturation. Conversely, as the potential decreases once more, the redeposition of dissolved Pt ions commences immediately for all particle sizes, resulting in a swift drop in ion concentration. Comparing the two square wave profiles (SW0.9V and SW0.98V) shows that a 80 mV increase in the UPL causes an 18-fold increase in the concentration of dissolved platinum within the ionomer. This heightened concentration notably accelerates redeposition, leading to a greater loss of ECSA due to Ostwald ripening, while also enhancing the migration of platinum into the membrane.

In contrast, when comparing the square wave at SW 0.90 V with the triangular

wave at the same potential TW 0.90 V, the triangular profile displays slower platinum dissolution, which is due to its more gradual increase in potential. Additionally, the concentration of Pt^{2+} reaches its peak at the UPL, with redeposition starting immediately after the potential begins to decline. The triangular load profile leads to less platinum dissolution and redeposition, thereby reducing both degradation and Ostwald ripening. Moreover, the shorter dwell time at higher Pt^{2+} concentrations results in a decrease in ion flux into the membrane, which minimizes platinum loss. This comparable result with experimental analyses illustrates the model's capability to be sensitive to varying potential cycling loads, which reflect real-world operating conditions. The alignment between the model predictions and experimental observations demonstrates that the model effectively captures the dynamics of platinum catalyst behavior under different cycling scenarios. This sensitivity to potential variations is crucial for accurately predicting the degradation mechanisms in PEMFC, thereby enhancing the model's reliability and applicability in practical settings.

Figures 2.9 illustrates that larger particles can more rapidly accept redeposited ions from the electrolyte than smaller particles, thereby accelerating their growth. This, combined with the higher dissolution rates of smaller particles, results in a shift in the particle size distribution toward larger particles, as shown in figure 2.9a. This phenomenon encompasses both redeposition and agglomeration mechanisms and highlights the increased susceptibility of smaller particles to corrosion. The evolution of particle radius, depicted in figure 2.9b, further confirms this trend, showing an increase in the average particle radius over time. The change in PRD enables the quantification of morphological alterations occurring within the active surface area, reflecting the effects of key degradation phenomena. Then, we can gain insights into how factors such as platinum dissolution, particle agglomeration, and corrosion impact the structural integrity of the catalyst. These morphological changes are crucial for understanding the overall performance and longevity of the catalyst in fuel cell applications, as they directly influence the electrochemical surface area and the catalyst's ability to facilitate the oxygen reduction reaction.

Figure 2.10 illustrates the temporal evolution of ECSA based on dataset (1). A comparison between the ECSA predicted by the developed degradation model and the accelerated stress test experimental data reveals a substantial and satisfactory level of agreement. Nevertheless, accurately tracking the degradation rate remains a significant challenge, primarily due to the complex interactions among various degradation processes affecting different components of the fuel cell. This issue becomes particularly pronounced as the end of the cell's operational lifespan approaches, where these interactions become increasingly evident. Furthermore, the degradation of the Pt catalyst is intricately linked to the internal states and parameters of the PEMFC. As the fuel cell operates under dynamic loading conditions, transient factors such as changes in temperature, humidity, and operating voltage can exert substantial influence on catalyst behavior. These transient conditions can lead to rapid fluctuations in reaction kinetics, potentially accelerating degradation mechanisms that the model may not fully capture. Continuous refinement of these models, alongside comprehensive experimental validation, is essential to enhance their predictive capabilities and better

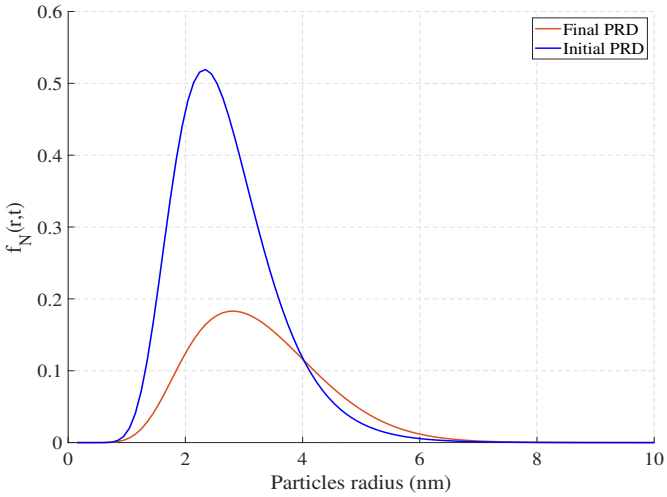

(a) Particle radius evolution

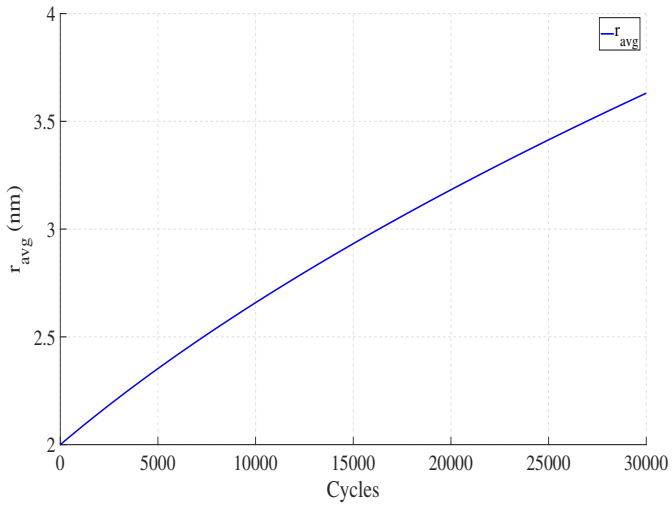

(b) ECSA evolution over 30 k cycles

Figure 2.9 – Comparison of particle radius and ECSA evolution

understand the multifaceted nature of fuel cell degradation. This ongoing effort will contribute to the development of more durable and efficient fuel cell technologies.

2.3.0.2 Catalyst Microstructure Evolution Analysis

At this stage, we conducted additional calculations to assess the ECSA response to various operating conditions. This involved a systematic examination of how different parameters, such as temperature, humidity, and voltage cycling profiles, influenced the ECSA over time. We compared these calculated results with the experimental dataset presented in table 2.2, with respect to initial conditions corresponding to the experimental setup.

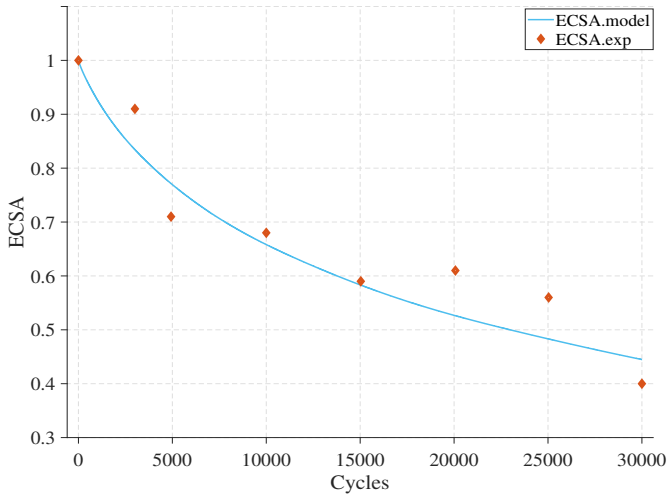

Figure 2.10 – ECSA evolution over 30k cycles

First, we analyzed the degradation pathways of the platinum catalyst under varying potential cycling conditions, observing how shifts in operational parameters and profiles affected the rate of catalyst degradation and the corresponding loss of ECSA. This validation process not only evaluates the accuracy of our model but also assesses its applicability in practical scenarios, while identifying the weaknesses that could be refined in future work, making it a robust tool for predicting catalyst aging. Ultimately, our comparison will highlight to understand how operational conditions affect catalyst performance, which can help us create more robust and efficient fuel cell control strategies.

Initially, we performed further calculations to evaluate the ECSA response to different load profiles, comparing our findings with experimental data from datasets (2), (3), and (4), as illustrated in figure 2.11.

Our analysis reveals significant electrochemical surface area losses, particularly with the SW profile, in contrast to the comparatively lower losses associated with the TW profile. These differences can be attributed to extended dwell times at elevated voltages, which accelerate the degradation of the Pt catalyst. Furthermore, when compared with dataset (4), the critical influence of the UPL on catalyst layer degradation becomes apparent. Operating the fuel cell at high UPL significantly impairs performance and exponentially exacerbates degradation effects. The model's consistency with the experimental data underscores its sensitivity to voltage profiles and emphasizes the pivotal role they play in Pt catalyst degradation.

The results shown in figure 2.12 illustrate the effect of relative humidity on Pt catalyst degradation. Increased levels of humidity are associated with greater electrochemical surface area loss, as electrochemical reactions are enhanced under higher relative humidity conditions. Additionally, exposure to higher humidity promotes increased ion diffusion, leading to greater platinum losses.

Under various temperatures, our simulated model demonstrates strong agreement

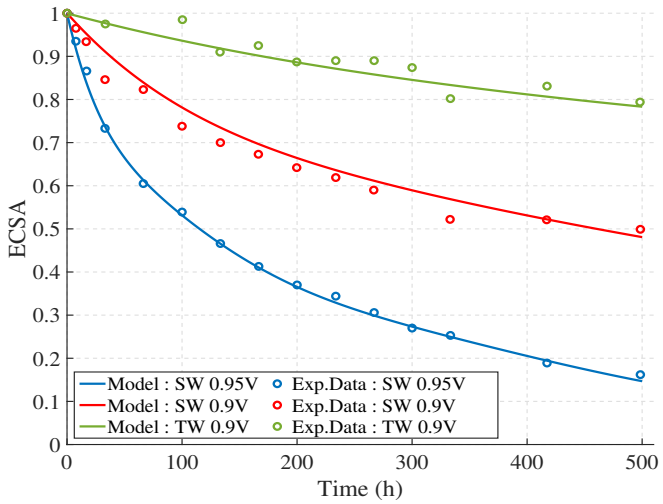

Figure 2.11 – Evolution of ECSA for datasets (2) & (3) & (4)

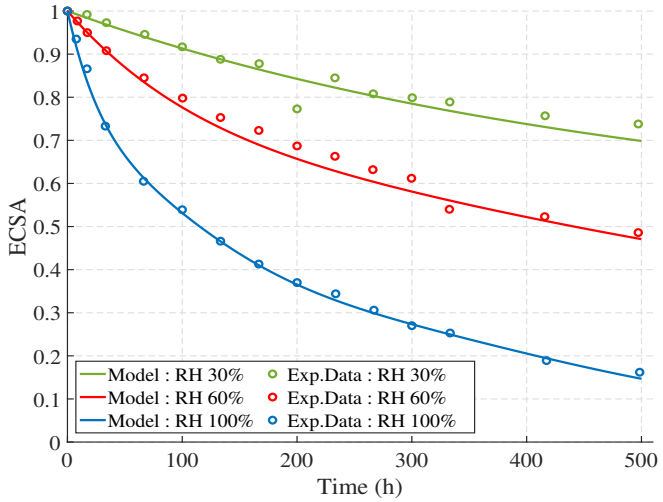

Figure 2.12 – Evolution of ECSA for datasets (4) & (5) & (6)

with the corresponding experimental data, as illustrated in figure 2.13. These results affirm the reliability of our predictive model across a range of temperature conditions. This enhancement can be attributed to our method of incorporating the temperature dependent reaction rate, as outlined in equation 2.13.

Finally, our model improves accuracy across various operating conditions, including voltage, relative humidity, and temperature. This capability can be further enhanced to predict the performance of PEM fuel cells by integrating the model into a macroscale framework and updating the parameters that influence system behavior during both transient and steady-state conditions. However, a slight deviation from the experimental data can be observed, primarily due to the incomplete consideration of the intricate effects of other degradation components. Furthermore, the degradation

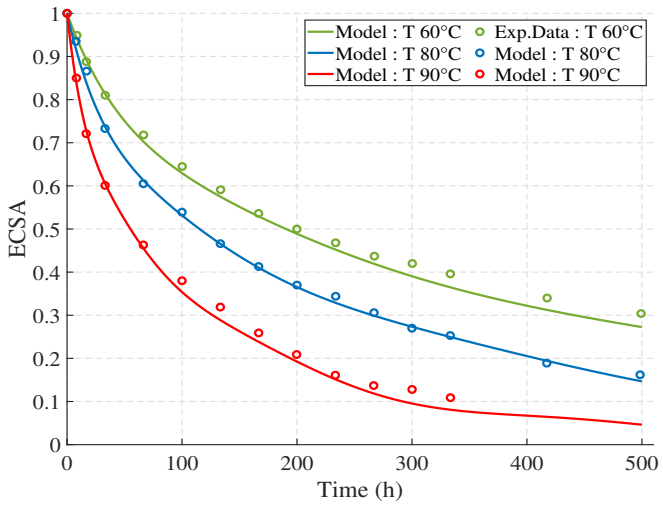

Figure 2.13 – Evolution of ECSA for datasets (4) & (7) & (8)

model relies on internal states, such as temperature and water activity in the catalyst layer, rather than directly on operating conditions. This dependency can affect the model's accuracy under dynamic conditions.

2.4 PEM Model Development

The membrane degradation model is presented and integrated with catalyst degradation to synthesize a membrane electrode assembly degradation model that incorporates the two most critical components [72]. Chemical degradation primarily involves the impact of membrane decomposition due to chemical reactions and contamination. It is regarded as the primary factor limiting the lifespan of membranes [80] and is characterized by decrease of the membrane thickness (MT) along with the release of byproducts such as HF, CO_2, and H_2SO_4. A reduction in membrane thickness leads to increased gas crossover and mechanical weakness, which can ultimately result in membrane failure. Consequently, the rate of chemical degradation can be estimated by monitoring the gas crossover rate and quantifying the release of fluoride ions.

The objective of this section is to investigate the effects of various operating conditions on the chemical degradation of the membrane, aiming to accurately quantify the degradation rate under different scenarios. The membrane degradation model incorporates essential processes, including the oxygen crossover from the cathode to the anode and the formation of hydrogen peroxide on the anode side, as illustrated in figure 2.14. This micro-scale information is then used to quantify changes in membrane thickness, offering a comprehensive understanding of the degradation dynamics.

The structural changes in the membrane are difficult to define, and direct observation during PEMFC operation requires a highly complex and demanding experimental

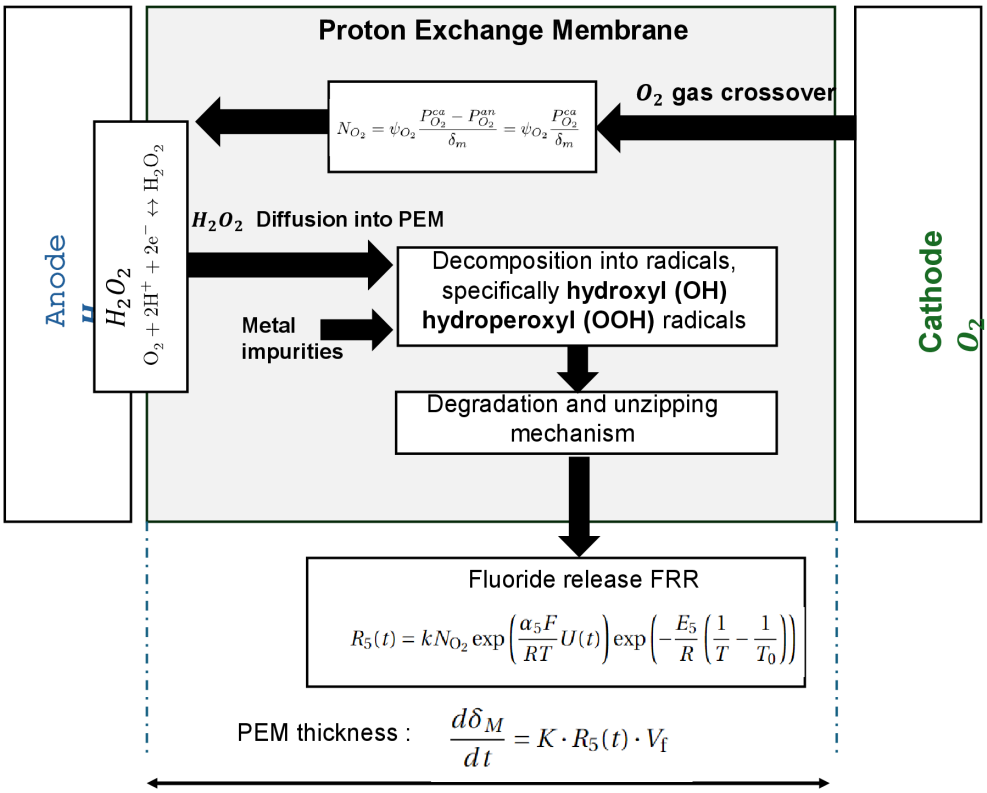

Figure 2.14 – Schematic Representation of Membrane Degradation

setup [156]. Treating the fuel cell as a black box further complicates the understanding of its chemical degradation processes. However, experimental analysis enables the detection and quantification of fluoride ions, perfluorosulfonic acid, and fluorinated organic compounds in the cell's wastewater, providing valuable insights into the degradation mechanisms [51, 55, 157]. Based on these analyses and experimental data, a degradation model can be validated to predict the membrane's microstructural changes over time.

2.4.1 Hydrogen peroxide formation

The formation of peroxides and radicals in PEM fuel cells is considered a key factor in membrane degradation. The process of H_2O_2 formation in PEMFCs is illustrated in figure 2.14. Initially, oxygen is transported through the gas diffusion layer and into the catalyst layer at the cathode. Due to the oxygen permeability in the ionomer, molecular oxygen can continue to diffuse through the membrane.

At the anode, a possible mechanism for H_2O_2 formation was described by LaConti et al. [50, 158], where at potentials lower than 0.695 V, the reaction 2.32 predominantly occurs via the H_2O_2 formation pathway, and water recombination can be neglected.

$$O_2 + 2H^+ + 2e^- \leftrightarrow H_2O_2 \tag{2.32}$$

The electrochemical formation rate of H_2O_2 is modeled using a simple kinetic law, based on the assumption that the reverse reaction is negligible.

$$R_{H_2O_2} = k_f^{'} c_{O_2} c_{H^+}^2 \tag{2.33}$$

In equation (2.33), only the forward rate term is considered because, at potentials of 0.6V vs. SHE and below, the oxidation rate of hydrogen peroxide (H_2O_2), which corresponds to the reverse reaction, is minimal. To estimate the kinetic rate constant $k_f^{'}$ at various potentials, The production rate of H_2O_2 against oxygen concentration is investigated [159]. The activation energies for the H_2O_2 formation reaction were determined using the Arrhenius equation. The kinetic constant per unit of active surface, $k_f^{'}$, is described by Ref. [159] as follows:

$$k_f' = k_f \exp\left(\frac{\alpha_{H_2O_2} F}{RT}\eta\right) \exp\left(-\frac{E_{H_2O_2}}{RT}\right) \tag{2.34}$$

In this equation, the overpotential η is measured in volts (V) relative to the standard hydrogen electrode (SHE), and $E_{H_2O_2}$ represents the activation energy for the formation of H_2O_2 on supported platinum catalysts.

Then, the formation of H_2O_2 occurs via an electrochemical reaction at the anode, accompanied by the reaction of H_2O_2 with fer Fe ions, which generates radicals that attack the polymer membrane. Chemical reactions within the membrane occur due to the coexistence of various species. Understanding the interactions among these different species requires further investigation for accurate modeling. Specifically, the reactions involving iron ions (Fe^{2+} and Fe^{3+}) and radicals $HO^{\cdot}, HOO^{\cdot}$ are of particular interest [54]. At this stage, we base our approach on a semi-empirical model as described in [51], which links fluoride release to membrane thickness through peroxide formation, as outlined in equation (2.34).

2.4.2 Fluoride release rate

Experimental analysis allows for the detection and quantification of fluoride ions, leading to the development of a semi-empirical equation that estimates the fluoride release rate based on equation (2.33). A mathematical expression for a semi-empirical law proposed by Chandesris et al. [51] to describe the fluoride release rate (FRR), which simulates the degradation of membrane molecular chains, is given by:

$$R_5(t) = k N_{O_2} \exp\left(\frac{\alpha_5 F}{RT} U(t)\right) \exp\left(-\frac{E_5}{R}\left(\frac{1}{T} - \frac{1}{T_0}\right)\right) \tag{2.35}$$

The variable N_{O_2} represents the oxygen crossover from the cathode to the anode, and it is influenced by factors such as membrane permeability, membrane thickness, and the partial oxygen pressure on the cathode side. This is denoted by:

$$N_{O_2} = \psi_{O_2} \frac{P_{O_2}^{ca} - P_{O_2}^{an}}{\delta_{mb}} = \psi_{O_2} \frac{P_{O_2}^{ca}}{\delta_{mb}} \tag{2.36}$$

where ψ_{O_2} is the oxygen permeability in the membrane, and $P_{O_2}^{ca}$ and $P_{O_2}^{an}$ are the partial pressures at the cathode and anode, respectively.

At the anode-membrane interface, the oxygen partial pressure tends toward zero, assuming that all the oxygen crossing over to the anode side either transforms into water or reacts with hydrogen. The parameter ψ_{O_2} represents the permeability, which depends on temperature and water content, as provided by the macro-scale model.

In this model, we suggest that the generation of radicals is mainly governed by the oxygen flux across the membrane and the cell voltage. In particular, the cell voltage impacts both the electrochemical production of peroxide and the concentration of iron ions, as noted by Wong and Kjeang [160]. This interaction subsequently affects the breakdown of peroxide into radicals. The two-electron oxygen reduction reaction responsible for peroxide formation can be described using a Butler-Volmer-type kinetic expression, as presented in equation (2.34).

The iron redox cycle, sustained when the cell voltage surpasses 0.7 V, exerts a complex influence that necessitates thorough analysis for complete understanding [160]. To simplify this interaction, it assumed that the relationship between peroxide formation and the iron redox cycle can be represented by a Butler-Volmer-type expression that includes an equivalent transfer coefficient, α_5.

The last term of equation (2.35) shows that all reactions involved in the chemical degradation of the membrane are dependent on temperature and adhere to an Arrhenius-type relationship. The activation energy E_5 reflects the effective activation energy for these different reactions.

2.4.3 Membrane thinning

The degradation rate of the ionomer is intricately influenced by the fluoride release rate, denoted as R_5, which is linked to the polymer chain structure. A straightforward model for membrane thinning has been established [51], incorporating the semi-empirical model of FRR. Since the FRR is normalized by the geometric active surface area of the membrane electrode assembly, the change in membrane thickness can be represented as proportional to the FRR multiplied by the volume of dry Nafion, denoted by:

$$\frac{d\delta_{mb}}{dt} = K \cdot R_5(t) \cdot V_{\mathrm{f}} \tag{2.37}$$

The degradation of the ionomer contributes to a reduction in the volume of dry Nafion, which is reflected in the thinning of the membrane, denoted by:

$$V_{\mathrm{f}} = \frac{1}{\rho_{ion}\chi_n} \tag{2.38}$$

Here, ρ_{ion} represents the density of dry Nafion, and χ_n is the mass fraction of

fluorine in Nafion. The constant K is an adjustable parameter that accounts for the fact that not all degraded ionomer fragments are recovered in the exhaust water, and that the ionomer fragments do not completely decompose into fluoride ions, which are the only ions measured.

Consequently, it can be inferred that the alteration in membrane thickness is likely directly proportional to the product of the FRR and the model proposed by Chandesris et al. [51], expressed as:

$$\frac{d\delta_{mb}}{dt} = k_5 \psi_{O_2} \frac{P_{O_2}}{\delta_{mb}} exp\left(\frac{\alpha_5 F}{RT} U(t)\right) exp\left(-\frac{E_5}{R}(\frac{1}{T} - \frac{1}{T_0})\right) \tag{2.39}$$

The degradation of the membrane requires further investigation, as this limitation hinders our understanding of PEM degradation. The complexity of multiple species involved in membrane degradation and the identification of their interactions present significant challenges. However, the accuracy of the model can be enhanced by assessing different conditions and employing feature extraction techniques based on characterization methods.

Symbol	Description	Value / Unit
Physical Parameters and Constants		
$\alpha_1, \alpha_2, \alpha_4$	Transfer coefficients for Pt dissolution, oxidation, and carbon corrosion	0.5 [-]
E_1^0	Standard equilibrium potential for Pt dissolution	1.188 [V]
E_2^0	Standard equilibrium potential for Pt oxidation	0.980 [V]
E_4^{eq}	Equilibrium potential for carbon corrosion reaction	0.2 [V]
$c^{ref}_{Pt^{2+}}$	Reference Pt ion concentration	1×10^{-3} [mol/cm^3]
$c^{ref}_{H^+}$	Reference proton concentration	1×10^{-3} [mol/cm^3]
G_i	Activation energy for reaction i	0.12 [eV]
k_b	Boltzmann constant	8.617×10^{-5} [eV/K]
σ_{Pt}	Surface tension of Pt nanoparticles	2.37×10^{-4} [J/cm^2]
σ_{PtO}	Surface tension of Pt oxide nanoparticles	1.00×10^{-4} [J/cm^2]
ω	Pt-O interaction energy	27×10^3 [J/mol]
Γ_{max}	Maximum Pt oxide coverage	2.8×10^{-9} [mol/cm^2]
$\Delta\mu^{PtO}_{ref}$	Chemical potential of Pt oxide	-42.3×10^3 [J/mol]
ρ_{Pt}	Pt metal density	21.45 [g/cm^3]
ρ_{PtO}	Pt oxide density	14.1 [g/cm^3]
ρ_{cc}	Carbon density	2.26 [g/cm^3]
M_{Pt}	Molar mass of Pt	195.1 [g/mol]
M_{PtO}	Molar mass of Pt oxide	211.0 [g/mol]
M_{cc}	Molar mass of carbon	12.01 [g/mol]
EW	Ionomer equivalent weight	1000 [g/mol]
V_{H_2O}	Molar volume of water	18 [cm^2/mol]
ρ_{ion}	Ionomer density	1.9 [g/cm^3]
χ_n	Mass fraction of fluorine	0.82 [-]
α_5	Equivalent transfer coefficient	0.54 [-]
E_5	Equivalent activation energy	75 [kJ/mol]
Fitting and Calibration Parameters		
k^{ref}_i	Reaction rate constant for reactions $i = 1, 2, 4$	$[\text{mol}/(\text{cm}^2 \cdot \text{s} \cdot \text{K})]$
k^{ref}_3	Rate constant for chemical dissolution	$[\text{mol}/(\text{cm}^2 \cdot \text{s})]$
k^{ref}_{cgl}	Coagulation rate constant	[1/s]
k_5	Equivalent Fluoride release constant	$[\mu\text{g}/(\text{cm}^2 \cdot \text{s})]$

Table 2.3 – Model Parameters for MEA Degradation

2.4.4 Results and Discussion

Experimental observations have demonstrated that chemical degradation is highly sensitive to operating conditions. The current numerical model further investigates this by examining the impact of various operating parameters on degradation behavior. In simulations conducted under AST, conditions are set to match those in figure 2.15, specifically: temperature at 95 °C, pressure at 2 atm, relative humidity at 50%, and an open circuit voltage. The initial membrane thickness is set to 25 μm. These baseline conditions are systematically adjusted in a parametric study to assess their influence on total mass loss and membrane thickness.

The impact of changes in membrane structure on chemical degradation is investigated. figure 2.15 presents simulation results demonstrating fluoride loss associated with variations in membrane thickness under different voltage cycle profiles. A strong relationship between chemical degradation and load cycling has been identified.

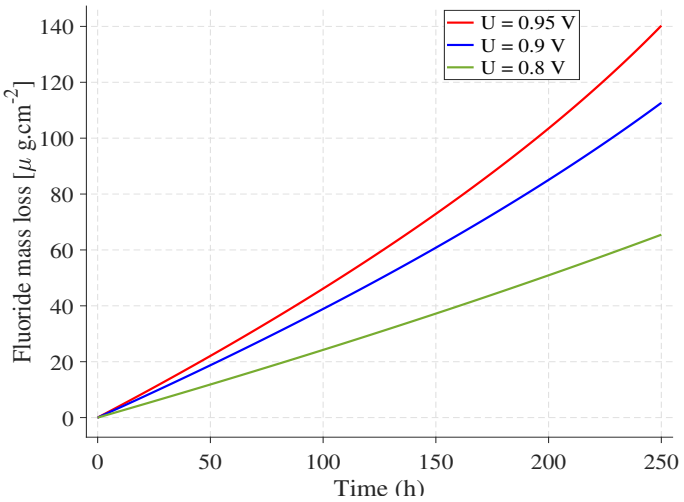

Figure 2.15 – Fluoride release accumulation

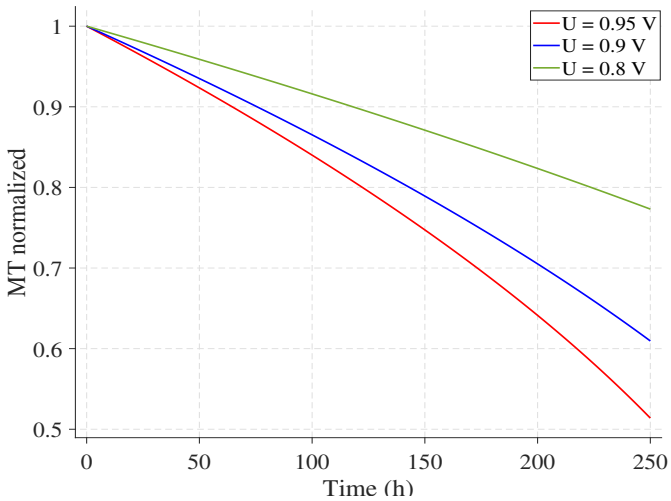

Figure 2.16 – MT evolution under different potentials

In figures 2.15 and 2.16, three different upper potential loads were effectively tested to assess the impact of cell potential on membrane degradation. The applied potentials were 0.95 V, 0.90 V, and 0.80 V. The results clearly indicate that higher UPLs lead to a substantial increase in fluoride release, with values ranging from two to three orders of magnitude greater than the fluoride release observed at 0.80 V.

Regarding the influence of load, it appears that the fluoride release mass increases as the load decreases. A similar trend is observed for the membrane thickness, as illustrated in figure 2.16.

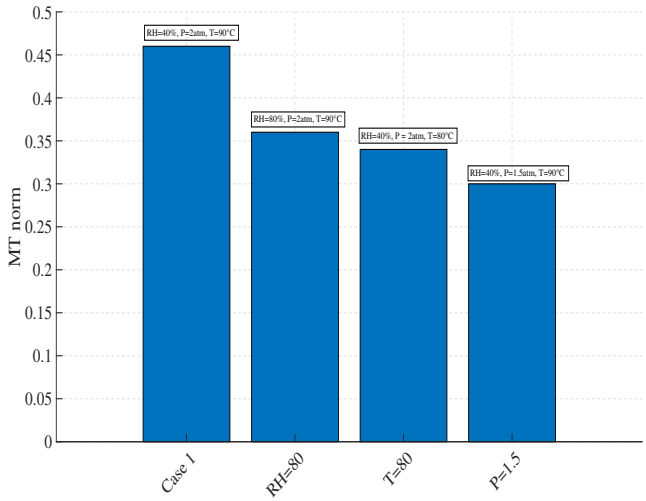

Figure 2.17 – MT degradation over 250 hours

Figure 2.17 demonstrates how temperature, relative humidity, and cathode pressure influence membrane degradation. As the operating temperature rises, the electro-

chemical reactions driving the degradation process are enhanced, resulting in a significant reduction in membrane thickness. According to Arrhenius law (2.35), with an activation energy of E_5, membrane degradation increases by 1.5 times when the temperature is elevated from 80 °C to 90 °C. Likewise, the initial permeability of oxygen gas through the membrane also increases with this temperature change. Consequently, elevated temperatures substantially accelerate chemical degradation.

Additionally, the generation of hydrogen peroxide (H_2O_2) is exacerbated by an elevated gas crossover rate. When contrasting the baseline condition at 1.5 atm with the high-pressure scenario at 2.0 atm, the latter leads to a more rapid degradation of the membrane. As a result, significant structural changes occur, adversely affecting its gas permeation characteristics. This heightened gas crossover flux further accelerates the chemical degradation of the membrane.

The simulation also indicates the membrane's mass loss and thickness across varying relative humidity levels, with the highest rate of chemical degradation occurring at low relative humidity values.

2.5 Summary and Conclusion

This chapter presents a microscale degradation model for the membrane electrode assembly in PEM fuel cells, focusing specifically on the catalyst layer and the proton exchange membrane. The model aims to assess the health state of PEMFCs by examining the degradation mechanisms impacting both platinum catalysts and the membrane under varying operational conditions.

A physics-based Pt catalyst degradation model is introduced to predict the change in electrochemical surface area during PEMFC aging, as influenced by different operating parameters. This model establishes links between operating conditions and the ECSA degradation rate, incorporating primary degradation mechanisms such as Pt dissolution, Ostwald ripening, coagulation, and corrosion. A component-level framework is emphasized as essential for accurately characterizing the aging of PEMFCs. Extending beyond the catalyst layer, this study incorporates a semi-empirical degradation model for membrane thickness, based on the fluoride release rate, to estimate membrane thinning over time. This integration enables a comprehensive view of degradation across both the membrane and electrodes. A microscale model was developed to simulate degradation over a range of parameters, including temperature and humidity, and validated using experimental data for catalyst degradation. However, further experimental data is needed for a complete evaluation of membrane degradation. Additionally, a detailed Pt catalyst model captures the dynamic behavior of platinum particles, making it useful in prognostic assessments to determine the aging state and predict future PEMFC losses. This information can guide timely maintenance interventions to extend the service life of PEMFCs.

Further refinement is essential, particularly in integrating the degradation model into a macroscale framework that can adjust PEMFC performance in real time to account for system changes due to degradation. Such integration is critical for enabling predictive control and gaining insights into how microscale degradation affects overall fuel cell performance. Additionally, understanding the direct influence of the fuel cell's internal states on degradation underscores the need for an advanced framework to support accurate prognostics. This will be talked about in the next chapter.

Future work could extend this model to incorporate the degradation of other components, such as the gas diffusion layer and bipolar plates. Addressing the interactions between degradation mechanisms in these different components presents a challenging but crucial step toward accurately predicting and analyzing PEMFC degradation. This chapter concludes by affirming the model's capacity to predict degradation and inform strategies to enhance PEMFC durability. The next chapter will focus on embedding the model into performance frameworks to better capture the impact of aging on overall system output and to evaluate its effectiveness in real-world applications.

3 Macro-Scale Model: PEM Fuel Cell Dynamic Model

Sommaire

3.1 Introduction . . . 70
3.2 PEMFC Dynamic Model . . . 72
3.2.1 Model Assumption . . . 73
3.2.2 Mass Transport across the MEA . . . 74
3.2.2.1 Gas transport through the electrode . . . 74
3.2.2.2 Water transport in the membrane . . . 76
3.2.2.3 Membrane gas crossover . . . 78
3.2.2.4 Vapor and water transport through MEA . . . 78
3.2.3 Heat Transport Model . . . 80
3.2.4 Terminal voltage Model . . . 81
3.3 Modeling Framework for Predicting PEMFC Degradation . . . 83
3.3.1 Analysis of Internal States and Parameters . . . 84
3.3.2 Performance . . . 86
3.3.3 Results and discussion . . . 88
3.3.3.1 Simulation under AST . . . 88
3.3.3.2 Simulation under NEDC . . . 89
3.4 Summary and Conclusion . . . 92

3.1 Introduction

This section introduces a framework for integrating a degradation model into a multiphysical dynamic PEM fuel cell system, aimed at predicting fuel cell lifetime and managing factors that affect component longevity and performance under variable load conditions [8, 161]. The primary objective of developing the macro-scale model is to manage and mitigate degradation by monitoring critical variables typically unmeasured but essential for the degradation model. To establish optimal operating conditions, it is vital to understand the real-time variations in the material properties of the PEMFC and the relationships between material degradation rates and operating conditions. There is currently a high demand for the development of an effective degradation model that can predict PEMFC performance over time [134, 162]. Furthermore, degradation of the MEA can also be influenced by the system's dynamic behavior, which must be accounted for in control strategies [163]. The microscale

model continuously updates the fuel cell's performance based on its health status, supporting the development of a more robust control architecture.

In the microscale model, the primary focus is on the membrane and catalyst, highlighting the importance of accurately capturing the internal states of the fuel cell. To achieve this, a 1D through-membrane model should be incorporated, acting as a virtual sensor to monitor internal conditions and provide real-time estimation and prediction of key physical processes, particularly water and heat transport. As discussed in the previous chapter, operating at low temperatures and high relative humidity can lower the degradation rate of the MEA. However, these conditions also heighten the risk of reversible degradation, such as flooding. The dynamic model facilitates the integration of transient state dynamics into a unified framework, enabling multi-layered control that ensures both performance optimization and effective operation of the PEM fuel cell. The framework must strike a balance between mitigating long-term degradation and maintaining short-term efficiency and reliability.

Existing PEM fuel cell models, such as computational fluid dynamics and lumped-parameter approaches, often struggle to fully capture mass transport mechanisms without incurring significant computational costs [164, 165]. In this chapter, we introduce a dynamic model for fuel cells that incorporates key mass transport processes, including two-phase flow within the gas diffusion layer. This model delivers results comparable to a one-dimensional approach, but without the need to solve complex partial differential equations. It employs a physics-based, two-phase, non-isothermal framework to capture critical through-plane transport phenomena in PEM fuel cells. By concentrating on the conditions within the membrane and catalyst layers, the model simplifies the system representation by excluding states associated with the gas diffusion and microporous layers.

This chapter presents a novel dual-scale modeling framework that integrates a multiphysics model with a degradation model tailored for PEM fuel cells. The multiphysics model provides insights into the internal states of the fuel cell, capturing essential variables such as cell voltage, relative humidity, and temperature at each time step, while also enabling interactions with auxiliary components like the compressor, humidifier, and cooling system. Concurrently, the degradation model addresses the key factors impacting PEM fuel cell performance and durability. By integrating these two models, the framework establishes a connection between microscopic degradation processes and macroscopic performance, along with operating parameters. This integration facilitates the estimation the effect of MEA degradation on fuel cell performance and durability under various operating conditions. To enhance the model's usability and reliability, it undergoes comparison through a comprehensive set of AST and is benchmarked against experimental data, ensuring accurate predictions for real-world applications.

3.2 PEMFC Dynamic Model

To accurately model fuel cells based on physical principles, it is essential to capture the dynamics in the through-plane direction. This section presents a reduced-order, one-dimensional, through-plane model of a PEM fuel cell. The model's main advantage lies in its ability to account for transient behaviors in both the membrane and gas states, while also being easily solvable at steady-state conditions.

Modeling PEM fuel cells involves capturing multiple mass transport mechanisms [23], with particular focus on the complex two-phase flow dynamics within the gas diffusion layers. To address these complexities, four partial differential equations (PDEs) describe the distributions of gas concentration, liquid saturation, temperature, and ionomer water content across the cell thickness. These parameters are governed by the following equations [117]:

$$\varepsilon_g \frac{\partial c_i}{\partial t} = \nabla \cdot (D_i \nabla c_i) + S_i \tag{3.1}$$

$$\frac{\varepsilon}{V_w} \frac{\partial s}{\partial t} = \nabla \cdot \left(\frac{\kappa}{V_w \mu} \left(\frac{\partial p_c}{\partial s} \right) \nabla s \right) + S_s \tag{3.2}$$

$$(\rho c_p) \frac{\partial T}{\partial t} = \nabla \cdot (k_T \nabla T) + S_T \tag{3.3}$$

$$\frac{\varepsilon_{ion}}{V_m} \frac{\partial \lambda}{\partial t} = \nabla \cdot \left(\frac{D_w}{V_m} \nabla \lambda + \frac{\xi}{F} i \right) + S_\lambda \tag{3.4}$$

In equation (3.1), only diffusive gas-phase transport is considered in the cell's porous layers, as research has demonstrated that convective transport has a negligible impact on mass transport in fuel cells. Equation (3.2) describes the liquid water saturation within the porous media, while equation (3.3) details conductive heat transfer across the cell layers, accounting for various sources of heat generation. Furthermore, equation (3.4) models water transport in the ionomer phase across the membrane and catalyst layers, incorporating both electro-osmotic drag and diffusion effects.

Our primary focus is on membrane hydration, temperature and water activity on the catalyst layer that effect the PEM fuel cell degradation and performance [166]. To accurately estimate membrane hydration, we need to consider vapor concentrations in the catalyst layers. We use a reduced-order model for mass transport across the MEA, which specifically addresses the conditions of the membrane and CLs. Conversely, the gas diffusion layer and microporous layer conditions introduce intermediate states between the controlled channel environment and the membrane and CL states. These intermediate states can often be consolidated into effective transport properties that remain relatively stable over short time periods [112].

For instance, liquid accumulation in the GDL typically occurs slowly, with minimal variation over just a few seconds. Therefore, in our reduced-order model, the dynamics of these intermediate states can be neglected, and their impact can be effectively captured using a simplified analytical approach for modeling transport properties

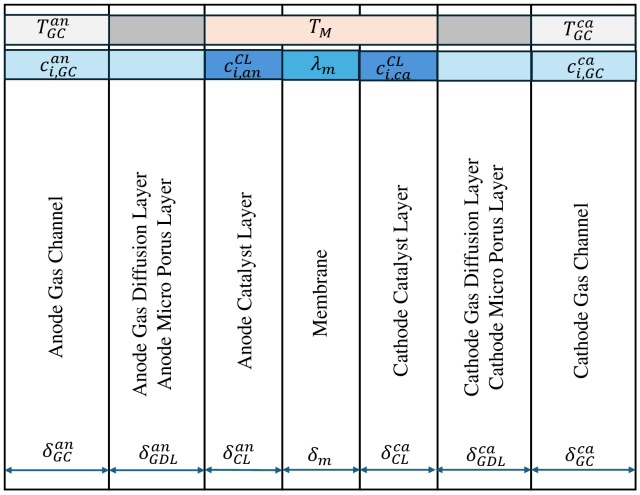

Figure 3.1 – Modeling domain and discretization

[166]. We incorporate liquid water saturation only in the cathode, as condensation typically does not occur in the anode under most operating conditions.

The PEM fuel cell is modeled as a series of five contiguous, homogeneous subdomains, representing a cell-area-averaged, through-plane cross-section of the porous layers. This configuration features a central PEM surrounded by two CLs and two GDLs, while the MPLs are not included. The gas channels (GCs) and bipolar plates at each end define the boundaries of the MEA, as illustrated in figure 3.1. The proposed multiphysical model can identify the distributions of liquid water and gas species in the through-plane direction without the need to solve partial differential equations. This model is based on several fundamental assumptions, with additional specific assumptions regarding various physical processes explained in the following subsections.

3.2.1 Model Assumption

The model is based on the following assumptions:

— **A(3.1) Ideal Gas Model:** All gas species are treated as ideal gases, and the influence of gravity is disregarded.

— **A(3.2) Constant Temperature:** The internal temperature within the catalyst-coated membrane (CCM) is assumed to be uniform and stable throughout its entirety.

— **A(3.3) Boundary Simplifications:** The flow within the gas channels (GCs) is modeled as boundary surfaces with a uniform spatial distribution.

— **A(3.4) Resistance Considerations:** The cell's ohmic resistance is considered to arise solely from the membrane.

— **A(3.5) Steady-State Mass Transport:** Mass transport processes in the gas diffusion layers are assumed to be in a quasi-steady state, with mass transport fluxes treated as uniform across the GDL.

— **A(3.6) Gas Phase Dynamics:** The dynamics of the gas phase are rapid enough that changes in reactant concentrations can be neglected. Only the concentrations of reactants at active sites are significant, and their distribution within the GDL thickness is not critical.

3.2.2 Mass Transport across the MEA

3.2.2.1 Gas transport through the electrode

We present the state equations for the reduced-order model, beginning with the reactant concentrations at the active sites, as their distribution within the MPL and GDL thickness is deemed non-essential according to assumption A(3.5). Utilizing the local current density, we can calculate the molar flux for each reactant. This molar flux, together with the known channel concentration, enables us to estimate the reactant concentration at the active sites.

$$c_{\mathrm{O_2,CL}} = c_{\mathrm{O_2,GC}} - R_{\mathrm{O_2}} \frac{i_{\mathrm{dens}}}{4F} \tag{3.5}$$

$$c_{\mathrm{H_2,CL}} = \frac{RT}{H_{H_2}} \left(c_{\mathrm{H_2,GC}} - R_{\mathrm{H_2}} \frac{i_{\mathrm{dens}}}{2F} \right) \tag{3.6}$$

where H_{H_2} represents Henry's Law constant for H_2. In this context, R_i denotes the total transport resistance of reactant i between the flow channel and the platinum sites. The concentration variables $c_{i,\mathrm{GC}}$ and $c_{i,\mathrm{CL}}$ represent the concentrations of oxygen ($i = O_2$) and hydrogen ($i = H_2$) in the flow channel and at the platinum sites, respectively. The transport resistance for each reactant is calculated by aggregating the diffusive resistances of oxygen and hydrogen species across different layer thicknesses, denoted as δ_{layer}.

$$R_i = \frac{\delta_{\mathrm{GDL}}}{D_i} + \frac{\delta_{\mathrm{CL}}}{D_i} + \frac{D_h}{S_h \cdot D_{i,ref}} \tag{3.7}$$

where D_h is the hydraulic diameter of the channel, and S_h is the Sherwood number. Additionally, $D_i = D_{i,\mathrm{ref}} D_0$ represents the effective diffusivity of species i within the layer. In equation (3.7), the left expression represents the first two terms, which illustrate the diffusive gas transport resistance across GDL and CL, while the last term denotes the convective transport resistance at the GDL-GC interface.

The various diffusion expressions are detailed in table 3.1. To calculate the Fickian gas diffusivities within the pore space of the partially flooded CLs and GDLs, we modify the Chapman–Enskog formula [167]. This modification incorporates the standard

Species	Diffusion Expression	Unit/Ref
O_2 diffuion in air	$D_{O_2,ref} = 0.28$	[cm^2/s]
H_2 diffuion in water vapor	$D_{H_2,ref} = 1.24$	[cm^2/s]
H_2O diffusion in hydrogen at anode	$D_{H_2O,ref} = 1.24$	[cm^2/s]
H_2O diffusion in air at cathode	$D_{H_2O,ref} = 0.36$	[cm^2/s]
Scaling factor for gas diffusion	$D_0 = \frac{\varepsilon}{\tau^2}(1-s)^3 \left(\frac{T}{T_{\text{ref}}}\right)^{1.5} \left(\frac{P_{\text{ref}}}{P}\right)$	[-]

Table 3.1 – Diffusion coefficients of various species

porous media correction factors for porosity ε and tortuosity τ , along with a saturation adjustment of $(1-s)^3$ [168]. The different parameters are detailed in table 3.1.

An interfacial resistance can develop at the platinum surface due to structural modifications of the Pt catalyst and the ionomer at the Pt/ionomer interface. This interaction reduces the effective Pt surface area, thereby decreasing oxygen permeability and impacting the oxygen flux near the Pt surface [169, 170]. In a typical PEMFC, oxygen transport resistance encompasses molecular diffusion resistance within both the GDL and the CL. Reference [169] provides a schematic illustration of the effective ionomer film area and platinum surface area. The ionomer area represents the portion of the ionomer film around a platinum particle that effectively participates in oxygen permeation. This area is assumed to be approximately proportional to the ECSA in the gas phase of the CL and is influenced by permeation resistance through the ionomer film surrounding the catalyst layer agglomerates, as shown in figure 3.2.

As ECSA decreases, a greater flux through the ionomer film is required to maintain the same total current density. This results in a steeper oxygen concentration gradient within the ionomer film, reducing oxygen availability at the Pt particle surfaces.

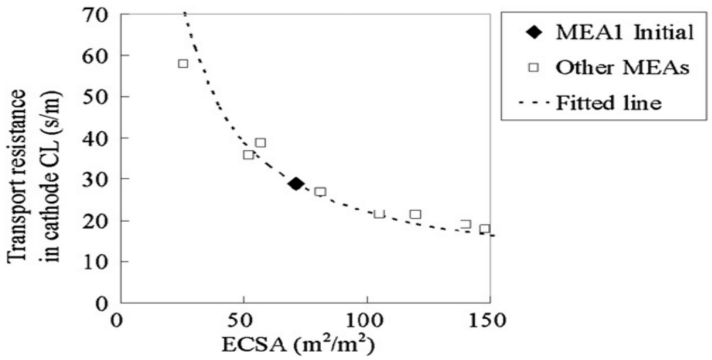

Figure 3.2 – The relationship between ECSA and transport resistance within CL [170]

To account for aging effects on transport mechanisms, particularly for oxygen, we must consider how platinum catalyst degradation during operation impacts these processes. This requires adjustments based on micro-scale information. Consequently, the effective oxygen resistance is modified accordingly and presented as follows:

$$R_{O_2}^{\text{eff}} = R_{O_2} + \frac{\beta_1}{ECS(t)} \tag{3.8}$$

where β_1 fitted parameter to link the impact of degradation on oxygen transport resistance, with $ECS(t)$ representing the active catalyst site (2.30), as quantified by the microscale model.

Parameters	AGC	AGDL	ACL	PEM	CCL	CGDL	CGC
δ layer thickness (μm)	300	160	10	25	10	160	300
ε pore volume fraction (-)	-	0.76	0.4	-	0.4	0.76	-
ε_{ion} ionomer volume fraction (-)	-	-	0.3	1	0.3	-	-
K^T thermal conductivity (W/mK)	-	1.6	0.27	0.3	0.27	1.6	-
(ρc_p) Volumetric heat capacity (J/cm^3K)	-	1.58	1.56	1.9	1.56	1.58	-

Table 3.2 – Parameters Used in the Model Adapted from [118]

3.2.2.2 Water transport in the membrane

In this section, we address the problem of water transport across the thickness of the membrane electrode assembly. Our main objective is to create a model that effectively represents the distribution of water content λ within the catalyst-coated membrane, focusing on three specific states [171]: the anode CL, the membrane itself, and the cathode CL. Water transport through the membrane is primarily governed by diffusion and electro-osmotic drag (EOD) [171]. It is also crucial to acknowledge that the equilibrium water content, along with the rates of sorption and desorption in the membrane, differs depending on whether the membrane is in contact with vapor or liquid water. This approach allows us to accurately model the distribution of λ, which directly influences the performance of the PEM fuel cell and parameters affecting degradation, such as oxygen and hydrogen crossover. Consequently, water transport fluxes within the membrane are represented by three ordinary differential equations:

$$\frac{\varepsilon_{\text{ion}}^{\text{an}}}{V_{\text{mb}}} \frac{d\lambda_{\text{CL}}^{\text{an}}}{dt} = -\frac{1}{\delta_{\text{CL}}^{\text{an}}} N_{\text{mb}}^{\text{an}} + S_{\text{ad}}^{\text{an}} \tag{3.9}$$

$$\frac{\varepsilon_{\text{ion}}^{\text{ca}}}{V_{\text{mb}}} \frac{d\lambda_{\text{CL}}^{\text{ca}}}{dt} = \frac{1}{\delta_{\text{CL}}^{\text{ca}}} \left(N_{\text{mb}}^{\text{ca}} + \frac{i_{\text{dens}}}{2F} \right) + S_{\text{ad}}^{\text{ca}} \tag{3.10}$$

$$\frac{\varepsilon_{\text{ion}}^{\text{mb}}}{V_{\text{mb}}} \frac{d\lambda_{\text{mb}}}{dt} = \frac{1}{\delta_{\text{mb}}} \left(N_{\text{mb}}^{\text{an}} - N_{\text{mb}}^{\text{ca}} \right) \tag{3.11}$$

where ε_{ion} is the ionomer volume fraction, which is assumed to be constant, as indicated in table 3.3. The variables $N_{\text{mb}}^{\text{an}}$ and $N_{\text{mb}}^{\text{ca}}$ represent the water flux through the thickness of the catalyst-coated membrane at the ACL and the CCL, respectively. Additionally, V_{mb} denotes the equivalent volume of the dry membrane, as expressed in equation (2.24). These states are essential for understanding the behavior of water

transport within the membrane, as they impact the overall performance and efficiency of the PEM fuel cell.

The water flux in the ionomer through the thickness of the CCM include the effects of electro-osmotic drag and diffusion is expressed by :

$$N_{\text{mb}} = \xi(\lambda)\frac{i_{dens}}{F} - \frac{1}{V_{\text{mb}}} D_w(\lambda)\frac{\partial \lambda}{\partial x} \tag{3.12}$$

The first term in(3.12) refers to water transported from the anode to the cathode by protons moving through the membrane. The number of water molecules accompanying each proton is referred to as the electro-osmotic drag coefficient (ξ), which is expressed as:

$$\xi(\lambda) = \frac{2.5 \cdot \lambda}{22} \tag{3.13}$$

The second term represents water generated at the cathode during the reaction, which tends to accumulate on that side. Some of this water diffuses back through the membrane towards the anode, a process known as "back diffusion" [172]. This typically occurs due to the significantly higher water concentration at the cathode compared to the anode. Where $D_w(\lambda)$ is the diffusion coefficient of water in Nafion expressed by [173]:

$$D_w(\lambda) = \varepsilon_{ion}^{1.5} \frac{3.842\lambda^3 - 32.03\lambda^2 + 67.74\lambda}{\lambda^3 - 2.115\lambda^2 + 33.013\lambda + 103.37} \times 10^{-6} \cdot \exp\left[\frac{20\text{kJ/mol}}{R}\left(\frac{1}{T_0} - \frac{1}{T}\right)\right] \tag{3.14}$$

The absorption and desorption of water vapor into and out of the ionomer occur over a finite period, typically on the order of an hour, rather than instantaneously. To account for the significant resistance at the ionomer-gas interface during water transport, the sorption source term S_{ad} is defined as [112]:

$$S_{\text{ad}} = \begin{cases} k_a \frac{1}{V_{mb}\delta_{\text{CL}}}(\lambda_{\text{eq}} - \lambda) & \text{if } \lambda < \lambda_{\text{eq}} \text{ (absorption)} \\ k_d \frac{1}{V_{mb}\delta_{\text{CL}}}(\lambda_{\text{eq}} - \lambda) & \text{if } \lambda > \lambda_{\text{eq}} \text{ (desorption)} \end{cases} \tag{3.15}$$

where λ_{eq} denotes the dynamic quasi-equilibrium water content for the ionomer, which depends on the water activity a_w given by:

$$\lambda_{\text{eq}} = 0.043 + 17.81 \cdot a_w - 39.85 \cdot a_w^2 + 36.0 \cdot a_w^3 \tag{3.16}$$

The water activity within the pores of the CL, denoted as a_w, is defined as the ratio of the total molar concentration of water vapor, c_v, to the saturated vapor concentration at the current temperature c_{sat} are given in table 3.3.

The interfacial water transfer coefficient, $k_{a,d}$, for the mass transfer of water vapor in Nafion membranes is given by Ge et al. [174]:

$$k_{a,d} = a_{a,d} f_v(\lambda) \exp\left[\frac{20\,\text{kJ/mol}}{R}\left(\frac{1}{T_0} - \frac{1}{T}\right)\right] \tag{3.17}$$

where a_a and a_d represent the absorption and desorption prefactors, respectively. Additionally, $f_v(\lambda)$, denoting the volume fraction of water in the ionomer, is given by equation (2.23).

Description	Parameter	Expression/Value [Unit]
Water activity	a_w	$\frac{c_v}{C_{\text{sat}}}$ [–]
Saturated vapor concentration	c_{sat}	$\frac{P_{\text{sat}}}{RT}$ [mol · cm^{-3}]
Saturation pressure	P_{sat}	$\exp\left(23.1963 - \frac{3816.44}{T-46.13}\right)$ [Pa]
Equivalent volume of dry membrane	V_m	$\frac{EW}{\rho_{\text{mb}}}$ [cm^3 · mol^{-1}]
Molar volume of liquid water	V_w	18 [cm^3 · mol^{-1}]
Absorption coefficient	a_a	3.53×10^{-3} [cm · s^{-1}]
Desorption coefficient	a_d	1.42×10^{-3} [cm · s^{-1}]

Table 3.3 – Physical parameters for water transport

3.2.2.3 Membrane gas crossover

The model accounts for the crossover of reactant gases through the membrane as a contributor to membrane degradation. As membrane thickness decreases, hydrogen crossover increases, which directly impacts PEMFC performance by contributing to performance loss. In this model, it is assumed that hydrogen migrating to the cathode reacts instantaneously with available oxygen, forming water and hydrogen peroxide. The total crossover fluxes are estimated using the following equation:

$$N_i = \psi_i \frac{P_i^{\text{ca}} - P_i^{\text{an}}}{\delta_{\text{mb}}} \tag{3.18}$$

where p_i^{ca} and p_i^{an} denote the partial pressures of the gas species i (e.g., H_2, O_2) at the cathode and anode, respectively. ψ_i denotes the corresponding membrane gas permeability of species i, which is given in table 3.4 for different species.

Species	Permeability [mol · cm^{-1} · bar^{-1} · s^{-1}]
O_2	$\psi_{O_2} = 6.74 \times 10^{-9} \exp\left(-\frac{21280}{RT}\right) + f_v \times 50.50 \times 10^{-9} \exp\left(-\frac{20470}{RT}\right)$
H_2	$\psi_{H_2} = 15.70 \times 10^{-9} \exp\left(-\frac{20280}{RT}\right) + f_v \times 45.00 \times 10^{-9} \exp\left(-\frac{18930}{RT}\right)$

Table 3.4 – Membrane gas permeability

3.2.2.4 Vapor and water transport through MEA

In terms of water vapor transport, we concentrate on the vapor concentrations within the CL, as these concentrations significantly impact the ionomer's ability to absorb water. Therefore, the dynamics of vapor within the CLs are represented by the following equations:

$$\varepsilon_{\mathrm{g},CL}^{\mathrm{an}} \frac{dc_{\mathrm{v},CL}^{\mathrm{an}}}{dt} = \frac{1}{\delta_{CL}^{\mathrm{an}}} \left(\frac{c_{\mathrm{v},GC}^{\mathrm{an}} - c_{\mathrm{v},CL}^{\mathrm{an}}}{R_{\mathrm{v}}^{\mathrm{an}}} \right) - S_{\mathrm{ad}}^{\mathrm{an}} \tag{3.19}$$

$$\varepsilon_{\mathrm{g},CL}^{\mathrm{ca}} \frac{dc_{\mathrm{v},CL}^{\mathrm{ca}}}{dt} = \frac{1}{\delta_{CL}^{\mathrm{ca}}} \left(\frac{c_{\mathrm{v},GC}^{\mathrm{ca}} - c_{\mathrm{v},CL}^{\mathrm{ca}}}{R_{\mathrm{v}}^{\mathrm{ca}}} \right) + S_{\mathrm{pc}}^{\mathrm{ca}} - S_{\mathrm{ad}}^{\mathrm{ca}} \tag{3.20}$$

$$\varepsilon_{\mathrm{CL}}^{\mathrm{ca}} \frac{ds_{\mathrm{CL}}^{\mathrm{ca}}}{dt} = \frac{1}{\delta_{\mathrm{CL}}^{\mathrm{ca}}} \left(\frac{s_{\mathrm{GDL}}^{\mathrm{ca}} - s_{\mathrm{CL}}^{\mathrm{ca}}}{R_{\mathrm{s}}^{\mathrm{ca}}} \right) - V_w S_{\mathrm{pc}}^{\mathrm{ca}} \tag{3.21}$$

The vapor concentration in the CL is influenced by the vapor flux entering or exiting the CL, as well as by source terms related to the ionomer's water absorption or desorption, represented by S_{ad} in equation (3.15). Additionally, the vapor concentration in the CCL accounts for phase change processes, denoted as S_{pc}. R_v is the resistance to vapor transport between the CL and the GC, which depends on vapor diffusion across different layers, as given by equation (3.7). The gas phase porosity, ε_g, is expressed as:

$$\varepsilon_g = (1 - s)\varepsilon$$

where ε represents the pore-space volume fraction and s indicates the liquid water saturation. For water transport, the source terms account for phase change processes, including evaporation and condensation, represented by S_{pc}. A commonly used approach in macro-homogeneous MEA modeling incorporates liquid-vapor phase change by assuming that mass transfer is driven by the difference between the vapor concentration and the vapor saturation concentration [118, 175, 176].

$$S_{\mathrm{pc}} = \begin{cases} k_{\mathrm{e}} s_{red} \left(c_v - c_{\mathrm{sat}}(T)\right) & \text{if } c_v < c_{\mathrm{sat}}(T),\ s_{red} > 0 \\ k_{\mathrm{c}} (1 - s_{red}) \left(c_v - c_{\mathrm{sat}}(T)\right) & \text{if } c_v \geq c_{\mathrm{sat}}(T) \end{cases} \tag{3.22}$$

Here, the coefficients k_e and k_c represent the evaporation/condensation transfer coefficients [118]. The dependence of the phase change interface on liquid water saturation is expressed through the reduced saturation.

$$s_{red} = \frac{s - s_{im}}{1 - s_{im}} \tag{3.23}$$

where s_{im} represents the immobile or inaccessible saturation, referring to liquid water that does not participate in transport pathways or phase changes, often due to spatial isolation. This value is estimated to be $s_{im} = 0.12$ [118]. Liquid accumulation transport in the CCL is influenced by capillary resistance to liquid water, which depends on its diffusivity, as well as on condensation and evaporation processes. The capillary resistance to liquid water is denoted by :

$$R_s = \frac{\delta_{GDL}}{D_s} + \frac{\delta_{CL}}{D_s} \tag{3.24}$$

The capillary liquid water diffusivity, denoted by D_{s}, is defined by the rate at which liquid water moves through the porous structure of the CCL due to capillary forces.

This diffusivity is influenced by several factors, including the pore size distribution, the connectivity of the pore network, and the viscosity of the liquid water, whic given by [177].

$$D_s = \frac{\kappa}{\mu}\frac{\partial p_c}{\partial s} \tag{3.25}$$

Where μ is the dynamic viscosity of water, and both the hydraulic permeability κ and the capillary pressure p_c depend on the water saturation. Many correlations have been proposed to describe the relationship between capillary pressure and saturation for various GDLs. Among these, the Leverett J-function is commonly used as a closure equation to model this relationship. The Leverett J-function, as detailed in the work of Leverett et al. [178], provides a framework for understanding how capillary pressure varies with water saturation in different GDLs.

$$p_c = -\frac{\sigma_l \cos\left(\theta_{\text{layer}}\right)}{\sqrt{\frac{\kappa_{\text{abs}}}{\varepsilon}}}\left[1.417s - 2.12s^2 + 1.263s^3\right] \tag{3.26}$$

Where σ_l represents the surface tension of liquid water, θ_{layer} indicates the contact angle of liquid water on the surface of the layer, and κ_{abs} represents the absolute (intrinsic) permeability of the porous medium.

The second parameter in the liquid water flux equation is the hydraulic permeability κ, which has a great impact on the liquid water distribution. It is modeled as [118]

$$\kappa = \left(10^{-6} + s_{\text{red}}^3\right)\kappa_{\text{abs}} \tag{3.27}$$

A reasonable estimate for the liquid water saturation at the CGDL/GC interface $s_{im} = 0.12$ can be found with the notion of equivalent capillaries in the GDL through which the liquid water is transported.

3.2.3 Heat Transport Model

The internal temperature in a PEM fuel cell plays a crucial role in MEA degradation. The dynamics of the membrane temperature are governed by:

$$\frac{dT_{mb}}{dt} = \frac{1}{(\rho c_p)_{mb}}\left(\frac{T_{mb} - T_{GC}}{\delta^{ca} R_T^{ca}} + \frac{T_{mb} - T_{GC}}{\delta^{an} R_T^{an}}\right) + \frac{S_T^{mb}}{(\rho c_p)_{mb}} + \frac{S_T^{ca}}{(\rho c_p)_{CL}} + \frac{S_T^{an}}{(\rho c_p)_{CL}} \tag{3.28}$$

The temperature of the membrane is affected by heat transfer from the gas and coolant channels, denoted as T_{GC}, as well as by various heat sources and sinks. The term S_T represents these heat sources. The total thickness of the cell layers on either side is represented by $\delta^{\text{an/ca}}$, while $R_T^{\text{an/ca}}$ indicates the overall heat transport resistance between the membrane and the gas channels. This resistance is the sum of conductive and convective heat transport resistances and is calculated as follows:

$$R_T = \frac{\delta_{\text{GDL}}}{k_{\text{T,GDL}}} + \frac{\delta_{\text{CL}}}{k_{\text{T,CL}}} + \frac{1}{h_{\text{conv}}} \tag{3.29}$$

where $k_{\text{T,layer}}$ denotes the effective thermal conductivity of the layer, h_{conv} represents the heat convection coefficient, and (ρc_p) is the volumetric heat capacity, as detailed in table 3.2. The heat source terms for equation (3.28) are provided in table 3.5.

Domain	**Heat Source Terms**
Anode CL (ACL)	$-S_{pc}H_{pc} + S_{\text{ad}}H_{\text{ad}} + H_{\text{HOR}}$
Cathode CL (CCL)	$-S_{pc}H_{pc} + S_{\text{ad}}H_{\text{ad}} + H_{\text{ORR}}$
Membrane	$R_{\text{mb}}\, i^2_{\text{dens}}$

Table 3.5 – Heat source terms for equation 3.28

The terms H_{ad} and H_{pc} denote the molar enthalpies of desorption and vaporization, respectively. The heat of reaction for the hydrogen oxidation reaction and the oxygen reduction reaction can be expressed as follows [112]:

$$H_{\text{HOR}} = \frac{i_{\text{dens}}}{\delta^{\text{an}}_{\text{CL}}} \left(\eta_{\text{HOR}} + \Pi_{\text{HOR}}\right) \tag{2.14}$$

$$H_{\text{ORR}} = \frac{i_{\text{dens}}}{\delta^{\text{ca}}_{\text{CL}}} \left(\eta_{\text{ORR}} + \Pi_{\text{ORR}}\right) \tag{2.15}$$

In these equations, Π_{HOR} and Π_{ORR} represent the Peltier coefficients for the HOR and ORR, respectively, while R_{mb} denotes the resistance of the membrane. The terms η_{HOR} and η_{ORR} correspond to the activation overpotentials associated with the HOR and ORR. Analyzing these heat contributions is essential for estimating the internal temperature state of PEM fuel cells, as they directly influence the electrochemical reactions and degradation mechanisms.

3.2.4 Terminal voltage Model

The performance of a fuel cell can be assessed based on the degraded parameters that affect its operation. The cell voltage U is derived from the difference between the open circuit voltage and the irreversible losses. These losses can be attributed to major factors such as activation losses, ohmic losses. The expression for the fuel cell voltage is given by:

$$U = U_{\text{OCV}} - \eta_{\text{ORR}} - \eta_{\text{HOR}} - \eta_{\text{ohm}} \tag{3.30}$$

In this equation, the term U_{OCV} represents the open circuit voltage of the fuel cell. The second term, η_{ORR}, accounts for the cathode activation overpotential, while η_{HOR} represents the anode activation overpotential. The term η_{ohm} describes the ohmic

losses due to ionic resistance . The voltage generated by the fuel cell is calculated by subtracting these losses from the open circuit voltage U_{OCV}, as given by:

$$U_{\mathrm{OCV}} = 1.229 - 8.5 \times 10^{-4} \, (T - 298.15) + \frac{RT}{4F} \ln\left(p_{\mathrm{H_2}} \cdot p_{\mathrm{O_2}}^{1/2}\right) \tag{3.31}$$

These losses, namely activation losses and ohmic losses, are comprehensively explained in reference [179]. The cathode activation loss is determined using the Tafel equation, where the current losses associated with membrane degradation are accounted for by including the current loss due to hydrogen crossover, expressed as follows:

$$\eta_{\mathrm{ORR}} = \frac{RT}{\alpha_{ca} F} \ln\left(\frac{i + i_{cross}}{i_{0,\mathrm{ca}}}\right) \tag{3.32}$$

where $i_{0,\mathrm{ca}}$ represents the exchange current density at the cathode. The activation loss resulting from the decay of the electrochemical active surface area can be described by the direct relationship between ECSA and the value of $i_{0,\mathrm{ca}}$, as mentioned in reference [179]. [112, 180]:

$$i_{0,ca} = i_{0,ca}^{ref} ECS(t) \left(\frac{P_{O_2}}{P_0}\right)^{\gamma} exp\left[-\frac{E_{ca}}{RT}\left(1 - \frac{T}{T_0}\right)\right] \tag{3.33}$$

where $ECS(t)$ is the effective surface area of catalyst layer, and θ denotes the oxide coverage. The term E_{ca} signifies the activation energy associated with the ORR. The exponential terms capture the effects of temperature and oxide coverage on the ORR kinetics, indicating that higher temperatures and lower oxide coverage lead to increased exchange current density.

Hydrogen crossover in a PEM fuel cell refers primarily to the performance losses associated with membrane degradation. This phenomenon can significantly impact the fuel cell's performance, particularly by increasing activation losses, which in turn reduces overall efficiency. The effect of hydrogen crossover can be quantified using the crossover current density, i_{cross}, expressed as

$$i_{\mathrm{cross}} = \frac{P_{H_2} \psi_{H_2}}{\delta_{mb}} \cdot 2F. \tag{3.34}$$

In this equation, P_{H_2} represents the partial pressure of hydrogen, ψ_{H_2} is the diffusion coefficient for hydrogen, δ_m is the thickness of the membrane, and F is Faraday's constant. This relationship indicates that the crossover current density is directly proportional to the partial pressure and diffusion coefficient while being inversely proportional to the membrane thickness.

The anode activation overpotential, η_{HOR}, accounts for the energy barrier that must be overcome for the HOR to occur at the anode. It is given by the equation

$$\eta_{\mathrm{HOR}} = \frac{RT}{\alpha_{an} F} \ln\left(\frac{i}{i_{0,\mathrm{an}}}\right). \tag{3.35}$$

Here, R is the universal gas constant, T is the membrane temperature, α_{an} is the

charge transfer coefficient for the anode, i is the current density, and $i_{0,\text{an}}$ is the exchange current density at the anode. This equation shows that the anode activation overpotential increases with the logarithm of the current density, indicating that higher currents require greater activation energy.

Ohmic losses, denoted as η_{ohm}, refer to the voltage drop due to electrical resistance faced by the flow of ions through the proton exchange membrane. This can be calculated as

$$\eta_{\text{ohm}} = R_{\text{ohm}} i, \tag{3.36}$$

where R_{ohm} is the ohmic resistance, defined by

$$R_{\text{ohm}} = \frac{\delta_{\text{mb}}}{\sigma_{\text{ion}}}. \tag{3.37}$$

In this context, δ_{mb} represents the membrane thickness, and σ_{ion} is the membrane conductivity, which is crucial for determining the efficiency of ion transport through the membrane. The membrane conductivity can be expressed as

$$\sigma_{\text{ion}} = (0.5139\lambda - 0.326) \exp\left(1268\left(\frac{1}{303} - \frac{1}{T}\right)\right), \tag{3.38}$$

where λ is the water activity in the membrane, and the exponential term accounts for the temperature dependence of the membrane conductivity.

By understanding these relationships and their implications, one can better model PEM fuel cell performance and adjust for degradation effects that lead to increased hydrogen crossover and efficiency losses, ultimately optimizing the design and operation of PEM fuel cells.

3.3 Modeling Framework for Predicting PEMFC Degradation

In previous work, a multiphysical model was developed to improve aging prediction in PEM fuel cells, specifically for optimizing control strategies. The primary objective of this PEMFC model is to establish a comprehensive approach that enables efficient determination of the effect of operating conditions on degradation for fuel cells in transport applications, thereby minimizing irreversible aging through control strategies. This model is constructed by integrating a localized, multi-scale framework that details electrochemical catalyst and membrane degradation mechanisms at the cell level with a broader fuel cell performance model. This multiphysical model can easily incorporate different scales within the fuel cell system as shown in figure 3.3, facilitating seamless inclusion of auxiliary components such as compressors, humidifiers, and cooling systems [8].

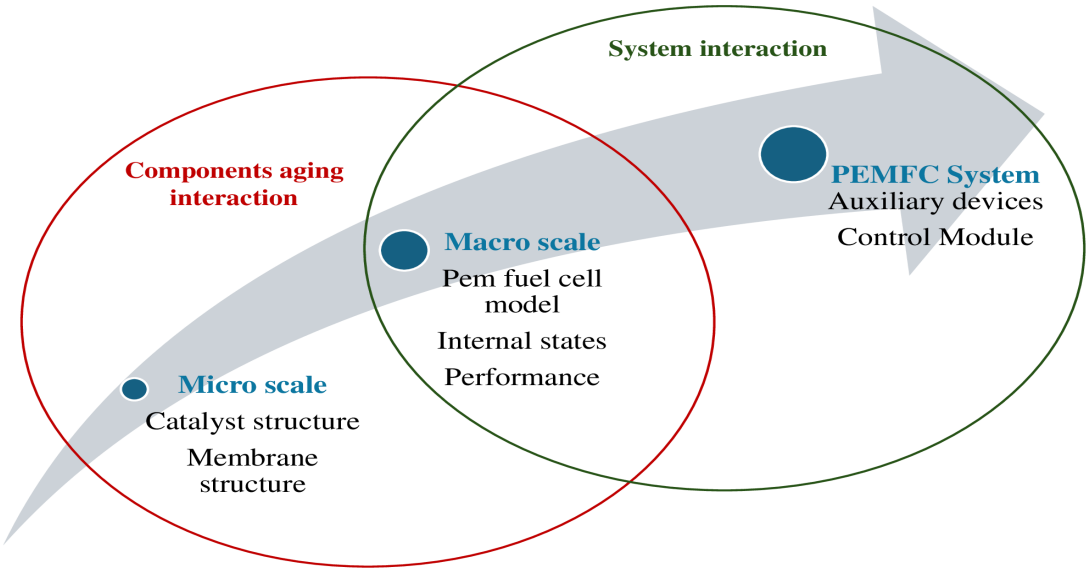

Figure 3.3 – Interactions across various levels within the fuel cell system

3.3.1 Analysis of Internal States and Parameters

The performance of a PEM fuel cell stack and system is shaped by numerous transient processes, each with a unique time constant. These interdependent processes create a complex, multiphysics, and multiscale environment. The convergence of degradation and transient effects across these time scales adds further complexity, making accurate predictions of system lifetime and remaining useful life challenging. Effective control strategies must account for the influence of these transient dynamics as well as localized effects within the membrane and catalyst layers. This modeling framework enables access to internal parameters, allowing for the tracking of transient effects as they accumulate and contribute to overall degradation over time.

In figure 3.4, the model's capability to estimate the internal states and parameters of the PEM fuel cell is illustrated. This capability enables detailed quantification of degradation mechanisms under both transient and steady-state conditions. By accurately capturing these internal dynamics, the model enhances predictive accuracy, providing more reliable estimations of fuel cell aging and remaining useful life. Additionally, the model's insights into internal states facilitate the development of control strategies aimed at managing and mitigating degradation, ultimately improving both performance and durability.

Furthermore, this model can estimate irreversible degradation effects, such as water accumulation (figure 3.4e), which decrease system performance. By addressing these degradation mechanisms, particularly under suboptimal operating conditions linked to water management, the model enables strategies to minimize aging and extend

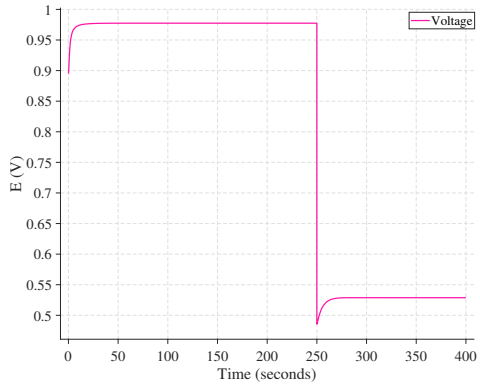

(a) Cell voltage

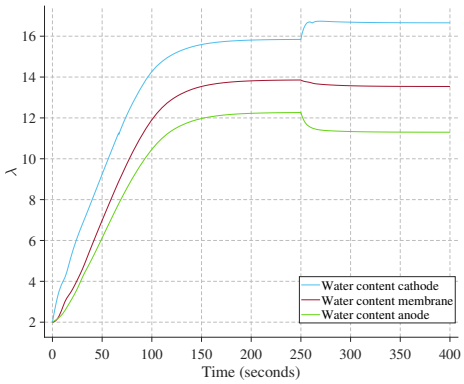

(b) Water content

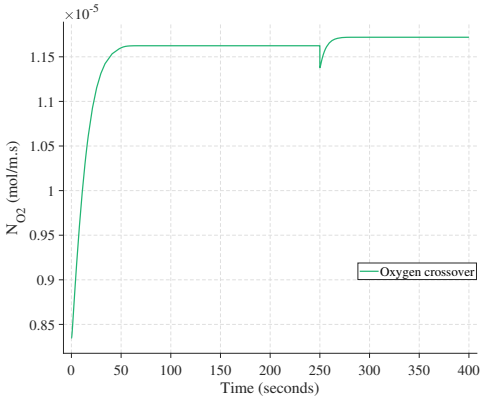

(c) Oxygen crossover

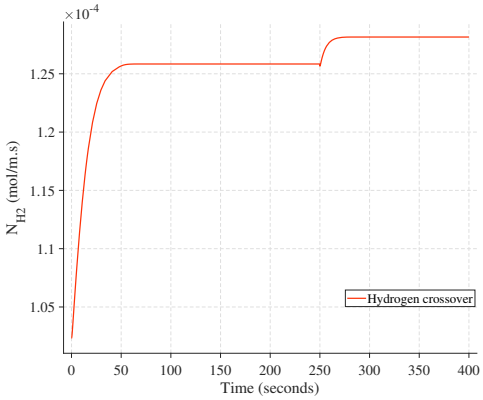

(d) Hydrogen crossover

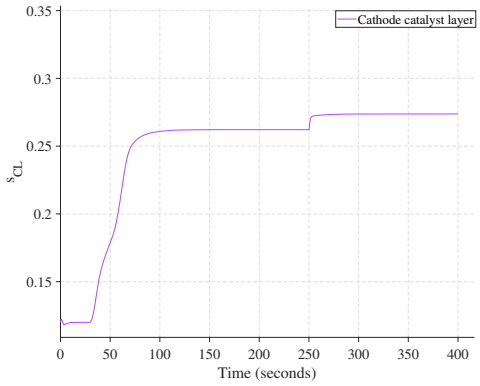

(e) Saturation

Figure 3.4 – Overview of PEM fuel cell parameters

fuel cell lifespan.

3.3.2 Performance

The degradation model of the MEA is integrated within a macro-scale fuel cell performance model to capture the coupled effects of operational and environmental factors on cell efficiency and durability. This integrated approach, as illustrated in figure 3.5, enables a comprehensive analysis of performance decline over time, facilitating predictive insights into fuel cell lifespan.

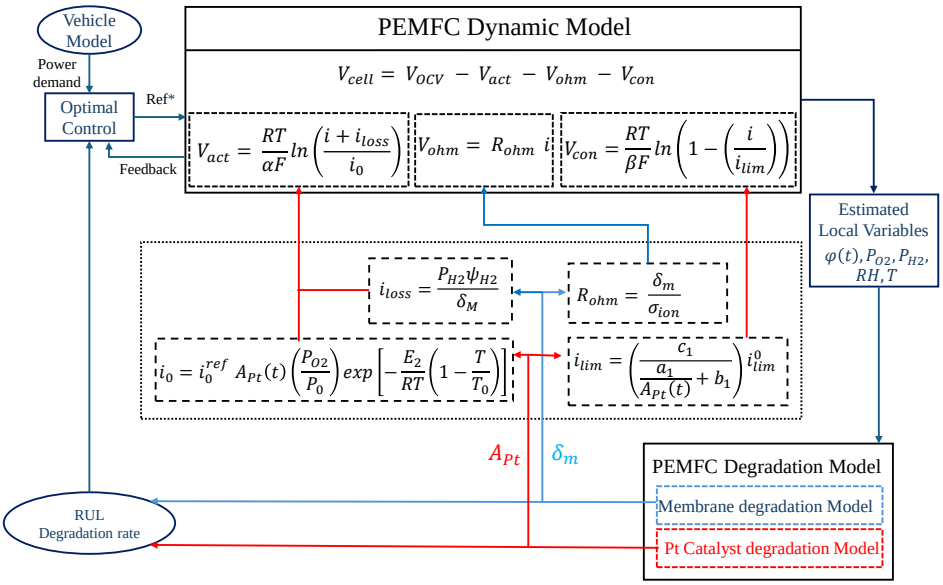

Figure 3.5 – Framework for coupling component level degradation to PEMFC performance model

Structural changes in the active catalyst sites and membrane thickness serve as key indicators of degradation, directly influencing activation losses by reducing the effectiveness of the oxygen reduction reaction (ORR) and increasing hydrogen permeability. Meanwhile, the integration of the degradation and performance models enhances the predictive accuracy of these factors.

The ECSA is determined using a micro-scale model applied specifically to the catalyst layer. This model tracks the progression of particle radius degradation over time while assuming uniform spatial development across the catalyst surface, thereby simplifying the integration with the macro-scale model and significantly reducing computational time. Additionally, changes in membrane thickness are leveraged to quantify hydrogen crossover as it progresses over time.

Conversely, the macro-scale model accounts for the dynamic influences of environmental conditions, allowing us to estimate internal fuel cell states, including

parameters like humidity, partial pressure, and membrane water content. Figure 3.6 provides a flowchart illustrating the interactions between these two submodels, detailing how the degradation indicators from the micro-scale model impact the overall performance predictions of the macro-scale model.

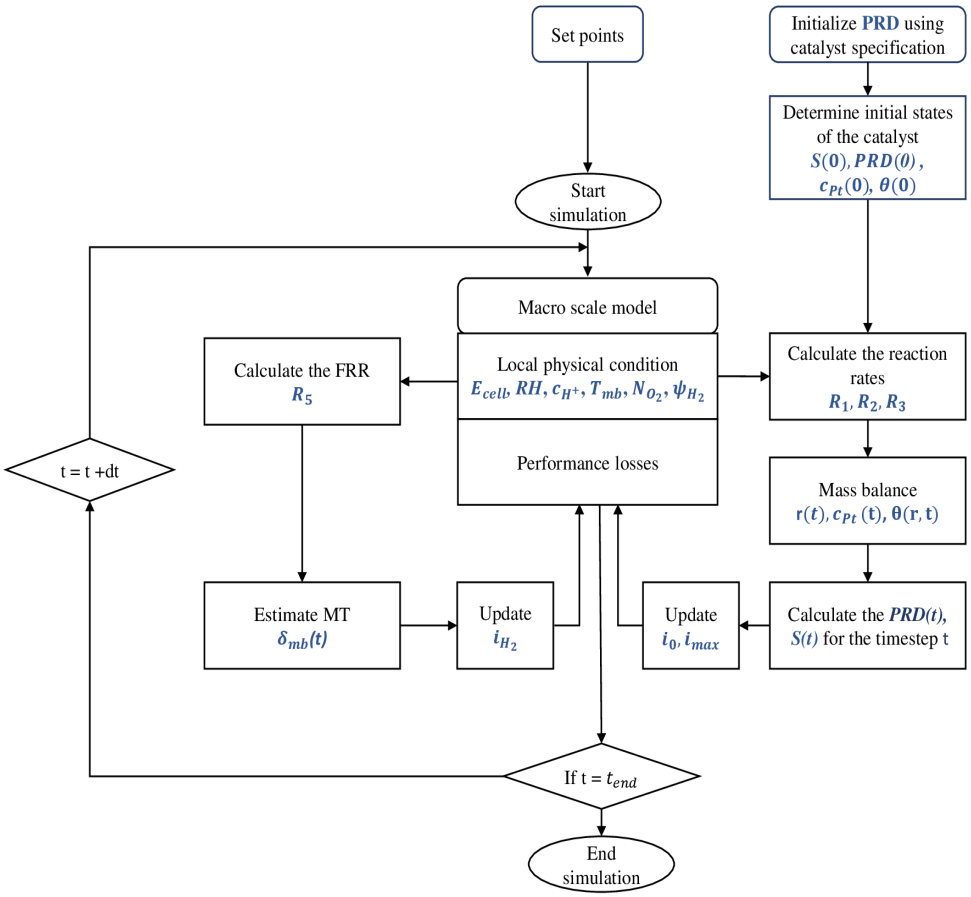

Figure 3.6 – Flowchart for simulating the dual-scale model of PEM fuel cell degradation

This integration enables real-time predictions of PEMFC aging resulting from catalyst and membrane degradation, such integration is essential for developing effective control strategies aimed at enhancing performance and durability, as it provides crucial insights into the internal states of the cells, which are rarely accessible through direct measurements. In addition, this framework is designed to systematically evaluate and manage the trade-offs between performance and durability. Moreover, the fuel cell model can be seamlessly extended to encompass the entire system, integrating all necessary auxiliary components to ensure optimal fuel cell operation.

3.3.3 Results and discussion

In this section, the simulation and validation processes will be enhanced using additional data from the experimental results.

3.3.3.1 Simulation under AST

The decay in open-circuit voltage (OCV) is commonly utilized as an indicator of State of Health (SoH) for proton exchange membrane fuel cells (PEMFCs). In this study, we compare the OCV drop predicted by our model, as shown in figure 3.7, with experimental data presented in [51]. The operating conditions are set to accelerate membrane degradation with the following parameters: relative humidity (RH) = 30%, temperature = 95° C, pressure $P = 2.5\,\text{bar}$, and idle current density $i_{\text{dens}} = 0.06\,\text{A/cm}^2$. The combined component-level model effectively captures the initial phase of the OCV curve, reflecting the rapid degradation of the electrochemically active surface area (ECSA) in the early stages, followed by stabilization. Furthermore, our model accurately represents the latter phase of the voltage drop, attributed to hydrogen crossover and membrane degradation.

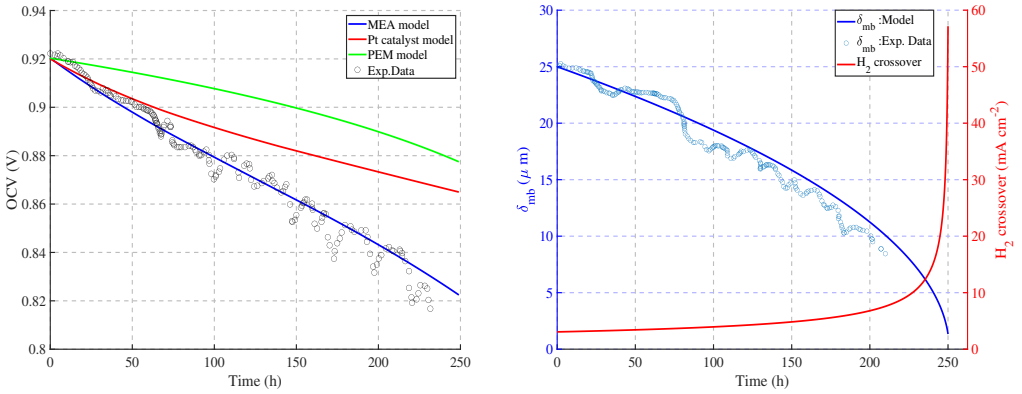

(a) The OCV change over time

(b) Changes in MT and i_{H_2}

Figure 3.7 – Comparative analysis of OCV and hydrogen crossover behavior over time.

In the second part, we ran the simulation model under Accelerated Stress Testing (AST) potential cycling, using a rectangular sweep between 0.6 V and 0.95 V. The RH was fixed at 50%, and the cell temperature was set to 80°C, with both anode and cathode pressures maintained at 1.5 bar. The membrane degradation rate was significantly influenced by the applied voltage near OCV and by the ECSA. Figure 3.8 illustrates that at the beginning of fuel cell operation lifetime, the loss of active surface area is dominant, accompanied by a linear increase in membrane degradation rate throughout the fuel cell's lifetime. In this case under the cited operation conditions, catalyst degradation becomes almost more significant over the fuel cell's lifetime, reaching a critical threshold first at 430 hours, while the membrane remains in good condition. Therefore, To enhance the overall health state of the PEMFC, it is vital to

optimize and balance the lifespan of each component, ensuring maximum utilization before reaching the failure threshold, ideally synchronizing their end-of-life (EOL) to maximize overall longevity. This can be achieved by monitoring relative humidity, which exhibits contradictory effects. Similarly, it is crucial to achieve optimal performance with minimal health degradation. Regarding temperature, operating at higher temperatures may enhance fuel cell performance, albeit with potential trade-offs associated with PEM fuel cell aging. However, this approach requires validation and refinement through further experimental data and investigation.

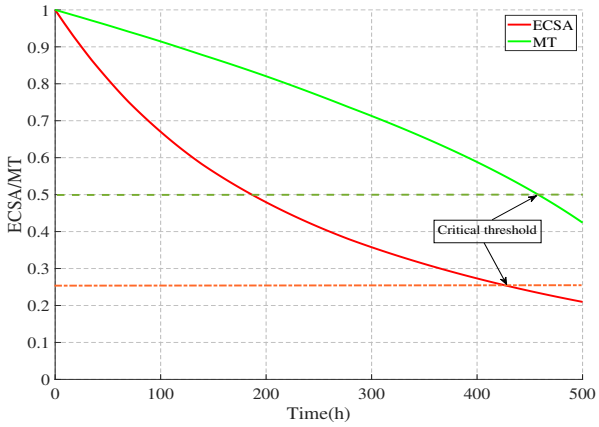

Figure 3.8 – ECSA and MT evolution over time

3.3.3.2 Simulation under NEDC

After analyzing the model's ability to capture the different operating conditions and observing that the simulated data aligns well with the experimental data, this section highlights the primary goal of this dual-scale model, which is to predict catalyst degradation during real-world driving cycles, specifically the the New European Driving Cycle (NEDC). The long-term dynamic durability test experiment aims to measure ECSA over a duration of 500 hours. All relevant details regarding the experiment, including specific tests , can be found in reference [181]. In this subsection, we do not consider any information regarding the membrane characteristics, as we neglect the impact of the membrane on performance during the first 500 hours under NEDC. Additional information and experimental data are needed to validate the overall degradation model.

The predicted ECSA loss and relative performance degradation under driving cycle conditions are presented in figure 3.10. Incorporating the detailed degradation model into a comprehensive performance model will enable the direct conversion of driving speed into voltage cycle data, as depicted in the figure 3.9. The results appear to be reasonable and suggest that with adequate validation data, this tool could prove to be valuable. However, fitting the model under AST conditions may explain the slight overestimation of degradation during the last 250 operational hours, as shown in

figure 3.10. To enhance precision, additional experimental data, particularly from fuel fell vehicles field data, is required.

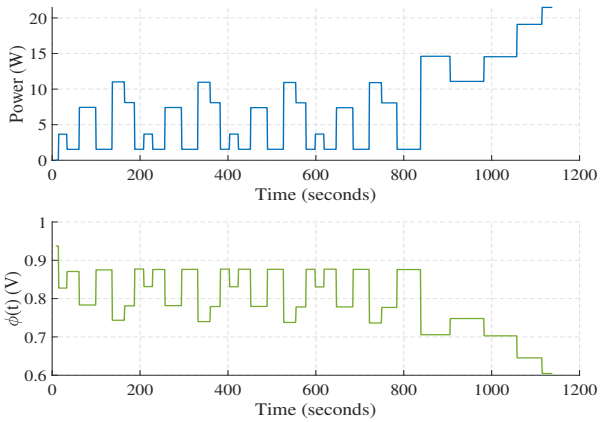

Figure 3.9 – Power and Voltage Load for FC-DLC

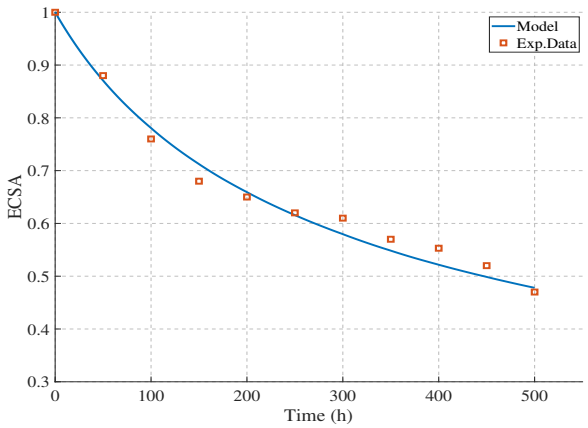

Figure 3.10 – ECSA evolution under NEDC

In figure 3.11, we examine the voltage drop rate calculated using the dual-scale model. It is therefore verified that this dual-scale model enables us to refine and update the voltage drop rate and performance losses.

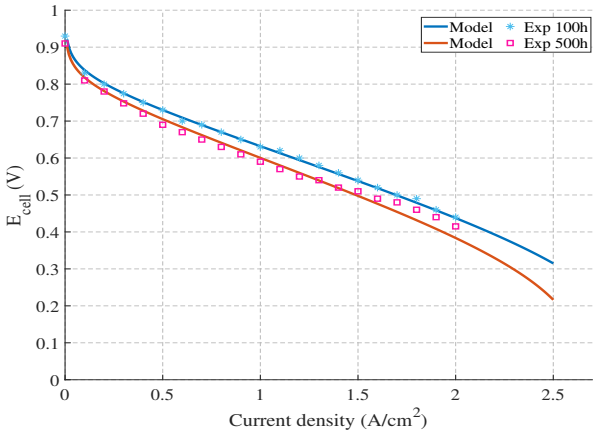

Figure 3.11 – Polarisation curve decay over time under NEDC

3.4 Summary and Conclusion

This study addresses the critical challenge of enhancing the durability of fuel cell components, specifically focusing on the Membrane Electrode Assembly in PEMFC. We propose an innovative dual-scale modeling framework that seamlessly integrates a multi-physics model with a degradation model. This integration facilitates accurate predictions of PEMFC behavior and performance across a range of operating conditions, thereby enabling the development and implementation of optimal control strategies. Additionally, our framework allows for the incorporation of auxiliary devices to effectively manage various parameters, aiming to reduce degradation and ensure the functional integrity of PEMFCs. Moreover, this modeling framework not only considers the internal states and performance metrics of the system but also assesses the impact of aging and the occurrence of irreversible faults. It is designed to capture the transient behavior of the system, providing a comprehensive understanding of its dynamics under varying conditions.

The degradation model serves as a reliable indicator for assessing the aging status of various PEMFC components, thus supporting real-time applications. This approach provides a comprehensive understanding of how factors such as pressure, temperature, voltage, and relative humidity influence PEMFC degradation rates, enabling a balanced optimization of operating conditions that enhances performance while adhering to the constraints of the membrane and platinum catalyst.

The model has been validated against accelerated stress tests and real-world data for the catalyst, including the New European Driving Cycle (NEDC), demonstrating its reasonable assumptions and predictive capabilities. However, accurately tracking the degradation rate remains challenging due to the complex interactions among components. Future work will focus on validating the overlapping degradation processes and refining the proposed models within this framework. Further investigation into the heterogeneity within the cell is also necessary, as variations in local operating conditions such as relative humidity, temperature, and pressure significantly impact MEA degradation across the segmented cell. Employing spatially resolved performance and degradation metrics for the MEA, rather than assuming uniform temporal degradation across the catalyst surface and membrane, is essential for improving the accuracy of our model.

4 Control Strategies for Enhancing PEMFC Longevity

Sommaire

4.1 Inroduction . . . 93
4.2 PEMFC system control overview and durability enhancement control . 95
4.2.1 Overview of two-layer control . . . 95
4.2.2 Durability enhancement control design . . . 96
4.3 Control Objective . . . 96
4.4 Modeling . . . 97
4.4.1 Assumptions . . . 98
4.4.2 MEA Degradation Modeling . . . 98
4.4.2.1 Modeling the Performance of PEMFC . . . 99
4.4.3 State-Space Model for Control . . . 101
4.4.4 Simulation Results . . . 103
4.5 Control Problem Formulation . . . 105
4.6 Control Method: Economic Model Predictive Control . . . 106
4.6.1 MPC principle and EMPC . . . 107
4.6.2 Application to the Fuel Cell Case . . . 109
4.6.3 EMPC Implementation Overview . . . 110
4.6.4 Simulation Results . . . 111
4.7 Experimental Results . . . 113
4.7.1 Test Bench Presentation . . . 113
4.7.2 Test Protocol . . . 113
4.7.3 Future Validation Results . . . 115
4.8 Summary and Conclusion . . . 116

4.1 Inroduction

Fuel cell durability challenges have prompted researchers to develop material solutions such as reversal tolerant anode catalysts, coated cathode catalysts, and membrane additives. While these innovations have improved lifetimes, they often fail to meet both cost and durability targets [182]. Although these materials enhance performance, they typically increase stack costs, and cost-saving measures, such as reducing platinum loading, can negatively impact durability. These shortcomings indicate that material solutions alone are insufficient and should be complemented

with active control strategies to maximize the potential of the materials and achieve more robust, cost-effective fuel cell performance [183].

The operation and control of PEM fuel cells require balancing performance optimization with extending the system's lifespan [184]. The longevity of a PEMFC depends largely on minimizing the structural degradation of key components, which can result from factors such as excessive potential loads, high temperatures, and low relative humidity [185]. A predictive degradation model should identify safe operational parameters tailored to the specific conditions of each component, ultimately prolonging their service life. This approach not only extends the lifespan of critical components but also reduces the risk of unscheduled shutdowns, thereby enhancing the overall reliability of the fuel cell system. To achieve this, a multi-stage process in model predictive control paradigm proposed in our project could be followed, as illustrated in figure 4.1.

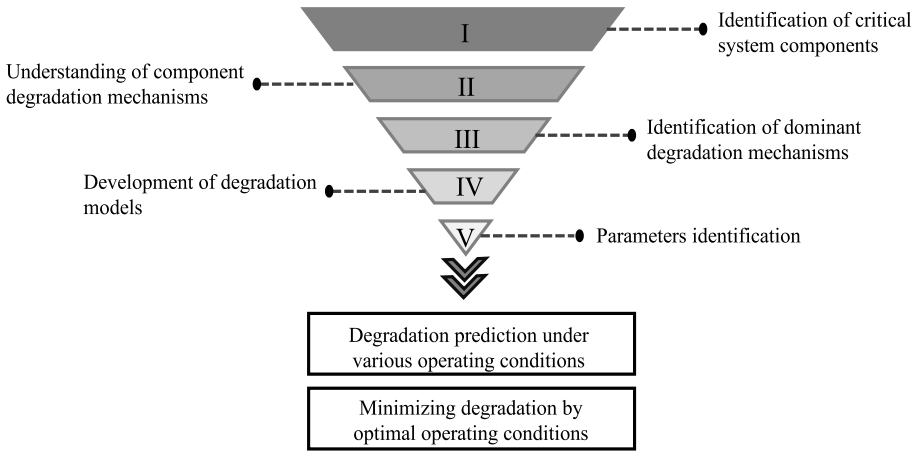

Figure 4.1 – Lifetime Management concept for PEM fuel cell systems

Performance degradation in PEM fuel cells is inevitable. However, the degradation rate can be minimized through a comprehensive understanding of the underlying mechanisms and the application of an optimal control strategy. Previous research has focused on low level controllers designed to prevent operational issues such as flooding, starvation, and thermal management by implementing closed-loop control systems based on static performance models [5, 6, 186].

In this chapter, we propose a novel health management method, focusing on the life extension of the PEMFC system, which addresses global degradation and performance of the PEMFC system [187]. Achieving high performance in PEMFC systems under long-term operating conditions requires careful consideration of the trade-off between degradation and efficiency. While higher temperatures enhance PEMFC performance, they also accelerate durability loss.

This chapter aims to develop a high-level optimal controller dealing with the trade-off between overall system efficiency retaining and the fuel cell's durability enhancement. The optimal control framework was first formulated in the economic model predictive control (EMPC) paradigm. In this framework, a specific study case is carried out to actively optimize temperature settings along the fuel cells' lifetime. To validate the proposed durability enhancement control approach, a 200 W PEMFC test bench is used and a comparative experimental study is being conducted. Once the degradation models are calibrated, the new optimal control strategy will be compared with experimental results obtained under the fixed nominal operating temperature specified by the manufacturer. This comparison will provide insights into the effectiveness of the proposed method in mitigating degradation relative to standard operational protocols.

4.2 PEMFC system control overview and durability enhancement control

4.2.1 Overview of two-layer control

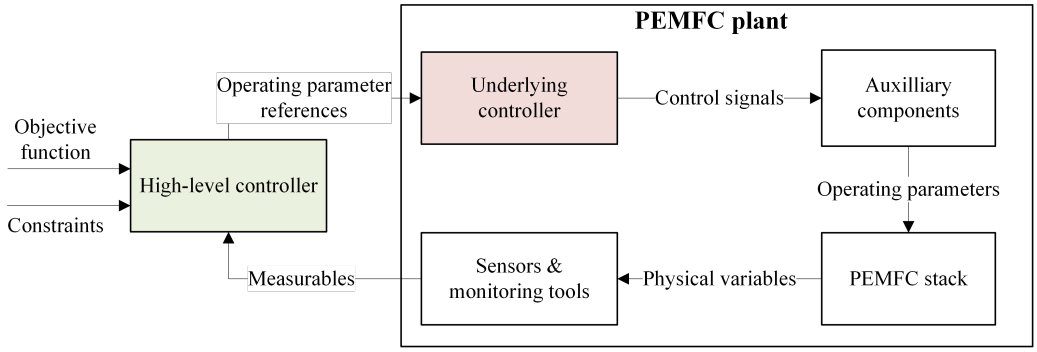

Figure 4.2 – Overview of the PEMFC system control

In here,

— PEMFC durability, system efficiency and life-cycle cost should considered as in the objective function or constraints.

— The operating parameters refer to the ones that are assigned by regulating the auxiliary actuators of a PEMFC system. They could contain stack temperature, reactant relative humidities, pressures and flow rate, as well as current if the load could be scheduled to some level via energy management module.

— The control signals are those assigned to the actuators, such as the voltage imposed on the air compressor for the air flow rate control.

— The measurables contain both the continuous regular measurements of the involved physical variables and the ones from some special and fuel cell-specific monitoring tools such as EIS.

4.2.2 Durability enhancement control design

The high-level controller is concerned and dedicated to durability enhancement. The design of this control could be conducted in the EMPC paradigm, which is illustrated in figure 4.3.

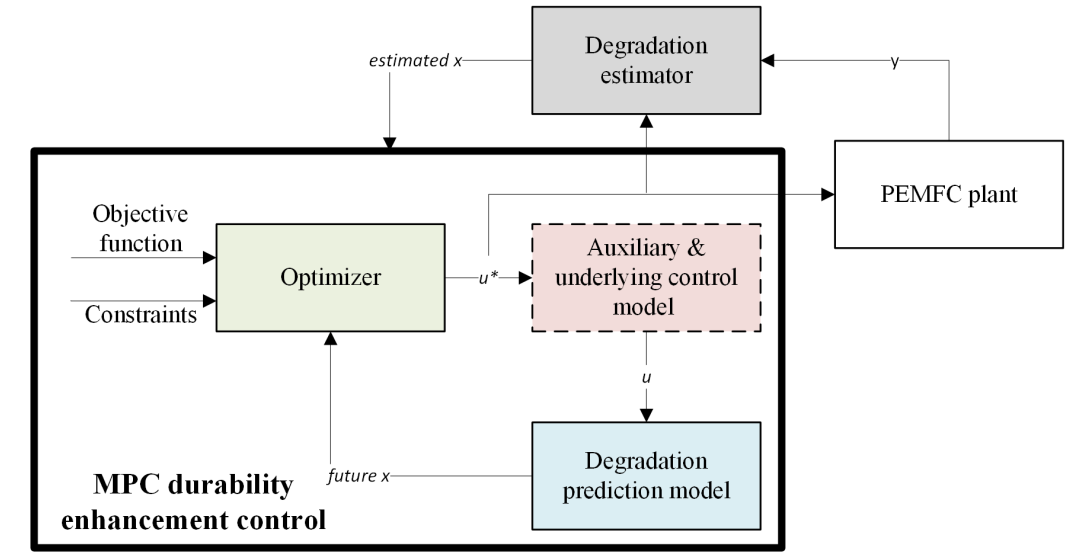

Figure 4.3 – Durability enhancement control in MPC paradigm

In the sequel, we will illustrate a study case concerning temperature control design dedicated to durability enhancement.

4.3 Control Objective

The control objectives for the PEMFC are twofold:

(O1) Minimize Degradation: This approach simultaneously considers both membrane and catalyst degradation, the two dominant aging mechanisms in transportation applications, thereby extending the operational lifespan.

(O2) Maximize Power Density: Maximizing power density is critical for enhancing the overall energy output of the fuel cell while ensuring it operates at optimal efficiency.

The overarching aim is to enhance the performance of PEMFCs while improving their components' reliability and durability. Although higher temperatures can boost the performance of PEMFCs, they also significantly reduce durability, creating a complex trade-off. This complicates the process of selecting an optimal operating temperature that strikes a balance between efficiency and longevity [188]. To tackle

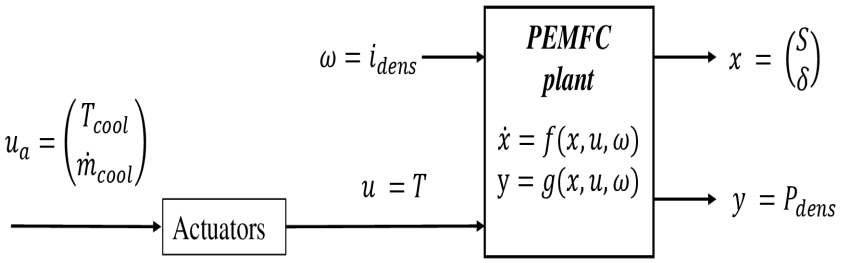

Figure 4.4 – Presentation of the input/output system

this challenge, this chapter presents models designed to predict the efficiency and durability of PEMFCs across various operating temperatures. These models have been utilized to identify the optimal operating temperature that supports extended target lifetimes.

Figure 4.4 illustrates the PEMFC plant input/output which is crucial to form the fuel cell predictive model for MPC design. The key input variables include temperature and charge demand, represented by current density (i_{dens}), both of which have a significant impact on degradation rates and overall performance. The influences of relative humidity and pressure on degradation are not addressed in this study and are held constant at their nominal operating values. The thermal management system tracks the optimal operating temperature by adjusting parameters such as the water flow rate $\dot{m}_{\text{cool}}$ and the cooling temperature T_{cool}. The optimal temperature is determined in real-time by a high-level controller based on the MPC approach. However, low-level control is not considered at this stage, as it is assumed that the cooling system responds adequately to the temperature reference. Ultimately, the primary output of the model, cell power, serves as a vital indicator of overall performance.

The dynamic relationships between the input variables and the output are defined by mathematical equations that capture the degradation mechanisms, i.e. the evolution of x.

4.4 Modeling

In this chapter, we simplify the model developed in the previous chapter to address challenges in control formulation due to data limitations and experimental material constraints. Our focus at this stage is on developing suitable health management strategies, where the degradation model is streamlined and integrated with the fuel cell performance model. This degradation model specifically captures the microscale evolution of the catalyst layer and membrane. Different from the models developed previously and to facilitate control design, we have introduced a simplified model that analyzes the fundamental mechanisms of catalyst degradation. This model examines

the interactions among two particle groups and considers the effects of two particle sizes instead of relying on a global particle distribution.

4.4.1 Assumptions

Based on the following assumptions, we simplify the Pt catalyst degradation model:
(A 4.1) : Agglomeration and carbon corrosion effects are neglected compared to dissolution and redeposition processes.
(A 4.2) : The degradation behavior is assumed to be uniform throughout the catalyst layer.
(A 4.3) : At any point during the aging process, two fictitious Pt particle groups with radii r_1 and r_2 represent the average behavior of particles smaller and larger than the mean radius r_{avg}, respectively ($r_1 < r_{avg}$ and $r_2 > r_{avg}$).
(A 4.4) : The total catalytic area is the sum of the areas of the two fictitious Pt particle groups, $S_1 + S_2 = S$.
(A 4.5) : Defining the deviations from the mean radius as $\Delta r_1 = r_{avg} - r_1$ and $\Delta r_2 = r_2 - r_{avg}$, we assume that $\frac{\Delta r_1}{r_{avg}}$ and $\frac{\Delta r_2}{r_{avg}}$ remain constant throughout the aging process.

4.4.2 MEA Degradation Modeling

The degradation model developed is defined by a series of differential equations that capture the critical processes affecting fuel cell performance, as detailed in Chapter 2. The temporal evolution of the ECSA considers variations in the particle size distribution across a spectrum of particle radii, represented by the following equation:

$$\frac{\partial f_N(r,t)}{\partial t} = -\frac{\partial}{\partial r}\left[f_N(r,t)\frac{dr}{dt}\right] \tag{4.1}$$

Equation (4.1) describes the rate of change of the ECSA, calculated by integrating the time-evolving particle size distribution $f_N(r,t)$. In this context, we do not consider the corrosion and agglomeration degradation mechanisms, and we assume there is no loss of platinum into the membrane. Instead, we focus on the primary degradation process, which is the dissolution and redeposition mechanism, commonly known as Ostwald ripening.

The second equation (4.2) presents the degradation of membrane thickness δ_{mb}

$$\frac{d\delta_{mb}}{dt} = -k_5 \psi_{O_2} \frac{P_{O_2}}{\delta_{mb}} \exp\left(\frac{\alpha_5 F}{RT} U(t)\right) \exp\left(-\frac{E_5}{R}\left(\frac{1}{T} - \frac{1}{T_0}\right)\right) \tag{4.2}$$

The membrane thickness variation is driven by oxygen partial pressure, cell voltage, and temperature-dependent reaction kinetics.

For the Pt catalyst degradation model in equation (4.1), rather than modeling every particle's electrochemical interaction in detail, we simplify the complexity of the physical processes governing degradation. In this approach, we assume that two

particle radius groups can effectively represent the average behavior of Pt catalyst degradation. This simplification captures the essential dynamic behaviors critical for effective control. The proposed model aims to maintain sufficient accuracy in predicting long-term degradation trends while enabling real-time implementation [189]. This approach ensures that the model remains computationally feasible for optimization while adequately representing the system's degradation dynamics. The reduction of the Pt catalyst degradation model is based on assumption **(A4)** [87, 189], which connects the catalytic area S to the average particle radius r_{avg} through the following approximation:

$$r_{\text{avg}} \approx \frac{3 \cdot V_{\text{Pt}}}{S} \tag{4.3}$$

Here, V_{Pt} denotes the mass loading of the Pt per unit volume of catalyst. The simplified aging model proposed by [189] and detailed in appendix 5.1 is expressed as follows:

$$\begin{aligned}\frac{dS}{dt} = &- k_1 \cdot \exp\left(\frac{F}{RT}\left(U - U_1^0\right)\right)(1-\theta) \cdot \frac{M_{\text{Pt}}}{\rho_{\text{Pt}}} \\ &\cdot \frac{\beta_1 F}{RT} \cdot \exp\left(\frac{\beta_1 F}{RT}\frac{S}{3V_{\text{Pt}}}\right) \cdot \frac{S^3}{9V_{\text{Pt}}^2} \frac{4\alpha_r \beta_r^2}{(1+\beta_r)(1-\alpha_r\beta_r)}.\end{aligned} \tag{4.4}$$

Here, β_1, as given in table 4.1, is a constant. The PRD coefficients α_r and β_r, which account for the differences in the radii of two hypothetical particle groups defined by the condition $r_1 < r_{\text{avg}} < r_2$, are assumed to remain constant throughout the degradation process. Specifically, it defined $\alpha_r = \frac{\Delta r_1}{\Delta r_2}$ and $\beta_r = \frac{\Delta r_2}{r_{\text{avg}}}$, where $\Delta r_1 = r_{\text{avg}} - r_1$ and $\Delta r_2 = r_2 - r_{\text{avg}}$. The platinum catalyst degradation model is presented as a first-order system, with the catalyst surface area S as the state variable. The Pt dissolution rate coefficient k_1 is temperature-dependent, as described in equation (2.13).

In this first-order system, the dynamics of platinum oxide coverage are neglected, treating it instead as a static function of the equivalent load input. The platinum oxide coverage, denoted as θ, depends on the cell potential U and is characterized by specific values at key voltage points and their interrelationships [86, 88]. Therefore, the mathematical representation of θ is given by:

$$\theta = \frac{1}{1 + \exp\left(22.4 \cdot (0.818 - U)\right)} \tag{4.5}$$

In this section, a degradation model is presented to predict the real-time degradation behavior of PEMFCs as a function of temperature and applied voltage. To correlate the health state with performance losses, a performance model is also introduced.

4.4.2.1 Modeling the Performance of PEMFC

Considering degradation effects, both the power density and fuel cell voltage become time-dependent. To estimate power density over time, it is necessary to account for voltage changes due to degradation. The power density throughout the fuel cell's

lifetime can be represented by:

$$P_{dens} = U \cdot i_{dens} \tag{4.6}$$

There is a strong correlation between the degradation of the MEA and the increase in voltage loss during the prolonged aging of a PEMFC. The voltage loss primarily consists of activation, ohmic, and concentration losses. The relationship governing the output voltage of a PEMFC, as detailed in the previous chapter, is given by:

$$U = U_{\text{ocv}} - \eta_{\text{act}} - \eta_{\text{ohm}} - \eta_{\text{conc}} \tag{4.7}$$

where U_{ocv} denotes the Nernst (open-circuit) voltage, η_{act} represents the activation losses (notably neglecting the activation losses due to the HOR), η_{ohm} refers to the ohmic losses, and η_{conc} accounts for the concentration losses due to reactant concentration drop at high load.

U_{ocv} depends on the fuel cell temperature T, as well as the partial pressures of hydrogen and oxygen:

$$U_{\text{ocv}} = 1.229 - 8.5 \times 10^{-4}(T - 298.15) + 4.308 \times 10^{-5} T \log\left(P_{\text{H}_2} P_{\text{O}_2}^{\frac{1}{2}}\right) \tag{4.8}$$

where the partial pressure of hydrogen P_{H_2}, which depends on the water content in the anode channel (assumed to be constant), is expressed as [190]:

$$P_{\text{H}_2} = \left(\frac{1}{2} P_{\text{sat}}\right) \left[\frac{1}{\exp\left(\frac{1.653 \cdot i_{\text{dens}}}{T^{1.334}}\right) \frac{RH_{\text{an}} P_{\text{sat}}}{P_{\text{an}}}} - 1 \right] \tag{4.9}$$

Similarly, the partial pressure of oxygen P_{O_2} is given by:

$$P_{\text{O}_2} = \frac{P_{\text{ca}} - RH_{\text{ca}} P_{\text{sat}}}{1 + 3.762 \exp\left(\frac{0.291 \cdot i_{\text{dens}}}{T^{0.832}}\right)} \tag{4.10}$$

In these expressions, P_{sat} represents the saturated water vapor pressure, as defined by equation in table 3.3, which is a function of the fuel cell temperature T. The terms RH_{an} and RH_{ca} denote the relative humidity of the anode and cathode, respectively, while P_{an} and P_{ca} correspond to the pressures at the anode and cathode, respectively.

The activation polarization voltage η_{act} can be calculated using the Tafel equation, which considers the impact of the ECSA on the exchange current density and the hydrogen crossover due to membrane degradation:

$$\eta_{\text{act}} = \frac{RT}{\alpha F} \log\left(\frac{i + i_{cross}}{i_0}\right) \tag{4.11}$$

$$i_0 = i_0^{\text{ref}} L_{Pt} S \left(\frac{P_{O_2}}{P_{\text{ref}}}\right)^{\gamma} \exp\left(-\frac{E_{\text{act}}}{RT}\left(1 - \frac{T}{303}\right)\right) \tag{4.12}$$

$$i_{\text{cross}} = \psi_{H_2} \frac{P_{H_2}}{\delta_{mb}} \cdot 2F \tag{4.13}$$

All parameters in equations (4.11), (4.12) and (4.13) are well defined in subsection 3.2.4.

Hydrogen crossover in a PEM fuel cell, caused by membrane degradation, can significantly impact the fuel cell's performance, particularly in terms of current losses i_{cross}. Additionally, catalyst degradation reduces the active sites available for the ORR.

The ohmic losses, denoted as η_{ohm}, in PEM fuel cells refer to the proton resistance in the membrane.

$$\eta_{\text{ohm}} = i_{\text{dens}} \cdot \delta_{mb} \frac{181.6 \cdot \left(1 + 0.03 \cdot i_{\text{dens}} + 0.062 \cdot \left(\frac{T}{303}\right)^2 \cdot i_{\text{dens}}^{2.5}\right)}{(\lambda - 0.634 - 3 \cdot i_{\text{dens}}) \cdot \exp\left(\frac{4.18 \cdot (T-303)}{T}\right)} \tag{4.14}$$

The concentration loss occurs due to the decrease in reactant concentration, resulting in a significant voltage drop at high current densities. This effect is especially pronounced as the current density approaches the limiting current density, i_L, at which point the supply rate of reactants becomes inadequate to support further increases in current. The concentration overpotential, denoted as η_{conc}, is given by:

$$\eta_{conc} = \beta_e \frac{RT}{4F} ln\left(1 - \frac{i}{i_{\text{L}}}\right) \tag{4.15}$$

Where β_e is an empirical parameter, and i_L is the limiting current density, which is related to the total oxygen transfer resistance R_{O_2}, including the catalyst degradation as illustrated in equation (3.7).

Finally, the voltage of the PEMFC, U, can be expressed as a function of the current density i_{dens}, temperature T, and the degradation states, including the catalyst electrochemical surface area S and membrane thickness δ_{mb}. This functional relationship allows for the formulation of an optimal control problem, which aims to generate an optimal trajectory for the PEMFC's operating conditions. By defining this trajectory, the control strategy can effectively balance performance, durability, and efficiency.

4.4.3 State-Space Model for Control

The degradation model presented here focuses on the slow dynamics of component structural properties, ignoring the transient behavior of the fuel cell system resulting from input changes. This transient behavior could be addressed in a lower-level layer of the model, allowing for the evaluation of its impact on degradation in future work to enhance overall fuel cell longevity. The aim is to decelerate the performance losses of PEMFC during long-term operation through health management based on an optimal temperature trajectory, while considering relative humidity and pressure fixed at nominal values. In this chapter, based on the two degradation models depicted in equations (4.2) and (4.4), the general structure of the damage dynamics is represented in a deterministic setting as follows:

$$\dot{x} = f(x,u,w) = \begin{cases} \dot{x}_1 = -K_1 \cdot \Gamma_2(x,u,w) \cdot x_1^3 \cdot \exp\left(\dfrac{1}{u_1} \cdot (c_{11}x_1 + c_{12}\Gamma_1(x,u,w) - c_{13})\right) \\ \dot{x}_2 = -K_2 \cdot \left(\dfrac{\Gamma_3(u,w)}{x_2}\right) \cdot exp\left(\dfrac{1}{u_1} \cdot (c_{21}\Gamma_1(x,u,w) - c_{22})\right) \end{cases} \tag{4.16}$$

$$y = g(x,u,w) \tag{4.17}$$

— x is the state vector:

$$x = \begin{bmatrix} S \\ \delta_{mb} \end{bmatrix}$$

with S and δ_{mb} representing the states.

— u is the input vector:

$$u = [T]$$

where T are the reference optimal inputs.

— w is the mesured disturbance :

$$w = [i_{dens}]$$

where i_{dens} is the disturbance.

— y is the output:

$$y = [P_{dens}]$$

where P_{dens} is the power density.

To mitigate the performance degradation of PEMFCs during long-term operation, an optimal temperature trajectory is developed. In this control strategy, the relative humidity at both the anode and cathode is maintained constant. In addition, the pressures at the cathode and anode are also kept constant, as given in table 4.2. Consequently, the fuel cell voltage, oxygen partial pressure and oxide coverage can be expressed as a function of the degradation state x, temperature u, and current density w , as follows:

$$U = \Gamma_1(x,u,w), \tag{4.18}$$

$$\theta = 1 - \Gamma_2(x,u,w). \tag{4.19}$$

$$P_{O_2} = \Gamma_3(u,w) \tag{4.20}$$

Finally, all model parameters used in the PEMFC degradation model are summarized in table 4.1.

Table 4.1 – Constants Used in the PEMFC Degradation Model

Symbol	Expression/Value	Description
K_1	$c_1 \frac{M_{pt}}{3\rho_{pt} V_{pt}} c_{11}$	Pt catalyst degradation constant
K_2	$c_2 \psi_{O_2} \exp\left(\frac{E_5}{RT_0}\right)$	Membrane degradation constant
c_1, c_2	-	Fitted parameters
c_{11}	$\frac{\beta_1 F}{3RV_{pt}}$	Physical constant
c_{12}	$\frac{F}{R}$	-
c_{13}	$\frac{G}{k_b} + c_{12} U_1^0$	-
c_{21}	$\frac{\alpha_5 F}{R}$	-
c_{22}	$\frac{E_5}{R}$	-
β_1	$\frac{\sigma_{pt} M_{pt}}{2F\rho_{pt}}$	-
$\Gamma_1(x,u,w)$	Eq.(4.18)	Applied voltage function
$\Gamma_2(x,u,w)$	Eq.(4.19)	Oxide coverage function
$\Gamma_3(u,w)$	Eq.(4.20)	Oxygen partial pressure function

4.4.4 Simulation Results

Simulations were conducted to assess model accuracy by comparing the simplified model with a detailed model of the Pt catalyst. The detailed model predicts changes in the ECSA based on the evolution of 50 particle radii. The results are presented in figure 4.5, illustrating the behavior under two square profiles: SW 0.9 V and SW 0.95 V cycling potentials, each with a 6-second period, as well as a low potential load of 0.6 V and upper potential load values of 0.9 V and 0.95 V.

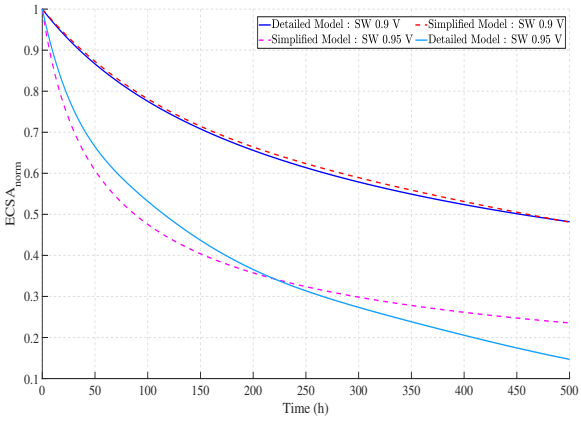

Figure 4.5 – Comparison of ECSA Evolution: Detailed vs. Simplified Model

By adjusting the degradation constant K_1, the simplified model accurately approximates the detailed model, achieving a mean absolute percentage error (MAPE) of 3% under the SW 0.9 V cycling condition. However, under the SW 0.95 V cycling profile,

the lumped model fails to replicate the detailed physical model accurately, resulting in a MAPE of 11%. This discrepancy occurs because the simplified model primarily focuses on the degradation mechanisms of dissolution and redeposition, while neglecting corrosion, which becomes critical at high UPL conditions. Furthermore, the lumped model overlooks Pt diffusion and migration, which intensify at high voltages due to the increased concentration of Pt ions.

Secondly, simulations were conducted to analyze the temperature on PEMFC. Based on experimental studies, the acceptable end-of-life (EoL) threshold for the membrane is established at 50% of its initial thickness, as indicated by the findings reported in [191] and [192]. Similarly, the acceptable health level for the ECSA is defined as 20% of its initial value, according to the experimental results presented by Kneer et al. [91].

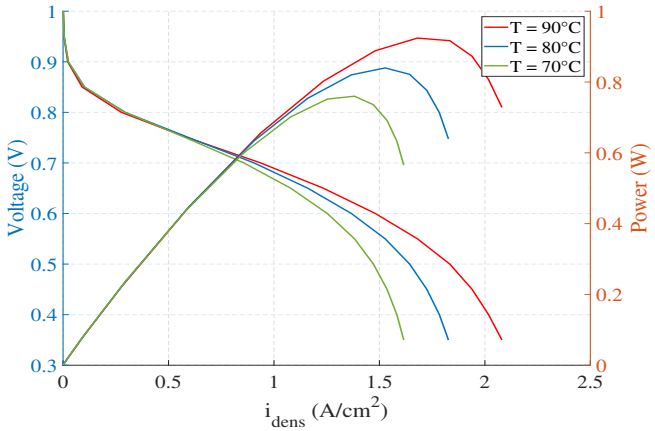

Figure 4.6 – Effect of Temperature on Polarization and Power Density

First, the polarization curve of the PEM fuel cell under varying temperature conditions offers valuable insights into the cell's performance, as illustrated in figure 4.6. As the temperature increases, there is a significant improvement in the fuel cell's efficiency, primarily due to reduced ohmic losses and enhanced proton conductivity, resulting in a more favorable polarization curve. Higher temperatures also contribute to a decrease in activation losses, further enhancing performance.

The simulation also indicates that while higher temperatures enhance performance, they simultaneously accelerate degradation. Specifically, elevated temperatures increase the rate of catalyst degradation and membrane thinning, as shown in figure 4.7.

The simulation, conducted over 1000 hours, demonstrates that in all cases, the ECSA reaches its critical degradation threshold before the membrane as shown 4.7 . This result emphasizes the crucial role of the Pt catalyst in fuel cells, highlighting the importance of optimizing operating conditions. To extend the fuel cell's lifetime, a balance must be achieved between maximizing performance and minimizing degradation. This underscores the need for a nuanced approach to operating conditions, particularly in managing temperature, to strike a balance between short-term efficiency gains and long-term durability.

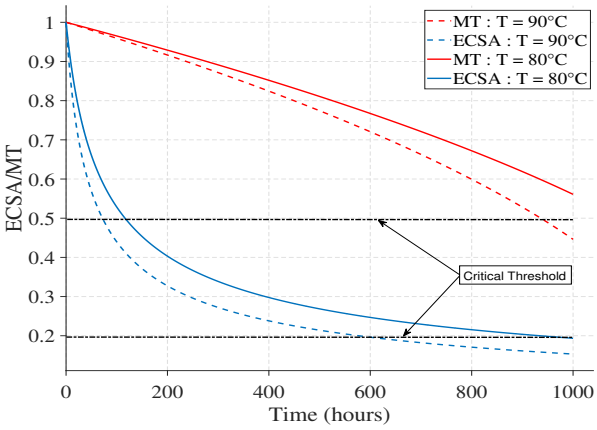

Figure 4.7 – ECSA and MT degradation under T = 80°C and T = 90°C

4.5 Control Problem Formulation

The control strategy is developed using model predictive control, which relies on solving a nonlinear programming problem to minimize a designated cost function. The objective of this approach is to minimize the cost function J, which is designed to balance multiple system goals, including the degradation state and system performance output. Specifically, the cost function J is formulated as a weighted combination of terms that represent these factors, each contributing to the overall system performance and longevity. The objective function is defined as follows:

$$\text{Minimize: } J = \int_{t}^{t+t_h} L(x,u,y)\,dt \tag{4.21}$$

subject to:

$$\begin{aligned} \dot{x} &= f(x,u,w) \\ y &= g(x,u,w) \\ T^{\text{Min}} &\leq T \leq T^{\text{Max}} \\ -\Delta T^{\text{Max}} &\leq \Delta T \leq \Delta T^{\text{Max}} \end{aligned}$$

To maintain optimal membrane hydration and avoid issues related to flooding and drying, the operating temperature of the PEMFC is controlled within a range between T^{Min} and T^{Max} [193]. Due to the significant rise and fall amplitudes in temperature, the variation in thermal stress within the PEMFC increases, which exacerbates the risk of damage to the microcracks at the end of the PEM and accelerates its expansion [194]. Therefore, it is essential to keep the temperature change amplitude within the limit ΔT^{Max}.

The next step involves designing the cost function. The objective is to minimize

the sum of the squared degradation states while penalizing rapid changes in degradation. This includes considering the degradation of critical components, such as the membrane and Pt catalyst, normalized to their initial states. Simultaneously, it is essential to maximize the power output of the PEM fuel cell over the prediction horizon t_h. The aim is to identify the optimal operating inputs that effectively balance degradation with acceptable efficiency, thereby maximizing the system's lifespan. The proper formulation of the cost function J is critical for ensuring that the control strategy not only maximizes immediate system performance but also takes into account long-term degradation. A well-constructed cost function will allow the MPC algorithm to optimize the system's operation over a prediction horizon. The explicit cost function for the Economic MPC is formulated as follows:

$$\text{Minimize: } J = W_d \int_t^{t+t_h} \|\Delta x\|^2 \; - W_p \int_t^{t+t_h} \|y - y_{\text{ref}}\|^2 \, dt, \tag{4.22}$$

where:

— W_d is a weighting factor that emphasizes the importance of minimizing the change in degradation states,

— W_p is a weighting factor that prioritizes maximizing the energy output of the PEM fuel cell,

— Δx represents the vector of changes in the degradation states,

— y represents the vector of power outputs from the fuel cell,

— y_{ref} represents the reference power output ,

— t_h is the prediction horizon at each time t.

By minimizing the squared difference between the current power $P(t)$ and the maximum achievable power $y_{\text{ref}} = P_{\max}(t)$, the function encourages operation close to peak performance without requiring a fixed reference value. Integrating the performance output is crucial, as it helps minimize power deviations over the prediction horizon due to degradation effects at high temperatures, while ensuring the highest possible performance.

4.6 Control Method: Economic Model Predictive Control

Given the problem formulation, the goal is to implement an optimal control strategy that addresses two primary objectives, **(O1)** and **(O2)**. Economic model predictive control, which does not require predefined reference trajectories [195], can be utilized as an effective optimal control approach. This method continuously optimizes the control inputs by considering the economic costs associated with degradation, efficiency, and system performance over a predictive horizon. By doing so, EMPC can actively minimize the degradation rate of critical components, such as the membrane and Pt catalyst, while simultaneously maximizing power output and efficiency.

This makes EMPC particularly advantageous in applications like fuel cell management [196], where balancing performance with durability is crucial for achieving a longer operational lifespan and minimizing maintenance. Implementing EMPC enables the system to adapt dynamically to varying operating conditions, aligning with the dual goals of sustained performance and extended lifespan.

4.6.1 MPC principle and EMPC

Model predictive control is an advanced method aims to optimize multivariable constrained control problem. It has been widely used in the process industries since the 1980s [197]. An objective function and a desired reference trajectory are used to compute the optimal control input sequence in an open-loop manner, with only the first element of the computed sequence being applied to the system. Predictive control tackles this optimization problem using the receding (or moving) horizon approach, as visually depicted in figure 4.8.

The controller, based on measurements obtained at time t, predicts the future dynamic behavior of the system over a prediction horizon T_p. It computes the optimal control input sequence over a control horizon T_c (where $T_c < T_p$) by optimizing a performance objective functional over the entire prediction horizon. However, only the initial part of the computed control input is applied to the system,as shown in figure 4.8a.

At each subsequent time step $t + \Delta t$, the process of prediction and optimization is repeated with updated measurements, shifting both the prediction and control horizons forward in time. This continuous-time receding horizon approach can be described as follows:

At time t: For the current state $x(t)$, solve an optimal control problem over a finite future interval $[t, t + T_p]$, taking into account current and future system constraints.
Apply the first control input: Only the initial portion of the computed control sequence, typically for a small interval Δt, is applied to the system.
Measure the system state at time $t + \Delta t$: Update the state $x(t + \Delta t)$ based on the system's response.
Recompute the optimization: At the next time step $t + \Delta t$, solve the optimal control problem again, now over the interval $[t + \Delta t, t + T_p + \Delta t]$, starting from the updated state $x(t + \Delta t)$.

In situations where available measurements do not fully capture the system's state, an observer can estimate the complete state $x(t + \Delta t)$ using the available data. MPC formulates control actions as an optimization problem, placing it within the domain of optimal control. This optimization takes into account constraints on inputs, outputs, and states, allowing for the real-time computation of an open-loop sequence of current and future control actions.

Economic Model Predictive Control is a specialized form of Model Predictive Control that operates without a predefined reference trajectory. Instead, its objective function

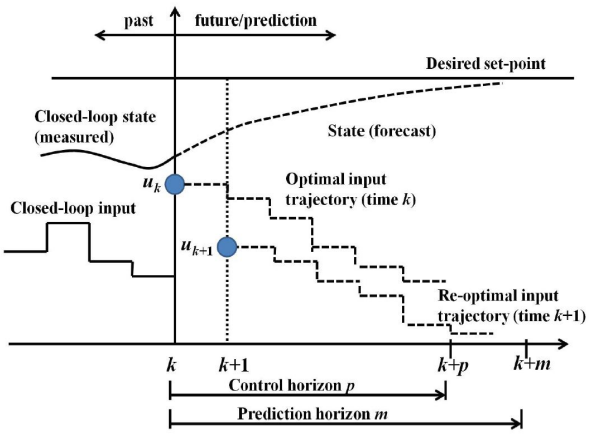

(a) Principle of MPC

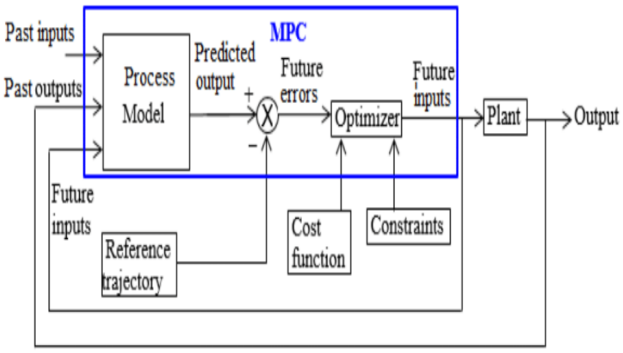

(b) Structure of MPC

Figure 4.8 – Principle and Structure of MPC [198]

explicitly incorporates the economic goals of the system. Typically, these economic objectives include minimizing costs related to production, distribution, and dispatch, while ensuring operational smoothness and adherence to safety standards. Essentially, EMPC controllers focus on optimizing the economic performance of system processes rather than merely tracking specified setpoints or reference trajectories [199]. This approach allows plants to operate at an optimal economic level. The Economic MPC strategy is implemented in a receding horizon manner, as illustrated in figure 4.8a. The objective function of the Economic MPC controller encompasses the economic objectives of the system under analysis. This thesis focuses on a class of systems described by the following dynamics:

$$\dot{x} = f(x, u, w) \tag{4.23}$$

where x denotes the dynamical state of the system, u the manipulated variable, and w the mesured disturbances. Additionally, the system is subject to a set of constraints

$$G(x, u, w) \leq 0$$

The system dynamics f and the set of constraints g can be either linear or non-linear. Furthermore, Economic MPC features a cost function that incorporates the economic objectives of the system, enabling the controller to directly optimize the economic variables. The cost function may also be linear or non-linear.

4.6.2 Application to the Fuel Cell Case

Our primary control objective is to maximize overall system efficiency while adhering to safety and operational constraints. To achieve this, we employ the EMPC framework to compute optimal temperature trajectory reference inputs. This approach minimizes fuel cell degradation by solving a long-term optimal control problem at each time step using nonlinear programming techniques.

Three cases are introduced to evaluate the impact of operational condition control on fuel cell power generation and degradation mechanisms, allowing for a comprehensive comparison and assessment of the proposed optimal control strategy. Although the decision variables and constraints remain consistent across all strategies, the optimization objective functions differ in each case. Furthermore, the model is subject to several constraints, assuming that the PEM fuel cell operates within specific temperature limits. The proposed constraints, along with all operating conditions and input constraints, are detailed in table 4.2.

Case 1: Minimizing Degradation While Considering System Efficiency Over the Prediction Horizon

In this approach, power density is maximized at each predictive horizon t_h throughout the operation of the fuel cell, considering the effects of MEA degradation. Additionally, this method allows for continuous adjustment of operational conditions over time, accounting for measured disturbances and variations in load demand throughout the fuel cell's lifetime. In this context, the objective is to optimize operating conditions and maintain system health while ensuring acceptable efficiency, as defined by the objective function in equation (4.24).

$$\text{Minimize: } J_1 = \int_t^{t_h} L(x,u,y)\,dt \tag{4.24}$$

subject to:

$$\dot{x} = f(x,u,w)$$
$$y = g(x,u,w)$$

Case 2: Maximize system efficiency without considering degradation dynamics

The objective is to maximize the power density during fuel cell operation. In this approach, degradation states are not included in the objective function ($W_d = 0$), focusing solely on the effect of state variables on power density output over the prediction horizon. The generated temperature trajectory will help quantify the degradation of the PEM and catalyst layer, enabling a comparison with the optimal trajectory. This allows for the analysis of the control approach.

Case 3: Nominal operating temperature

In this case, we establish a fixed nominal operating temperature of $T = 80°C$ for the entire lifespan of the fuel cell system. This temperature is specifically chosen to maximize the system's total efficiency throughout its lifetime, with the optimal value determined at the initial time and maintained constant during operation. By comparing this case with Case 1, we will highlight the importance of continuously optimizing the temperature throughout the fuel cell's lifetime, where operational conditions may change over time.

Table 4.2 – Parameters and Ranges Used in the PEMFC Degradation Model

Parameter	**Value**
Temperature	60°C to 90°C
RH_{an}	70%
RH_{ca}	70%
P_{an}	1.5 bar
P_{ca}	1.5 bar

4.6.3 EMPC Implementation Overview

In this work, the EMPC framework is designed to optimize the temperature trajectory in PEM fuel cells, accounting for both performance and degradation. To address the distinct dynamics of degradation, temperature, and load variations, we carefully define the prediction and control horizons. The optimal selection of these configurations are subjects for future investigation. The goal of this work is to introduce a new health management approach, considering aging effects and performance optimization, and to analyze its effectiveness in mitigating the fuel cell aging degradation.

— **Prediction Horizon:**
Given the slow degradation rate in PEMFCs—which can extend over several hours or even days—we set a prediction horizon of $t_h = 10hours$. This duration is chosen to capture long-term degradation effects while balancing computational efficiency, ensuring that control decisions consider the gradual degradation over a meaningful timespan.

— **Control Horizon:**
The temperature in PEMFCs has a relatively slow response rate, making it infeasible to adjust temperature optimally at very small time steps. Instead, *a control step time of one hour* is implemented, ensuring that temperature adjustments align with the system's thermal dynamics. This hourly adjustment interval provides sufficient time for the temperature to respond effectively to changes, while also allowing for optimization without introducing excessive computational burden.

— **Handling Load Variations:**
During each prediction horizon, the load disturbances can vary quickly and often unpredictably. Instead of attempting to track each small fluctuation, we use the mean load value over time step. This approximation smooths the high-frequency variations in load, simplifying the control problem and making it feasible to incorporate fast-changing disturbances without requiring continuous, small-step adjustments. This approach aligns with prior studies on disturbance prediction strategies, such as in [196].

This approach allows EMPC to balance system performance and degradation effectively within practical computational limits, making it a sound basis for further development in PEMFC health management.

4.6.4 Simulation Results

The simulation was conducted using a varying load profile. During the first 400 hours, a current density of $i_{\text{dens}} = 0.1\,\text{A/cm}^2$ was applied, representing near-idling conditions. Then, the current density was increased to $0.5\,\text{A/cm}^2$, and from 700 hours onward, it was set to $1.5\,\text{A/cm}^2$, representing higher load conditions.

In figure 4.9a, the optimal temperature trajectories are shown for the defined load profiles, taking into account the degradation effects as defined in Case 1. Initially, under near-idling conditions, the temperature drops rapidly within 3 hours to limit the degradation of the platinum catalyst and membrane, maintaining it at a minimal value. This temperature reduction reflects the significant impact of degradation under near-idling conditions, where power generation is minimal, prioritizing the extension of PEMFC lifespan over efficiency.

Once the load increases to $0.7\,\text{A/cm}^2$, the temperature rises quickly to reach the optimal range, and then gradually increases, striking a balance between maintaining efficiency and limiting degradation of the fuel cell. This gradual increase is explained by the tendency of the catalyst degradation rate to stabilize over time.

Under high load demand, the optimal temperature trajectory continues to rise to maximize power density. In this scenario, the degradation rate is relatively low, allowing for higher operating temperatures that improve proton conductivity while reducing both ohmic and activation losses. This leads to enhanced power output until the maximum temperature is reached, at which point the degradation of the platinum catalyst stabilizes. Consequently, higher temperatures under high load conditions

support improved efficiency and performance without significantly compromising durability.

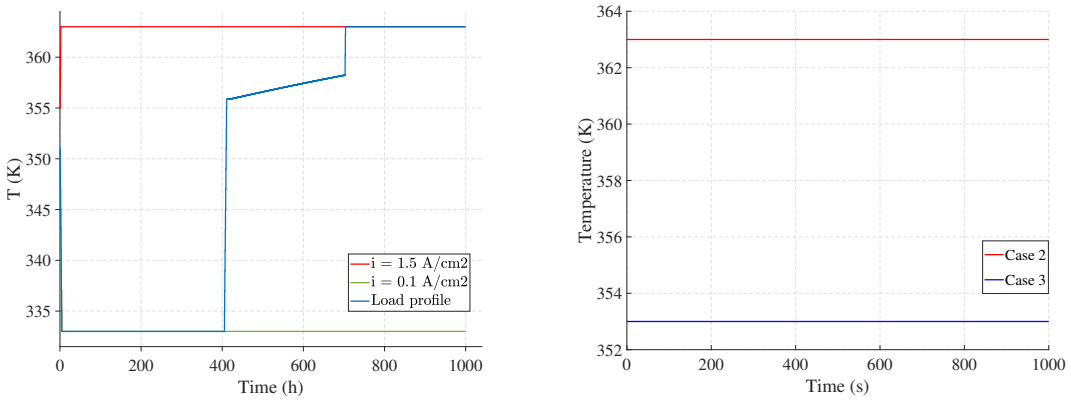

(a) Temperature trajectory for case (1)

(b) Temperature trajectory for case (2) & (3)

Figure 4.9 – Temperature trajectory

In the second case 4.9b, which aims to maximize power density without accounting for degradation mechanisms in the cost function, the operating temperature reaches and is maintained at its peak during both idling and load conditions. This behavior can be attributed to the controller's inability to predict deviations in power density due to degradation over a 10-hour period.

In this stage, we will evaluate this approach's ability to maintain optimal efficiency over time and balance efficiency with durability. This will be achieved by comparing the power density generated under different conditions and assessing the system's durability. The setup alternates the load between idle conditions and high load over a 20-hour period.

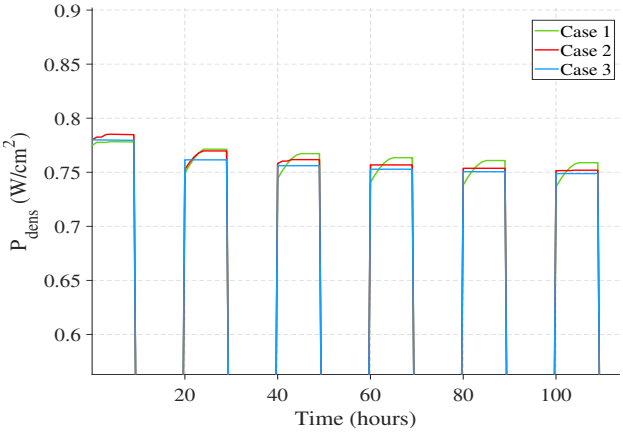

Figure 4.10 – Power density for case (1) & (2) &(3)

In figure 4.10, the power density is shown over the first 60 hours. As observed, the power density in case 2 fails to remain stable and decreases over time due to

degradation effects from the high temperature at low load. In contrast, the control strategy in Case 1 optimizes temperature based on operating conditions, adjusting temperature with load, raising it under high load and lowering it under low load. This approach helps to sustain power generation more effectively over time despite degradation.

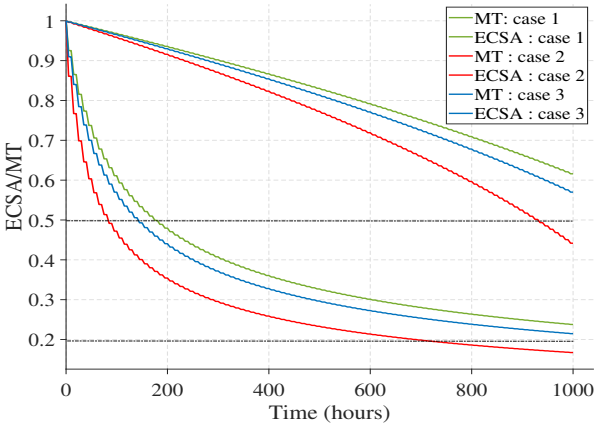

Figure 4.11 – Degradation in different cases

In figure 4.11, we evaluate the degradation effects across different cases to assess the effectiveness of the newly proposed approach in mitigating PEM fuel cell degradation and enhancing overall performance. Durability improvements are demonstrated by comparing the degradation states at the end of the simulation period. As shown, the optimal control strategy effectively extends the lifetime of the membrane electrode assembly. This novel approach, which involves dynamically adjusting the temperature over time, shows significant potential for enhancing overall system durability. To further validate this approach, an experimental test will be conducted to validate its effectiveness and quantify the expected lifetime gains.

4.7 Experimental Results

4.7.1 Test Bench Presentation

The experimental setup planned for this research is designed to simulate real-world operating conditions of PEMFC. This setup will facilitate enable the evaluation of the overall system performance, thereby providing a robust platform for validating the proposed predictive multiscale framework.

4.7.2 Test Protocol

The test protocol will be structured to systematically evaluate the effects of various operating conditions on the degradation of the PEMFC components. The protocol

will involve testing two 200W PEMFC stacks under different conditions to ensure comprehensive analysis. The key components of the experimental procedure are as follows:

1. **Test Duration and Load Cycling:**
   - The experimental tests will be conducted for a total duration of **200 hours**.
   - A well-defined load profile will be applied, consisting of two distinct load stages: **idle condition** and **high load**.
   - The load profile will follow a **24-hour period** with alternating conditions, ensuring that both operational extremes are captured over the course of the experiment.
   - This alternating load profile is designed to replicate varying operational states and provide insights into the degradation behavior of the fuel cell under dynamic load conditions.
2. **Characterization Technique:**
   - Every **48 hours**, electrochemical impedance spectroscopy (EIS) measurements will be conducted to characterize the fuel cell's performance and degradation. This will be performed on both test stacks to monitor their condition over time.
3. **Performance and Degradation Model Identification:**
   - **Stack 1** will be used for **parameter identification** of both the performance and degradation models. Data from this stack will inform the calibration of the models used for the simulations.
   - A **polarization curve** will be conducted at three different temperatures to evaluate the stack's performance across a range of thermal conditions.
4. **Degradation Model Under Temperature Variations:**
   - The degradation model will be identified based on data obtained from testing under two different temperature conditions to identify the influence of temperature on fuel cell degradation.
5. **Nominal Operating Conditions for Stack 1:**
   - **Stack 1** will be operated under nominal conditions, following the defined load profile, to simulate standard operating conditions for the fuel cell system, and will be used as a benchmark to evaluate the proposed approach.
6. **Optimized Temperature and Cooling System for Stack 2:**
   - **Stack 2** will be operated with an optimized temperature profile, integrating a cooling system consisting of a cooling pump and fan to regulate the temperature more effectively during testing.
   - The cooling system's performance will be assessed to ensure the stack operates within the desired trajectory for optimal performance and durability.
7. **Validation of Predictive Degradation Model:**

— Characterization techniques, including EIS, will be applied to **Stack 2** to verify the accuracy of the predictive degradation model.
— The data from Stack 2 will be used to update and improve the model's predictive accuracy during the test, as illustrated in figure 4.2, ensuring that the EMPC updates its states. The obtained results will be compared with those from the first stack, permitting the validation of this novel approach.

4.7.3 Future Validation Results

As we advance with this research, we anticipate that validation results from upcoming experimental tests will demonstrate the efficacy of the proposed health management strategy in mitigating degradation. A key focus will be to evaluate the effect of the prediction horizon on the strategy's effectiveness and limitations. The experimental phase also aims to quantify the health benefits achieved through this approach and to validate our modeling assumptions on degradation mitigation, while currently neglecting uncertainty effects.

In Model Predictive Control, predictions over long horizons tend to be highly sensitive to model accuracy, which requires thorough evaluation based on experimental results. As these models are further refined, we expect they will support the development of more sophisticated control strategies that can dynamically adapt to varying operational conditions, ultimately leading to longer-lasting and more efficient PEMFC systems.

4.8 Summary and Conclusion

This chapter presents a health management strategy using EMPC to generate an optimal temperature trajectory, reducing degradation while enhancing fuel cell performance. This approach effectively couples health state prediction with performance enhancement, focusing on minimizing membrane and catalyst degradation while maximizing power density to improve both efficiency and durability. The health state prediction is based on a developed degradation model, and the operating temperature trajectory is optimized using a nonlinear programming method.

The EMPC strategy has demonstrated its capability to optimize PEM fuel cell longevity under varying load conditions by employing a dynamic temperature adjustment approach, where temperature is optimized based on load demands. This method effectively sustained power output over time by mitigating degradation effects. In contrast, maintaining a fixed maximum temperature to maximize initial power density led to accelerated degradation and a noticeable decline in performance. Additionally, holding a constant nominal temperature without adjusting for load increases degradation during idling conditions, which adversely impacts overall performance.

The results underscore the critical role of adaptive temperature control in balancing power density with degradation rates, thereby prolonging PEM fuel cell performance. By reducing temperature during low-load periods, the EMPC strategy minimizes the adverse effects of high temperatures, offering a sustainable solution for long-term applications. Future work may focus on refining this adaptive control framework to incorporate degradation uncertainties.

Conclusion and Perspectives

Summary

In this thesis, a comprehensive microscale degradation model for PEM fuel cells has been developed, focusing on the catalyst layer and proton exchange membrane within the membrane-electrode assembly to estimate aging losses due to material microstructure evolution. The model aims to accurately assess the health state of the PEMFC by examining the primary degradation mechanisms affecting its two most critical components, enabling performance predictions under various operating conditions. A performance model was introduced to provide critical information about the internal conditions of an operating fuel cell and update the performance losses. This allows for the introduction of a novel PEMFC model that transforms the static performance model by making it depend on aging states. Lastly, a health management strategy based on MPC was developed to extend the fuel cell's lifetime by optimizing its temperature trajectory.

Degradation Modeling and Analysis

The Pt catalyst and membrane are core components in PEMFCs, highlighting the need for a model that can serve as a health state indicator and provide insights into the degradation rate as a function of controlled operating conditions. This presents a significant challenge, as the underlying physical degradation phenomena are typically modeled using complex, coupled mechanisms that are still not fully understood and require further investigation.

To address this, this thesis takes a step further by proposing a model framework that can help avoid unexpected aging losses. First, a physics-based model for Pt catalyst degradation is introduced to quantify the reduction in electrochemical surface area during PEMFC aging. This model captures critical factors such as cycling load, temperature, and humidity, which influence the degradation rate. It also incorporates key mechanisms like platinum dissolution, Ostwald ripening, coagulation, and corrosion. The proposed model is validated using a range of experimental data from two different operating conditions, where acceptable quantitative agreement with available measurements is achieved. Additionally, a semi-empirical degradation model is introduced to address membrane thinning over time, offering a more comprehensive perspective on PEMFC degradation by integrating both catalyst and membrane degradation processes.

The results demonstrate the model's effectiveness in capturing complex degradation mechanisms; however, further investigation and development are needed. First,

considering the aging effects of other components, such as the gas diffusion layer and bipolar plate corrosion, can enhance the degradation analysis and improve the prediction accuracy of PEMFCs. Secondly, the interactions between different degradation components are important, such as quantifying the effect of platinum band formation on membrane degradation and vice versa. These interactions add complexity to the model, making it reliant on a deeper understanding of degradation mechanisms. Meanwhile, a hybrid approach to improve the model could be a promising way to enhance prediction accuracy, depending on the available data.

Dual-Scale Modeling Framework

The dual-scale model plays a crucial role in improving the prognosis of health states under both steady-state and transient conditions, enabling effective control strategies. The degradation of the MEA depends on the internal states and parameters of the PEM fuel cell, yet sensor measurements providing such vital information are rarely available, where they could be approximated by the proposed multiphysical dynamic model. Meanwhile, this framework makes the performance of the system time-dependent and upgrades the multiphysical PEMFC model from a static to an aging-dependent model.

On the other hand, this multi-physics model can easily incorporate different scales within the fuel cell system, allowing for the seamless inclusion of auxiliary components such as compressors, humidifiers, and cooling systems, supporting the design of optimal control strategies. The importance of model coupling is illustrated by its ability to predict the performance of PEM fuel cells over time, under real-world conditions such as the New European Driving Cycle supports the model's reasonable assumptions and predictive capabilities.

Future work should focus on enhancing this framework by further investigating the heterogeneity within the fuel cell. Variations in local operating conditions, such as relative humidity, temperature, and pressure, significantly impact platinum dissolution rates and kinetic losses across the cell. To improve the model's accuracy, it is essential to incorporate spatially resolved MEA performance and degradation, rather than assuming uniform degradation across the components over time.

Health Management Strategy

The thesis also introduces an Economic Model Predictive Control strategy to optimize temperature, mitigating degradation while maintaining performance. This approach showcases the advantages of adaptive temperature control, particularly under fluctuating load conditions. By dynamically adjusting temperature, the EMPC strategy reduces degradation during idle periods and better manages under load demands compared to static temperature settings. Results emphasize the critical role of optimal control in balancing power density with degradation rates, offering a pathway to enhanced PEMFC durability for long-term applications.

Future work needs to focus on improving predictive control by configuring MPC

parameters, such as the prediction horizon, and assessing their impact. Additionally, expanding the control approach to include transient dynamics by incorporating the auxiliary system controller and considering the dynamic behavior of the system with respect to aging and reversible degradation is essential. Meanwhile, the control strategy depends on the model's accuracy, internal state observation, and aging condition assessment. This requires the development of advanced methods for health state estimation by combining historical data with hybrid models, as well as improvements to the physics-based model.

Bibliography

[1] Laetitia Dubau, Luis Castanheira, Frédéric Maillard, et al. “A review of PEM fuel cell durability: materials degradation, local heterogeneities of aging and possible mitigation strategies”. In: *Wiley Interdisciplinary Reviews: Energy and Environment* 3.6 (2014), pp. 540–560 (cit. on pp. 15, 18).

[2] Georg A Futter, Arnulf Latz, and Thomas Jahnke. “Physical modeling of chemical membrane degradation in polymer electrolyte membrane fuel cells: Influence of pressure, relative humidity and cell voltage”. In: *Journal of Power Sources* 410 (2019), pp. 78–90 (cit. on pp. 15, 18, 24, 32).

[3] Frank A de Bruijn, VAT Dam, and GJM Janssen. “Durability and degradation issues of PEM fuel cell components”. In: *Fuel cells* 8.1 (2008), pp. 3–22 (cit. on pp. 15, 18, 20, 25).

[4] Marine Jouin, Rafael Gouriveau, Daniel Hissel, et al. “Degradations analysis and aging modeling for health assessment and prognostics of PEMFC”. In: *Reliability Engineering & System Safety* 148 (2016), pp. 78–95. ISSN: 0951-8320. DOI: 10.1016/j.ress.2015.12.003 (cit. on pp. 15, 18, 27).

[5] María Laura Sarmiento Carnevali. “Modeling and control of PEM fuel cells”. In: (2017) (cit. on pp. 15, 94).

[6] Carl F Lorenzo and Walter C Merrill. “Life extending control-a concept paper”. In: *1991 American Control Conference*. IEEE. 1991, pp. 1081–1095 (cit. on pp. 15, 38, 94).

[7] Marta Zagorowska, Ouyang Wu, James R Ottewill, et al. “A survey of models of degradation for control applications”. In: *Annual Reviews in Control* 50 (2020), pp. 150–173 (cit. on pp. 15, 38).

[8] Christophe Robin, Mathias Gerard, Alejandro A Franco, et al. “Multi-scale coupling between two dynamical models for PEMFC aging prediction”. In: *international journal of hydrogen energy* 38.11 (2013), pp. 4675–4688 (cit. on pp. 15, 70, 83).

[9] Sara I Zandalinas, Felix B Fritschi, and Ron Mittler. “Global warming, climate change, and environmental pollution: recipe for a multifactorial stress combination disaster”. In: *Trends in Plant Science* 26.6 (2021), pp. 588–599 (cit. on p. 17).

[10] Jia Ying Yong, Vigna K Ramachandaramurthy, Kang Miao Tan, et al. "A review on the state-of-the-art technologies of electric vehicle, its impacts and prospects". In: *Renewable and sustainable energy reviews* 49 (2015), pp. 365–385 (cit. on p. 17).

[11] Eurostat. *Greenhouse Gas Emissions by Source Sector, EU*. https://ec.europa.eu/eurostat/statistics-explained/index.php?title=File:Greenhouse_gas_emissions_by_source_sector,_EU,_2020.png. 2021 (cit. on p. 17).

[12] Bahattin Tanç, Hüseyin Turan Arat, Ertuğrul Baltacıoğlu, et al. "Overview of the next quarter century vision of hydrogen fuel cell electric vehicles". In: *International Journal of Hydrogen Energy* 44.20 (2019), pp. 10120–10128 (cit. on p. 17).

[13] Xueqin Lü, Yan Qu, Yudong Wang, et al. "A comprehensive review on hybrid power system for PEMFC-HEV: Issues and strategies". In: *Energy conversion and Management* 171 (2018), pp. 1273–1291 (cit. on p. 17).

[14] Atanu Roy and Sabyasachi Pramanik. "A review of the hydrogen fuel path to emission reduction in the surface transport industry". In: *International Journal of Hydrogen Energy* 49 (2024), pp. 792–821 (cit. on p. 17).

[15] Yun Wang, Daniela Fernanda Ruiz Diaz, Ken S Chen, et al. "Materials, technological status, and fundamentals of PEM fuel cells–a review". In: *Materials today* 32 (2020), pp. 178–203 (cit. on p. 18).

[16] Marie-Cécile Pera, Daniel Hissel, Hamid Gualous, et al. *Electrochemical components*. John Wiley & Sons, 2013 (cit. on p. 18).

[17] Xiao Xia Wang, Mark T Swihart, and Gang Wu. "Achievements, challenges and perspectives on cathode catalysts in proton exchange membrane fuel cells for transportation". In: *Nature Catalysis* 2.7 (2019), pp. 578–589 (cit. on p. 18).

[18] Ming Chen, Chen Zhao, Fengman Sun, et al. "Research progress of catalyst layer and interlayer interface structures in membrane electrode assembly (MEA) for proton exchange membrane fuel cell (PEMFC) system". In: *ETransportation* 5 (2020), p. 100075 (cit. on p. 18).

[19] Yonghong Bing, Hansan Liu, Lei Zhang, et al. "Nanostructured Pt-alloy electrocatalysts for PEM fuel cell oxygen reduction reaction". In: *Chemical Society Reviews* 39.6 (2010), pp. 2184–2202 (cit. on p. 18).

[20] Julio Luna, Samir Jemei, Nadia Yousfi-Steiner, et al. "Nonlinear predictive control for durability enhancement and efficiency improvement in a fuel cell power system". In: *Journal of Power Sources* 328 (2016), pp. 250–261 (cit. on p. 18).

[21] Basil Kouvaritakis and Mark Cannon. "Model predictive control". In: *Switzerland: Springer International Publishing* 38 (2016) (cit. on p. 18).

[22] Hao Liu, Jian Chen, Daniel Hissel, et al. "Prognostics methods and degradation indexes of proton exchange membrane fuel cells: A review". In: *Renewable and Sustainable Energy Reviews* 123 (2020), p. 109721 (cit. on p. 18).

[23] Frano Barbir. *PEM fuel cells: theory and practice*. Academic press, 2012 (cit. on pp. 20, 72).

[24] Patrick Schneider, Mariah Batool, Andres O Godoy, et al. "Impact of platinum loading and layer thickness on cathode catalyst degradation in PEM fuel cells". In: *Journal of The Electrochemical Society* 170.2 (2023), p. 024506 (cit. on p. 20).

[25] Mingzhang Pan, Chengjie Pan, Chao Li, et al. "A review of membranes in proton exchange membrane fuel cells: Transport phenomena, performance and durability". In: *Renewable and Sustainable Energy Reviews* 141 (2021), p. 110771 (cit. on p. 21).

[26] Ghassemzadeh Lida and Holdcroft Steven. "Quantifying the Structural Changes of Perfluorosulfonated Acid Ionomer upon Reaction with Hydroxyl Radicals". In: (2013) (cit. on p. 21).

[27] Tushar Kanti Maiti, Jitendra Singh, Prakhar Dixit, et al. "Advances in perfluorosulfonic acid-based proton exchange membranes for fuel cell applications: A review". In: *Chemical Engineering Journal Advances* 12 (2022), p. 100372 (cit. on p. 21).

[28] Nadia Yousfi-Steiner, Ph Moçotéguy, D Candusso, et al. "A review on PEM voltage degradation associated with water management: Impacts, influent factors and characterization". In: *Journal of power sources* 183.1 (2008), pp. 260–274 (cit. on p. 22).

[29] N Yousfi-Steiner, Ph Moçotéguy, D Candusso, et al. "A review on polymer electrolyte membrane fuel cell catalyst degradation and starvation issues: Causes, consequences and diagnostic for mitigation". In: *Journal of Power Sources* 194.1 (2009), pp. 130–145 (cit. on p. 22).

[30] Yuichiro Tabuchi, Takeshi Shiomi, Osamu Aoki, et al. "Effects of heat and water transport on the performance of polymer electrolyte membrane fuel cell under high current density operation". In: *Electrochimica Acta* 56.1 (2010), pp. 352–360 (cit. on p. 22).

[31] Daniel Hissel and Marie-Cécile Pera. "Diagnostic & health management of fuel cell systems: Issues and solutions". In: *Annual Reviews in Control* 42 (2016), pp. 201–211 (cit. on pp. 22, 41).

[32] Carole Lebreton, Michel Benne, Cédric Damour, et al. "Fault Tolerant Control Strategy applied to PEMFC water management". In: *International Journal of Hydrogen Energy* 40.33 (2015), pp. 10636–10646 (cit. on p. 22).

[33] Wolfgang Schmittinger and Ardalan Vahidi. "A review of the main parameters influencing long-term performance and durability of PEM fuel cells". In: *Journal of power sources* 180.1 (2008), pp. 1–14 (cit. on pp. 22, 25, 26).

[34] PJ Ferreira, Y Shao-Horn, D Morgan, et al. "Instability of Pt/ C electrocatalysts in proton exchange membrane fuel cells: a mechanistic investigation". In: *Journal of the Electrochemical Society* 152.11 (2005), A2256 (cit. on pp. 22, 23).

[35] Andraž Pavlišič, Primož Jovanovič, Vid Simon Šelih, et al. "Platinum dissolution and redeposition from Pt/C fuel cell electrocatalyst at potential cycling". In: *Journal of The Electrochemical Society* 165.6 (2018), F3161–F3165 (cit. on p. 22).

[36] Konrad Ehelebe, Julius Knöppel, Markus Bierling, et al. "Platinum dissolution in realistic fuel cell catalyst layers". In: *Angewandte Chemie* 133.16 (2021), pp. 8964–8970 (cit. on p. 22).

[37] Martin Prokop, Monika Drakselova, and Karel Bouzek. "Review of the experimental study and prediction of Pt-based catalyst degradation during PEM fuel cell operation". In: *Current Opinion in Electrochemistry* 20 (2020), pp. 20–27 (cit. on p. 22).

[38] Serhiy Cherevko. "Stability and dissolution of electrocatalysts: Building the bridge between model and "real world" systems". In: *Current Opinion in Electrochemistry* 8 (2018), pp. 118–125 (cit. on pp. 22, 43).

[39] Paulo J Ferreira and Yang Shao-Horn. "Formation mechanism of Pt single-crystal nanoparticles in proton exchange membrane fuel cells". In: *Electrochemical and Solid-State Letters* 10.3 (2007), B60 (cit. on pp. 22, 23, 43).

[40] Felix N Büchi, Minoru Inaba, and Thomas J Schmidt. *Polymer electrolyte fuel cell durability*. Springer, 2009 (cit. on pp. 23, 33).

[41] Wu Bi and Thomas F Fuller. "Modeling of PEM fuel cell Pt/C catalyst degradation". In: *Journal of Power Sources* 178.1 (2008), pp. 188–196 (cit. on pp. 23, 30, 43, 44).

[42] Jingxin Zhang, Brian A Litteer, Wenbin Gu, et al. "Effect of hydrogen and oxygen partial pressure on Pt precipitation within the membrane of PEMFCs". In: *Journal of the electrochemical society* 154.10 (2007), B1006 (cit. on pp. 23, 49).

[43] Weibo Zheng, Liangfei Xu, Zunyan Hu, et al. "Dynamic modeling of Pt degradation and mitigation strategies in polymer electrolyte membrane fuel cells". In: *eTransportation* 12 (2022), p. 100171 (cit. on p. 23).

[44] N Macauley, L Ghassemzadeh, C Lim, et al. "Pt band formation enhances the stability of fuel cell membranes". In: *ECS Electrochemistry Letters* 2.4 (2013), F33 (cit. on p. 23).

[45] Stefan Helmly, Renate Hiesgen, Tobias Morawietz, et al. "Microscopic investigation of platinum deposition in PEMFC cross-sections using AFM and SEM". In: *Journal of The Electrochemical Society* 160.6 (2013), F687 (cit. on p. 23).

[46] Andrea Impagnatiello, Carolina Ferreira Cerqueira, Pierre-Eugène Coulon, et al. "Degradation mechanisms of supported Pt nanocatalysts in proton exchange membrane fuel cells: an operando study through liquid cell transmission electron microscopy". In: *ACS Applied Energy Materials* 3.3 (2020), pp. 2360–2371 (cit. on p. 24).

[47] Isaac Martens, Raphaël Chattot, and Jakub Drnec. "Decoupling catalyst aggregation, ripening, and coalescence processes inside operating fuel cells". In: *Journal of Power Sources* 521 (2022), p. 230851 (cit. on p. 24).

[48] A Honji, T Mori, K Tamura, et al. "Agglomeration of platinum particles supported on carbon in phosphoric acid". In: *Journal of The Electrochemical Society* 135.2 (1988), p. 355 (cit. on p. 24).

[49] Natalia Macauley, Dennis D Papadias, Joseph Fairweather, et al. "Carbon corrosion in PEM fuel cells and the development of accelerated stress tests". In: *Journal of The Electrochemical Society* 165.6 (2018), F3148–F3160 (cit. on pp. 24, 44).

[50] AB LaConti, M Hamdan, and RC McDonald. "Mechanisms of membrane degradation". In: *Handbook of fuel cells* 3 (2003), pp. 647–662 (cit. on pp. 24, 25, 62).

[51] M Chandesris, R Vincent, L Guetaz, et al. "Membrane degradation in PEM fuel cells: From experimental results to semi-empirical degradation laws". In: *International Journal of Hydrogen Energy* 42.12 (2017), pp. 8139–8149 (cit. on pp. 24, 31, 62–65, 88).

[52] Adam Z Weber. "Gas-crossover and membrane-pinhole effects in polymer-electrolyte fuel cells". In: *Journal of The Electrochemical Society* 155.6 (2008), B521 (cit. on p. 24).

[53] Natalia Macauley, Mark Watson, Michael Lauritzen, et al. "Empirical membrane lifetime model for heavy duty fuel cell systems". In: *Journal of Power Sources* 336 (2016), pp. 240–250 (cit. on pp. 25, 33).

[54] I Elferjani, G Serre, B Ter-Ovanessian, et al. "A coupling approach between metallic bipolar plates corrosion and membrane chemical degradation in the proton exchange membrane fuel cells". In: *International Journal of Hydrogen Energy* 46.63 (2021), pp. 32226–32241 (cit. on pp. 25, 63).

[55] Peng Ren, Pucheng Pei, Yuehua Li, et al. "Degradation mechanisms of proton exchange membrane fuel cell under typical automotive operating conditions". In: *Progress in Energy and Combustion Science* 80 (2020), p. 100859 (cit. on pp. 25, 27, 62).

[56] Pawel Gazdzick, Jens Mitzel, Daniel Garcia Sanchez, et al. "Evaluation of reversible and irreversible degradation rates of polymer electrolyte membrane fuel cells tested in automotive conditions". In: *Journal of Power Sources* 327 (2016), pp. 86–95 (cit. on p. 26).

[57] Jean-Marc Le Canut, Rami M Abouatallah, and David A Harrington. "Detection of membrane drying, fuel cell flooding, and anode catalyst poisoning on PEMFC stacks by electrochemical impedance spectroscopy". In: *Journal of The Electrochemical Society* 153.5 (2006), A857 (cit. on p. 26).

[58] DA McKay, WT Ott, and AG Stefanopoulou. "Modeling, parameter identification, and validation of reactant and water dynamics for a fuel cell stack". In: *ASME International Mechanical Engineering Congress and Exposition*. Vol. 42169. 2005, pp. 1177–1186 (cit. on p. 26).

[59] Wensheng He, Guangyu Lin, and Trung Van Nguyen. "Diagnostic tool to detect electrode flooding in proton-exchange-membrane fuel cells". In: *AIChE Journal* 49.12 (2003), pp. 3221–3228 (cit. on p. 26).

[60] J St-Pierre, DP Wilkinsor, S Knights, et al. "Relationships between water management, contamination and lifetime degradation in PEFC". In: *Journal of New Materials for Electrochemical Systems* 3.2 (2000), pp. 99–106 (cit. on p. 26).

[61] Yoshitsugu Sone, Per Ekdunge, and Daniel Simonsson. "Proton conductivity of Nafion 117 as measured by a four-electrode AC impedance method". In: *Journal of the Electrochemical Society* 143.4 (1996), p. 1254 (cit. on p. 26).

[62] Xinyu Huang, Roham Solasi, YUE Zou, et al. "Mechanical endurance of polymer electrolyte membrane and PEM fuel cell durability". In: *Journal of Polymer Science Part B: Polymer Physics* 44.16 (2006), pp. 2346–2357 (cit. on p. 26).

[63] Zhixiang Liu, Lizhai Yang, Zongqiang Mao, et al. "Behavior of PEMFC in starvation". In: *Journal of power sources* 157.1 (2006), pp. 166–176 (cit. on p. 26).

[64] Mark Mathias, Joerg Roth, Jerry Fleming, et al. "Handbook of fuel cells—fundamentals, technology and applications". In: *Fuel cell technology and applications* 3 (2003), pp. 517–537 (cit. on p. 27).

[65] Timothy W Patterson and Robert M Darling. "Damage to the cathode catalyst of a PEM fuel cell caused by localized fuel starvation". In: *Electrochemical and Solid-State Letters* 9.4 (2006), A183 (cit. on p. 27).

[66] Sumit Kundu, Michael Fowler, Leonardo C. Simon, et al. "Reversible and irreversible degradation in fuel cells during Open Circuit Voltage durability testing". In: *Journal of Power Sources* 182.1 (2008), pp. 254–258. ISSN: 0378-7753. DOI: https://doi.org/10.1016/j.jpowsour.2008.04.009 (cit. on p. 27).

[67] Deborah J Myers, Xiaoping Wang, Matt C Smith, et al. "Potentiostatic and potential cycling dissolution of polycrystalline platinum and platinum nanoparticle fuel cell catalysts". In: *Journal of The Electrochemical Society* 165.6 (2018), F3178–F3190 (cit. on p. 27).

[68] Tsutomu Ioroi, Zyun Siroma, Shin-ichi Yamazaki, et al. "Electrocatalysts for PEM fuel cells". In: *Advanced Energy Materials* 9.23 (2019), p. 1801284 (cit. on p. 27).

[69] Rodney L Borup, Ahmet Kusoglu, Kenneth C Neyerlin, et al. "Recent developments in catalyst-related PEM fuel cell durability". In: *Current Opinion in Electrochemistry* 21 (2020), pp. 192–200 (cit. on p. 28).

[70] Ludivine Franck-Lacaze, Caroline Bonnet, E Choi, et al. "Ageing of PEMFC's due to operation at low current density: Investigation of oxidative degradation". In: *international journal of hydrogen energy* 35.19 (2010), pp. 10472–10481 (cit. on p. 28).

[71] R Singh, PC Sui, KH Wong, et al. "Modeling the effect of chemical membrane degradation on PEMFC performance". In: *Journal of The Electrochemical Society* 165.6 (2018), F3328–F3336 (cit. on pp. 28, 32).

[72] Marine Jouin, Rafael Gouriveau, Daniel Hissel, et al. "Degradations analysis and aging modeling for health assessment and prognostics of PEMFC". In: *Reliability Engineering & System Safety* 148 (2016), pp. 78–95 (cit. on pp. 28, 61).

[73] Sumit Kundu, Michael W Fowler, Leonardo C Simon, et al. "Open circuit voltage durability study and model of catalyst coated membranes at different humidification levels". In: *Journal of Power Sources* 195.21 (2010), pp. 7323–7331 (cit. on p. 28).

[74] M Gummalla, VV Atrazhev, D Condit, et al. "Degradation of polymer-electrolyte membranes in fuel cells: II. Theoretical model". In: *Journal of The Electrochemical Society* 157.11 (2010), B1542 (cit. on p. 28).

[75] Ruichun Jiang, H Russell Kunz, and James M Fenton. "Investigation of membrane property and fuel cell behavior with sulfonated poly (ether ether ketone) electrolyte: Temperature and relative humidity effects". In: *Journal of Power Sources* 150 (2005), pp. 120–128 (cit. on p. 29).

[76] Mahmoud M Saleh, Takeoshi Okajima, Masahiko Hayase, et al. "Exploring the effects of symmetrical and asymmetrical relative humidity on the performance of H2/air PEM fuel cell at different temperatures". In: *Journal of Power Sources* 164.2 (2007), pp. 503–509 (cit. on p. 29).

[77] Jianlu Zhang, Yanghua Tang, Chaojie Song, et al. "PEM fuel cell relative humidity (RH) and its effect on performance at high temperatures". In: *Electrochimica Acta* 53.16 (2008), pp. 5315–5321 (cit. on p. 29).

[78] Wu Bi, Qunhui Sun, Yulin Deng, et al. "The effect of humidity and oxygen partial pressure on degradation of Pt/C catalyst in PEM fuel cell". In: *Electrochimica Acta* 54.6 (2009), pp. 1826–1833 (cit. on p. 29).

[79] YH Lai and DA Dillard. "Mechanical durability characterization and modeling of ionomeric membranes". In: *Handbook of fuel cells* (2010) (cit. on p. 29).

[80] Craig S Gittleman, Frank D Coms, and Yeh-Hung Lai. "Membrane durability: physical and chemical degradation". In: *Polymer electrolyte fuel cell degradation* (2012), pp. 15–88 (cit. on pp. 29, 61).

[81] Jianlu Zhang, Zhong Xie, Jiujun Zhang, et al. “High temperature PEM fuel cells”. In: *Journal of power Sources* 160.2 (2006), pp. 872–891 (cit. on p. 29).

[82] Wu Bi and T Fuller. “Temperature effects on PEM fuel cells Pt/C catalyst degradation”. In: *ECS Transactions* 11.1 (2007), p. 1235 (cit. on p. 29).

[83] Takeshi Yoda, Hiroyuki Uchida, and Masahiro Watanabe. “Effects of operating potential and temperature on degradation of electrocatalyst layer for PEFCs”. In: *Electrochimica acta* 52.19 (2007), pp. 5997–6005 (cit. on p. 29).

[84] Hamid Kazemi Esfeh and Mohd Kamaruddin Abd Hamid. “Temperature effect on proton exchange membrane fuel cell performance Part II: Parametric study”. In: *Energy Procedia* 61 (2014), pp. 2617–2620 (cit. on p. 29).

[85] Andres Jacome. “Estimation précise et robuste de l’état de vieillissement de piles PEMFC par observateurs bayésiens dans le cadre d’une approche basée modèle”. PhD thesis. Université Bourgogne Franche-Comté, 2021 (cit. on p. 30).

[86] Robert M Darling and Jeremy P Meyers. “Kinetic model of platinum dissolution in PEMFCs”. In: *Journal of the Electrochemical Society* 150.11 (2003), A1523 (cit. on pp. 30, 45, 48–50, 54, 99).

[87] Robert M Darling and Jeremy P Meyers. “Mathematical model of platinum movement in PEM fuel cells”. In: *Journal of the Electrochemical Society* 152.1 (2004), A242 (cit. on pp. 30, 99).

[88] Steven G Rinaldo, Jürgen Stumper, and Michael Eikerling. “Physical theory of platinum nanoparticle dissolution in polymer electrolyte fuel cells”. In: *The Journal of Physical Chemistry C* 114.13 (2010), pp. 5773–5785 (cit. on pp. 30, 52, 54, 99).

[89] Steven G Rinaldo, Wendy Lee, Jürgen Stumper, et al. “Catalyst degradation: nanoparticle population dynamics and kinetic processes”. In: *ECS Transactions* 50.2 (2013), p. 1505 (cit. on pp. 30, 48).

[90] Manik Mayur, Mathias Gerard, Pascal Schott, et al. “Lifetime prediction of a polymer electrolyte membrane fuel cell under automotive load cycling using a physically-based catalyst degradation model”. In: *Energies* 11.8 (2018), p. 2054 (cit. on p. 31).

[91] Alexander Kneer and Nadja Wagner. “A semi-empirical catalyst degradation model based on voltage cycling under automotive operating conditions in PEM fuel cells”. In: *Journal of The Electrochemical Society* 166.2 (2019), F120 (cit. on pp. 31, 104).

[92] M Chandesris, V Médeau, N Guillet, et al. “Membrane degradation in PEM water electrolyzer: Numerical modeling and experimental evidence of the influence of temperature and current density”. In: *International Journal of Hydrogen Energy* 40.3 (2015), pp. 1353–1366 (cit. on p. 31).

[93] Akeel A Shah, TR Ralph, and FC Walsh. "Modeling and simulation of the degradation of perfluorinated ion-exchange membranes in PEM fuel cells". In: *Journal of The Electrochemical Society* 156.4 (2009), B465 (cit. on p. 32).

[94] Larisa Karpenko-Jereb, Christof Sternig, Clemens Fink, et al. "Membrane degradation model for 3D CFD analysis of fuel cell performance as a function of time". In: *international journal of hydrogen energy* 41.31 (2016), pp. 13644–13656 (cit. on p. 33).

[95] Tao Xie and Charlene A Hayden. "A kinetic model for the chemical degradation of perfluorinated sulfonic acid ionomers: Weak end groups versus side chain cleavage". In: *Polymer* 48.19 (2007), pp. 5497–5506 (cit. on p. 33).

[96] Weibo Zheng, Liangfei Xu, Zunyan Hu, et al. "Dynamic modeling of chemical membrane degradation in polymer electrolyte fuel cells: Effect of pinhole formation". In: *Journal of Power Sources* 487 (2021), p. 229367 (cit. on p. 33).

[97] Jae Young Shim, Shohji Tsushima, and Shuichiro Hirai. "Experimental and modeling studies on the effect of oxygen partial pressure on membrane degradation in PEMFCs". In: *Journal of the Electrochemical Society* 156.6 (2009), B690 (cit. on p. 33).

[98] Simon Morando, Samir Jemei, Daniel Hissel, et al. "ANOVA method applied to proton exchange membrane fuel cell ageing forecasting using an echo state network". In: *Mathematics and Computers in Simulation* 131 (2017), pp. 283–294 (cit. on p. 34).

[99] RE Silva, Rafael Gouriveau, Samir Jemei, et al. "Proton exchange membrane fuel cell degradation prediction based on adaptive neuro-fuzzy inference systems". In: *International Journal of Hydrogen Energy* 39.21 (2014), pp. 11128–11144 (cit. on p. 34).

[100] Marine Jouin, Rafael Gouriveau, Daniel Hissel, et al. "Prognostics of PEM fuel cell in a particle filtering framework". In: *International Journal of Hydrogen Energy* 39.1 (2014), pp. 481–494 (cit. on p. 34).

[101] Pucheng Pei, Qianfei Chang, and Tian Tang. "A quick evaluating method for automotive fuel cell lifetime". In: *International Journal of Hydrogen Energy* 33.14 (2008). TMS07: Symposium on Materials in Clean Power Systems, pp. 3829–3836. ISSN: 0360-3199. DOI: https://doi.org/10.1016/j.ijhydene.2008.04.048 (cit. on p. 34).

[102] Pyoungho Choi and Ravindra Datta. "Sorption in proton-exchange membranes: an explanation of Schroeder's paradox". In: *Journal of the Electrochemical Society* 150.12 (2003), E601 (cit. on p. 35).

[103] Thomas E Springer, TA Zawodzinski, and Shimshon Gottesfeld. "Polymer electrolyte fuel cell model". In: *Journal of the electrochemical society* 138.8 (1991), p. 2334 (cit. on pp. 35, 36).

[104] Dawn M Bernardi and Mark W Verbrugge. "Mathematical model of a gas diffusion electrode bonded to a polymer electrolyte". In: *AIChE journal* 37.8 (1991), pp. 1151–1163 (cit. on p. 35).

[105] Ryan Anderson, Lifeng Zhang, Yulong Ding, et al. "A critical review of two-phase flow in gas flow channels of proton exchange membrane fuel cells". In: *Journal of Power Sources* 195.15 (2010), pp. 4531–4553 (cit. on p. 35).

[106] Alireza Goshtasbi, Pablo García-Salaberri, Jixin Chen, et al. "Through-the-membrane transient phenomena in PEM fuel cells: A modeling study". In: *Journal of The Electrochemical Society* 166.7 (2019), F3154 (cit. on p. 35).

[107] Georg A Futter, Pawel Gazdzicki, K Andreas Friedrich, et al. "Physical modeling of polymer-electrolyte membrane fuel cells: Understanding water management and impedance spectra". In: *Journal of Power Sources* 391 (2018), pp. 148–161 (cit. on p. 35).

[108] Jay T Pukrushpan, Huei Peng, and Anna G Stefanopoulou. "Control-oriented modeling and analysis for automotive fuel cell systems". In: *J. Dyn. Sys., Meas., Control* 126.1 (2004), pp. 14–25 (cit. on pp. 35–37).

[109] Kyung Won Suh. *Modeling, analysis and control of fuel cell hybrid power systems*. University of Michigan, 2006 (cit. on pp. 35–37).

[110] Denise A McKay, Jason B Siegel, William Ott, et al. "Parameterization and prediction of temporal fuel cell voltage behavior during flooding and drying conditions". In: *Journal of Power Sources* 178.1 (2008), pp. 207–222 (cit. on p. 36).

[111] M Zaglio, Alexander Wokaun, John Mantzaras, et al. "1D-Modelling and Experimental Study of the PEFC Dynamic Behaviour at Load Increase". In: *Fuel Cells* 11.4 (2011), pp. 526–536 (cit. on p. 36).

[112] Alireza Goshtasbi, Benjamin L Pence, and Tulga Ersal. "Computationally efficient pseudo-2D non-isothermal modeling of polymer electrolyte membrane fuel cells with two-phase phenomena". In: *Journal of The Electrochemical Society* 163.13 (2016), F1412 (cit. on pp. 36, 72, 77, 81, 82).

[113] J Zhou, A Putz, and M Secanell. "A mixed wettability pore size distribution based mathematical model for analyzing two-phase flow in porous electrodes". In: *Journal of The Electrochemical Society* 164.6 (2017), F530 (cit. on p. 36).

[114] Daniel R Baker, David A Caulk, Kenneth C Neyerlin, et al. "Measurement of oxygen transport resistance in PEM fuel cells by limiting current methods". In: *Journal of The Electrochemical Society* 156.9 (2009), B991 (cit. on p. 36).

[115] Lalit M Pant, Michael R Gerhardt, Natalia Macauley, et al. "Along-the-channel modeling and analysis of PEFCs at low stoichiometry: Development of a 1+ 2D model". In: *Electrochimica Acta* 326 (2019), p. 134963 (cit. on p. 36).

[116] Hao Wu, Peter Berg, and Xianguo Li. "Steady and unsteady 3D non-isothermal modeling of PEM fuel cells with the effect of non-equilibrium phase transfer". In: *Applied Energy* 87.9 (2010), pp. 2778–2784 (cit. on p. 36).

[117] Alireza Goshtasbi, Benjamin L Pence, Jixin Chen, et al. "A mathematical model toward real-time monitoring of automotive PEM fuel cells". In: *Journal of The Electrochemical Society* 167.2 (2020), p. 024518 (cit. on pp. 36, 72).

[118] Roman Vetter and Jürgen O Schumacher. "Free open reference implementation of a two-phase PEM fuel cell model". In: *Computer Physics Communications* 234 (2019), pp. 223–234 (cit. on pp. 36, 76, 79, 80).

[119] Daniel S Hussey, Dusan Spernjak, Adam Z Weber, et al. "Accurate measurement of the through-plane water content of proton-exchange membranes using neutron radiography". In: *Journal of Applied Physics* 112.10 (2012) (cit. on p. 36).

[120] Takahiro Suzuki, Yuichiro Tabuchi, Shohji Tsushima, et al. "Measurement of water content distribution in catalyst coated membranes under water permeation conditions by magnetic resonance imaging". In: *International journal of hydrogen energy* 36.9 (2011), pp. 5479–5486 (cit. on p. 36).

[121] Jens Eller, Tomas Rosén, Federica Marone, et al. "Progress in in situ X-ray tomographic microscopy of liquid water in gas diffusion layers of PEFC". In: *Journal of The Electrochemical Society* 158.8 (2011), B963 (cit. on p. 36).

[122] S. Jemeï, D. Hissel, M.C. Péra, et al. "On-board fuel cell power supply modeling on the basis of neural network methodology". In: *Journal of Power Sources* 124.2 (2003), pp. 479–486. ISSN: 0378-7753. DOI: 10.1016/S0378-7753(03)00799-7 (cit. on p. 37).

[123] Z Abdin, CJ Webb, and E MacA Gray. "PEM fuel cell model and simulation in Matlab–Simulink based on physical parameters". In: *Energy* 116 (2016), pp. 1131–1144 (cit. on p. 37).

[124] Joshua Golbert and Daniel R. Lewin. "Model-based control of fuel cells (2): Optimal efficiency". In: *Journal of Power Sources* 173.1 (2007), pp. 298–309. ISSN: 0378-7753. DOI: https://doi.org/10.1016/j.jpowsour.2007.04.062 (cit. on p. 37).

[125] Julio Luna, Samir Jemei, Nadia Yousfi-Steiner, et al. "Nonlinear predictive control for durability enhancement and efficiency improvement in a fuel cell power system". In: *Journal of Power Sources* 328 (2016), pp. 250–261. ISSN: 0378-7753. DOI: https://doi.org/10.1016/j.jpowsour.2016.08.019 (cit. on p. 37).

[126] Hui Li, Yanghua Tang, Zhenwei Wang, et al. "A review of water flooding issues in the proton exchange membrane fuel cell". In: *Journal of Power Sources* 178.1 (2008), pp. 103–117. ISSN: 0378-7753. DOI: https://doi.org/10.1016/j.jpowsour.2007.12.068 (cit. on p. 37).

[127] Jiamin Xu, Caizhi Zhang, Ruijia Fan, et al. "Modelling and control of vehicle integrated thermal management system of PEM fuel cell vehicle". In: *Energy* 199 (2020), p. 117495. ISSN: 0360-5442. DOI: https://doi.org/10.1016/j.energy.2020.117495 (cit. on p. 38).

[128] Ten-Huei Guo, Philip Chen, and Link Jaw. "Intelligent life-extending controls for aircraft engines". In: *AIAA 1st Intelligent Systems Technical Conference*. 2004, p. 6468 (cit. on p. 38).

[129] James W Fuller. *Model predictive controller with life extending control*. US Patent 7,203,554. Apr. 2007 (cit. on p. 38).

[130] P Kallappa, Michael S Holmes, and Asok Ray. "Life-extending control of fossil fuel power plants". In: *Automatica* 33.6 (1997), pp. 1101–1118 (cit. on p. 39).

[131] Jeffrey Caplin and Asok Ray. "Life extending control of gas turbine engines for aircraft propulsion". In: *Proceedings of the 36th IEEE Conference on Decision and Control*. Vol. 5. IEEE. 1997, pp. 4700–4701 (cit. on p. 39).

[132] Zhiguang Hua, Zhixue Zheng, Elodie Pahon, et al. "Health indicators for PEMFC systems life prediction under both static and dynamic operating conditions". In: *IECON 2020 the 46th annual conference of the IEEE industrial electronics society*. IEEE. 2020, pp. 3963–3968 (cit. on p. 41).

[133] Jiayu Chen, Dong Zhou, Chuan Lyu, et al. "A novel health indicator for PEMFC state of health estimation and remaining useful life prediction". In: *International Journal of Hydrogen Energy* 42.31 (2017), pp. 20230–20238 (cit. on p. 41).

[134] Thomas Jahnke, Georg Futter, Arnulf Latz, et al. "Performance and degradation of Proton Exchange Membrane Fuel Cells: State of the art in modeling from atomistic to system scale". In: *Journal of Power Sources* 304 (2016), pp. 207–233 (cit. on pp. 42, 70).

[135] Lei Fan, Jianhua Gao, Yanda Lu, et al. "Analysis of the Influence of Component Degradation on Different Degradation Indexes of PEMFC". In: *Energies* 16.23 (2023), p. 7806 (cit. on p. 42).

[136] SR Dhanushkodi, M Tam, S Kundu, et al. "Carbon corrosion fingerprint development and de-convolution of performance loss according to degradation mechanism in PEM fuel cells". In: *Journal of Power Sources* 240 (2013), pp. 114–121 (cit. on p. 44).

[137] N Seriani and F Mittendorfer. "Platinum-group and noble metals under oxidizing conditions". In: *Journal of Physics: Condensed Matter* 20.18 (2008), p. 184023 (cit. on p. 44).

[138] Rod Borup, Jeremy Meyers, Bryan Pivovar, et al. "Scientific aspects of polymer electrolyte fuel cell durability and degradation". In: *Chemical reviews* 107.10 (2007), pp. 3904–3951 (cit. on p. 44).

[139] Angel A Topalov, Serhiy Cherevko, Aleksandar R Zeradjanin, et al. "Towards a comprehensive understanding of platinum dissolution in acidic media". In: *Chemical Science* 5.2 (2014), pp. 631–638 (cit. on p. 44).

[140] Darrick V Heyd and David A Harrington. "Platinum oxide growth kinetics for cyclic voltammetry". In: *Journal of Electroanalytical Chemistry* 335.1-2 (1992), pp. 19–31 (cit. on p. 45).

[141] David A Harrington. "Simulation of anodic Pt oxide growth". In: *Journal of Electroanalytical Chemistry* 420.1-2 (1997), pp. 101–109 (cit. on p. 45).

[142] BE Conway, B Barnett, H Angerstein-Kozlowska, et al. "A surface-electrochemical basis for the direct logarithmic growth law for initial stages of extension of anodic oxide films formed at noble metals". In: *The Journal of chemical physics* 93.11 (1990), pp. 8361–8373 (cit. on p. 45).

[143] Heather A Baroody and Erik Kjeang. "Predicting platinum dissolution and performance degradation under drive cycle operation of polymer electrolyte fuel cells". In: *Journal of The Electrochemical Society* 168.4 (2021), p. 044524 (cit. on p. 46).

[144] Patrick Schneider, Christian Sadeler, Anne-Christine Scherzer, et al. "Fast and reliable state-of-health model of a PEM cathode catalyst layer". In: *Journal of The Electrochemical Society* 166.4 (2019), F322 (cit. on pp. 46, 54).

[145] Srikanth Arisetty, Yuxiu Liu, Wenbin Gu, et al. "Modeling platinum oxide growth of PEMFC cathode catalysts". In: *ECS Transactions* 69.17 (2015), p. 273 (cit. on p. 47).

[146] Ambrož Kregar, Matija Gatalo, Nik Maselj, et al. "Temperature dependent model of carbon supported platinum fuel cell catalyst degradation". In: *Journal of Power Sources* 514 (2021), p. 230542 (cit. on p. 47).

[147] Masanobu Uchimura, Seiho Sugawara, Yosuke Suzuki, et al. "Electrocatalyst durability under simulated automotive drive cycles". In: *Ecs Transactions* 16.2 (2008), p. 225 (cit. on p. 47).

[148] Ryan O'hayre, Suk-Won Cha, Whitney Colella, et al. *Fuel cell fundamentals*. John Wiley & Sons, 2016 (cit. on p. 48).

[149] Steven G Rinaldo, Wendy Lee, Jürgen Stumper, et al. "Mechanistic principles of platinum oxide formation and reduction". In: *Electrocatalysis* 5 (2014), pp. 262–272 (cit. on p. 48).

[150] Josef C Meier, Ioannis Katsounaros, Carolina Galeano, et al. "Stability investigations of electrocatalysts on the nanoscale". In: *Energy & Environmental Science* 5.11 (2012), pp. 9319–9330 (cit. on p. 48).

[151] Lim Kim, Chul Goo Chung, Yong Wook Sung, et al. "Dissolution and migration of platinum after long-term operation of a polymer electrolyte fuel cell under various conditions". In: *Journal of Power Sources* 183.2 (2008), pp. 524–532 (cit. on p. 48).

[152] Steven G Rinaldo, Wendy Lee, Jürgen Stumper, et al. "Nonmonotonic dynamics in Lifshitz-Slyozov-Wagner theory: Ostwald ripening in nanoparticle catalysts". In: *Physical Review E* 86.4 (2012), p. 041601 (cit. on p. 48).

[153] Peter W Voorhees and ME Glicksman. "Solution to the multi-particle diffusion problem with applications to Ostwald ripening—II. Computer simulations". In: *Acta metallurgica* 32.11 (1984), pp. 2013–2030 (cit. on p. 48).

[154] Rangachary Mukundan, Andrew M Baker, Ahmet Kusoglu, et al. "Membrane accelerated stress test development for polymer electrolyte fuel cell durability validated using field and drive cycle testing". In: *Journal of The Electrochemical Society* 165.6 (2018), F3085–F3093 (cit. on p. 51).

[155] Marvin Messing and Erik Kjeang. "Empirical modeling of cathode electrode durability in polymer electrolyte fuel cells". In: *Journal of Power Sources* 451 (2020), p. 227750 (cit. on pp. 53, 54).

[156] Xiaoyan Luo, Lida Ghassemzadeh, and Steven Holdcroft. "Effect of free radical-induced degradation on water permeation through PFSA ionomer membranes". In: *International Journal of Hydrogen Energy* 40.46 (2015), pp. 16714–16723 (cit. on p. 62).

[157] Ka Hung Wong and Erik Kjeang. "Macroscopic in-situ modeling of chemical membrane degradation in polymer electrolyte fuel cells". In: *Journal of The Electrochemical Society* 161.9 (2014), F823 (cit. on p. 62).

[158] Pavel S Ruvinskiy, Antoine Bonnefont, Cuong Pham-Huu, et al. "Using ordered carbon nanomaterials for shedding light on the mechanism of the cathodic oxygen reduction reaction". In: *Langmuir* 27.14 (2011), pp. 9018–9027 (cit. on p. 62).

[159] Vijay A Sethuraman, John W Weidner, Andrew T Haug, et al. "Hydrogen peroxide formation rates in a PEMFC anode and cathode: Effect of humidity and temperature". In: *Journal of The Electrochemical Society* 155.1 (2007), B50 (cit. on p. 63).

[160] Ka Hung Wong and Erik Kjeang. "Mitigation of chemical membrane degradation in fuel cells: understanding the effect of cell voltage and iron ion redox cycle". In: *ChemSusChem* 8.6 (2015), pp. 1072–1082 (cit. on p. 64).

[161] Mathieu Bressel, Mickael Hilairet, Daniel Hissel, et al. "Remaining useful life prediction and uncertainty quantification of proton exchange membrane fuel cell under variable load". In: *IEEE Transactions on Industrial Electronics* 63.4 (2016), pp. 2569–2577 (cit. on p. 70).

[162] A Verma and R Pitchumani. "Influence of transient operating parameters on the mechanical behavior of fuel cells". In: *International Journal of Hydrogen Energy* 40.26 (2015), pp. 8442–8453 (cit. on p. 70).

[163] Philippe Moçotéguy, Bastian Ludwig, and Nadia Steiner. "Influence of ageing on the dynamic behaviour and the electrochemical characteristics of a 500 We PEMFC stack". In: *International journal of hydrogen energy* 39.19 (2014), pp. 10230–10244 (cit. on p. 70).

[164] Daming Zhou, Fei Gao, Ahmed Al-Durra, et al. "Development of a multiphysical 2-D model of a PEM fuel cell for real-time control". In: *IEEE Transactions on Industry Applications* 54.5 (2018), pp. 4864–4874 (cit. on p. 71).

[165] Horng-Wen Wu. "A review of recent development: Transport and performance modeling of PEM fuel cells". In: *Applied energy* 165 (2016), pp. 81–106 (cit. on p. 71).

[166] Alireza Goshtasbi and Tulga Ersal. "LQ-MPC design for degradation-conscious control of PEM fuel cells". In: *2019 American Control Conference (ACC)*. IEEE. 2019, pp. 1555–1560 (cit. on pp. 72, 73).

[167] RB Bird, WE Stewart, and EN Lightfoot. "Transport Phenomena. John Wiley & Sons, Inc". In: *New York, NY* 1 (2002) (cit. on p. 74).

[168] Tomas Rosén, Jens Eller, Jinfen Kang, et al. "Saturation dependent effective transport properties of PEFC gas diffusion layers". In: *Journal of The Electrochemical Society* 159.9 (2012), F536 (cit. on p. 75).

[169] Liang Hao, Koji Moriyama, Wenbin Gu, et al. "Modeling and experimental validation of Pt loading and electrode composition effects in PEM fuel cells". In: *Journal of The Electrochemical Society* 162.8 (2015), F854 (cit. on p. 75).

[170] Shinji Jomori, Nobuaki Nonoyama, and Toshihiko Yoshida. "Analysis and modeling of PEMFC degradation: Effect on oxygen transport". In: *Journal of Power Sources* 215 (2012), pp. 18–27 (cit. on p. 75).

[171] Ling Xu, Zunyan Hu, Chuan Fang, et al. "A reduced-dimension dynamic model of a proton-exchange membrane fuel cell". In: *International Journal of Energy Research* 45.12 (2021), pp. 18002–18017 (cit. on p. 76).

[172] Colleen Spiegel. *PEM fuel cell modeling and simulation using MATLAB*. Elsevier, 2011 (cit. on p. 77).

[173] Cortney K Mittelsteadt and John Staser. "Simultaneous water uptake, diffusivity and permeability measurement of perfluorinated sulfonic acid polymer electrolyte membranes". In: *ECS Transactions* 41.1 (2011), p. 101 (cit. on p. 77).

[174] Shanhai Ge, Xuguang Li, Baolian Yi, et al. "Absorption, desorption, and transport of water in polymer electrolyte membranes for fuel cells". In: *Journal of the Electrochemical Society* 152.6 (2005), A1149 (cit. on p. 77).

[175] David L Fritz and Jeffrey S Allen. "Evaporation modeling for proton exchange membrane fuel cells". In: *ECS transactions* 25.1 (2009), p. 49 (cit. on p. 79).

[176] Hao Wu, Xianguo Li, and Peter Berg. "On the modeling of water transport in polymer electrolyte membrane fuel cells". In: *Electrochimica Acta* 54.27 (2009), pp. 6913–6927 (cit. on p. 79).

[177] Valentin Sulzer, Peyman Mohtat, and Jason B Siegel. "Reduced-order modeling of PEM fuel cells using asymptotic analysis". In: (2022) (cit. on p. 80).

[178] MoC Leverett. "Capillary behavior in porous solids". In: *Transactions of the AIME* 142.01 (1941), pp. 152–169 (cit. on p. 80).

[179] Yongqiang Wang, Scott J Moura, Suresh G Advani, et al. "Power management system for a fuel cell/battery hybrid vehicle incorporating fuel cell and battery degradation". In: *International Journal of Hydrogen Energy* 44.16 (2019), pp. 8479–8492 (cit. on p. 82).

[180] NP Subramanian, TA Greszler, J Zhang, et al. "Pt-oxide coverage-dependent oxygen reduction reaction (ORR) kinetics". In: *Journal of The Electrochemical Society* 159.5 (2012), B531 (cit. on p. 82).

[181] Jian Zuo, Hong Lv, Daming Zhou, et al. "Long-term dynamic durability test datasets for single proton exchange membrane fuel cell". In: *Data in Brief* 35 (2021), p. 106775 (cit. on p. 89).

[182] E Endoh. "Highly durable PFSA membranes". In: *Handbook of Fuel Cells* 5 (2009), pp. 361–374 (cit. on p. 93).

[183] Gregor S Harzer, Jan N Schwämmlein, Ana Marija Damjanović, et al. "Cathode loading impact on voltage cycling induced PEMFC degradation: a voltage loss analysis". In: *Journal of The Electrochemical Society* 165.6 (2018), F3118–F3131 (cit. on p. 94).

[184] Mahmood Shafiee and Isaac Animah. "Life extension decision making of safety critical systems: An overview". In: *Journal of Loss Prevention in the Process Industries* 47 (2017), pp. 174–188 (cit. on p. 94).

[185] N Zhao, Y Chu, Z Xie, et al. "Effects of fuel cell operating conditions on proton exchange membrane durability at open-circuit voltage". In: *Fuel Cells* 20.2 (2020), pp. 176–184 (cit. on p. 94).

[186] Xi Chen, Jianghai Xu, Qian Liu, et al. "Active disturbance rejection control strategy applied to cathode humidity control in PEMFC system". In: *Energy Conversion and Management* 224 (2020), p. 113389 (cit. on p. 94).

[187] Qi Li, Tianle Su, Liangzhen Yin, et al. "Health Management for PEMFC System Long-Term Operation Based on Optimal Temperature Trajectory Real-Time Optimization". In: *IEEE Transactions on Industrial Electronics* (2024) (cit. on p. 94).

[188] Maher AR Sadiq Al-Baghdadi. "Modelling of proton exchange membrane fuel cell performance based on semi-empirical equations". In: *Renewable energy* 30.10 (2005), pp. 1587–1599 (cit. on p. 96).

[189] Xian Zhang and Pierluigi Pisu. "Prognostic-oriented fuel cell catalyst aging modeling and its application to health-monitoring and prognostics of a pem fuel cell". In: *International Journal of Prognostics and Health Management* 5.1 (2014) (cit. on pp. 99, 139).

[190] Donghai Hu, Yuteng Wang, Jianwei Li, et al. "Investigation of optimal operating temperature for the PEMFC and its tracking control for energy saving in vehicle applications". In: *Energy Conversion and Management* 249 (2021), p. 114842 (cit. on p. 100).

[191] Dilip Ramani, Yadvinder Singh, Francesco P Orfino, et al. "Characterization of membrane degradation growth in fuel cells using X-ray computed tomography". In: *Journal of The Electrochemical Society* 165.6 (2018), F3200 (cit. on p. 104).

[192] C Lim, L Ghassemzadeh, F Van Hove, et al. "Membrane degradation during combined chemical and mechanical accelerated stress testing of polymer electrolyte fuel cells". In: *Journal of Power Sources* 257 (2014), pp. 102–110 (cit. on p. 104).

[193] Eunho Choi, Segeun Jang, Sang Moon Kim, et al. "Patterned mesoporous TiO2 microplates embedded in Nafion® membrane for high temperature/low relative humidity polymer electrolyte membrane fuel cell operation". In: *Renewable Energy* 180 (2021), pp. 203–212 (cit. on p. 105).

[194] Zhiming Zhang, Zhihao Chen, Kunpeng Li, et al. "A multi-field coupled PEMFC model with force-temperature-humidity and experimental validation for high electrochemical performance design". In: *Sustainability* 15.16 (2023), p. 12436 (cit. on p. 105).

[195] David Angeli. "Economic model predictive control". In: *Encyclopedia of Systems and Control*. Springer, 2021, pp. 665–671 (cit. on p. 106).

[196] Walid Touil, Zhongliang Li, Rachid Outbib, et al. "Model predictive control energy management strategy of fuel cell hybrid electric vehicle". In: *IECON 2022–48th Annual Conference of the IEEE Industrial Electronics Society*. IEEE. 2022, pp. 1–8 (cit. on pp. 107, 111).

[197] James Blake Rawlings, David Q Mayne, Moritz Diehl, et al. *Model predictive control: theory, computation, and design*. Vol. 2. Nob Hill Publishing Madison, WI, 2017 (cit. on p. 107).

[198] Mohamadou Nassourou. "Robust Economic Model Predictive Control of Smart Grids". In: (2021) (cit. on p. 108).

[199] Stefan Loew, Abhinav Anand, and Andrei Szabo. "Economic model predictive control of Li-ion battery cyclic aging via online rainflow-analysis". In: *Energy Storage* 3.3 (2021), e228 (cit. on p. 108).

ANNEXES

5 Appendix

5.1 Pt Catalyst Model Simplification

This appendix provides an overview of the simplified Pt catalyst model employed in our control approach. To streamline the model, we consider only two representative particle radii rather than the full particle radius distribution. We assume a single degradation mechanism, specifically Ostwald ripening, and deliberately neglect chemical dissolution effects to focus on core degradation dynamics in a reduced-complexity framework.

To begin, let $f_N(r_i, t) = N_i$ denote the particle count for each specific particle group with radius r_i. We discretize the particle radius distribution into a defined number of groups $i \in [1, M]$, where each group corresponds to a fixed particle number at radius r_i. Rather than modeling the evolution of the entire particle distribution, we simplify further by fixing the number of particles in each radius group while allowing only the radius to vary over time, described by the equation:

$$\frac{dr_i}{dt} = -\frac{M_{\mathrm{Pt}}}{\rho_{\mathrm{Pt}}} R_1(r_i, t)$$

The surface area $S(t)$ is given by:

$$S(t) = \sum_i 4\pi r_i^2 N_i$$

To simplify our analysis, we define the following constants:

$$U_a = \exp\left(\frac{FU}{RT}\right)$$

$$U_b = \exp\left(\frac{FU_1^0}{RT}\right)$$

Additionally, we define the function $U_c(r_i)$:

$$U_c(r_i) = \exp\left(\frac{F}{RT}\frac{\beta_1}{r_i}\right)$$

where $\beta_1 = \frac{\sigma_{\mathrm{Pt}} M_{\mathrm{Pt}}}{2F\rho_{\mathrm{Pt}}}$.
The rate of change of the surface area S over time is given by:

$$\frac{dS}{dt} = \sum_i \frac{d}{dt}(4\pi r_i^2 N_i) = \sum_i 8\pi r_i N_i \frac{dr_i}{dt} = -8\pi \frac{M_{\mathrm{Pt}}}{\rho_{\mathrm{Pt}}} \sum_i r_i N_i R_1(r_i, t)$$

This expression indicates that the change in surface area over time depends on the radius r_i, the particle count N_i, and the rate of the degradation mechanism $R_1(r_i, t)$ for each particle group i.

Neglecting Pt diffusion into the membrane, steady-state concentration is achieved only when the rate of Pt atom dissolution equals the rate of Pt ion redeposition:

$$\frac{dc_{\mathrm{Pt}}}{dt} = V_{\mathrm{Pt}} \sum_i 4\pi r_i^2 N_i R_1(r_i, t) = 0$$

This implies that $R_1(r_i, t) = 0$. From this, we can derive:

$$k_1 (1 - \theta(r, t)) \left[\frac{U_a}{U_b} U_c(r_i) - \frac{c_{\mathrm{Pt}^{2+}}}{c^{\mathrm{ref}}_{\mathrm{Pt}^{2+}}} \frac{U_b}{U_a U_c(r_i)} \right] = 0 \tag{5.1}$$

Based on assumption (A 4), we have:

$$\frac{c_{\mathrm{Pt}^{2+}}}{c^{\mathrm{ref}}_{\mathrm{Pt}^{2+}}} = \left(\frac{U_a}{U_b} \right)^2 \left(U_c(r_{\mathrm{avg}}) \right)^2$$

where r_{avg} is the equivalent average radius.

Using a Taylor expansion on the derivative of the platinum ion concentration and substituting the electrochemically active surface area (ECSA) for particle groups 1 and 2, as discussed by Zhang et al. [189], we obtain the following approximations:

$$S_1 \approx S \cdot \frac{\Delta r_2}{r_2} \Big/ \left(\frac{\Delta r_1}{r_1} + \frac{\Delta r_2}{r_2} \right) \tag{5.2}$$

$$S_2 \approx S \cdot \frac{\Delta r_1}{r_1} \Big/ \left(\frac{\Delta r_1}{r_1} + \frac{\Delta r_2}{r_2} \right) \tag{5.3}$$

Consequently, the time derivative of S can be expressed as follows:

$$\frac{dS}{dt} = -8\pi \frac{M_{\mathrm{Pt}}}{\rho_{\mathrm{Pt}}} k_1 (1 - \theta) \frac{U_a}{U_b} \sum_{i=1}^{2} \frac{S_i}{4\pi r_i} \left(\frac{U_c(r_i)}{U_c(r_{\mathrm{avg}})} - \frac{U_c(r_{\mathrm{avg}})}{U_c(r_i)} \right) \tag{5.4}$$

where the average radius is defined as:

$$r_{\mathrm{avg}} = \frac{3 V_{\mathrm{Pt}}}{S} \tag{5.5}$$

Additionally, the function $U_c(r_{\mathrm{avg}})$ is given by:

$$U_c(r_{\mathrm{avg}}) = \exp\left(\frac{F}{RT} \frac{\beta_1}{r_{\mathrm{avg}}} \right) \tag{5.6}$$

Thus, we can restate the expression for the derivative of S:

$$\frac{dS}{dt} = -8\pi \frac{M_{\mathrm{Pt}}}{\rho_{\mathrm{Pt}}} k_1 (1-\theta) \frac{U_a}{U_b} U_c(r_{\mathrm{avg}}) \sum_{i=1}^{2} \frac{S_i}{4\pi r_i} \left(\frac{U_c(r_i)}{U_c(r_{\mathrm{avg}})} - \frac{U_c(r_{\mathrm{avg}})}{U_c(r_i)} \right) \tag{5.7}$$

This leads to:

$$\frac{dS}{dt} = -2 \frac{M_{\mathrm{Pt}}}{\rho_{\mathrm{Pt}}} k_1 (1-\theta) \frac{U_a}{U_b} \exp\left(\frac{F\beta_1}{RT} \frac{S}{3V_{\mathrm{Pt}}} \right) \cdot \left(\frac{S_1}{r_1} \frac{2F\beta_1}{RT} \left(\frac{\Delta r_1}{r_{\mathrm{avg}} r_1} \right) - \frac{S_2}{r_2} \frac{2F\beta_1}{RT} \left(\frac{\Delta r_2}{r_{\mathrm{avg}} r_2} \right) \right) \tag{5.8}$$

In summary, the final expression for the time derivative of the surface area S can be presented as:

$$\frac{dS}{dt} = -k_1 (1-\theta) \frac{M_{\mathrm{Pt}}}{\rho_{\mathrm{Pt}}} \exp\left(\frac{F}{RT} (U - U_1^0) \right) \exp\left(\frac{F\beta_1}{RT} \frac{S}{3V_{\mathrm{Pt}}} \right) \cdot \left(\frac{S^3}{9V_{\mathrm{Pt}}^2} \cdot \frac{4\alpha_r \beta_r^2}{(1+\beta_r)(1-\alpha_r \beta_r)} \right) \tag{5.9}$$

where we define $\frac{\Delta r_2}{r_{\mathrm{avg}}} = \beta_r$ and $\Delta r_1 = \alpha_r \Delta r_2$.